Optimization in Wireless Sensor and Machine-Type Communication Networks

by

Ghasem Naddafzadeh Shirazi

B.Sc., Shiraz University, Iran, 2006
M.Eng., National University of Singapore, Singapore, 2009

A THESIS SUBMITTED IN PARTIAL FULFILLMENT OF
THE REQUIREMENTS FOR THE DEGREE OF

DOCTOR OF PHILOSOPHY

in

The Faculty of Graduate and Postdoctoral Studies

(Electrical and Computer Engineering)

THE UNIVERSITY OF BRITISH COLUMBIA

(Vancouver)

April 2014

Abstract

Wireless sensor networks (WSNs) are systems used for detecting events and gathering information from an area of interest in many different application domains, from home and industry automation, to healthcare and transportation, to environmental monitoring. With regard to the communication task involved in WSNs, they can also be seen as an instance of the new paradigm, known as machine-type communication (MTC). Similar to traditional wireless sensors, MTC-enabled devices can communicate together without direct human interference.

Energy efficiency for the sake of longevity is perhaps the most challenging requirement for many WSNs and MTC networks. In this thesis, we consider ultra-wideband (UWB) transmission technology for energy-efficient communication in WSNs. UWB achieves frugal use of energy by transmitting with low spectral efficiency when compared to legacy wireless technologies. This also allows it to operate license-exempt in many jurisdictions around the world. More recently, however, wireless service operators consider the use of cellular technology also for low data-rate applications originally only served by WSN-type technology. In particular, long-term evolution (LTE) technology has moved into the focus for joint personal-communication and MTC networks. Recent releases of the LTE standard and ongoing work items

in LTE standardization specifically accommodate low-cost and low-power MTC.

This thesis presents contributions that improve the performance of UWB WSN and LTE MTC networks in several aspects, namely lifetime, localization accuracy, and coverage. A common theme of these different contributions are the use of optimization methods for obtaining scalable, robust, and/or low-complexity solutions.

We first address the lifetime maximization problem in a UWB-based WSN designed for multiple event detection. The key contribution is the joint optimization of transmission and routing parameters of sensor nodes so that the energy consumption is distributed as evenly as possible among the entire WSN. We then investigate the challenges of localization in WSNs and provide a convex solution which is robust to measurement uncertainties. In the last part of this thesis we focus on providing coverage for low-cost LTE MTC networks, where the challenge is to develop efficient transmission strategies that maximize the coverage of MTC devices in an LTE cell.

Preface

The material presented in this thesis is entirely based on research performed by myself under the supervision of Prof. Lutz Lampe in the Department of Electrical and Computer Engineering (ECE) at the University of British Columbia (UBC). Below is a list of publications related to the work presented in this thesis, which includes commentaries on the role of collaborators.

Publications Related to Chapter 2

- Ghasem Naddafzadeh Shirazi and Lutz Lampe, "Lifetime Maximization in UWB Sensor Networks for Event Detection", *IEEE Trans. Signal Processing*, vol. 59, no. 9, pp. 4411 – 4423, September 2011.

- Ghasem Naddafzadeh Shirazi and Lutz Lampe, "Lifetime Maximization in UWB Sensor Networks for Event Detection Applications", in IEEE International Conference on Communications (ICC), pp. 1 – 6, Cape Town, South Africa, May 2010.

Publications Related to Chapter 3

- Ghasem Naddafzadeh Shirazi, Michael Botros Shenouda, and Lutz Lampe, "Second Order Cone Programming for Sensor Network Localization with Anchor Position Uncertainty", *IEEE Trans. Wireless Communications*, vol. 13, no. 2, pp. 749 – 763, February 2014.

- Ghasem Naddafzadeh Shirazi and Lutz Lampe, "Second Order Cone Programming for Robust Localization in Mobile Sensor Networks", in IEEE Global Communication Conference (Globecom), 4th International Workshop on Wireless Networking and Control for Unmanned Autonomous Vehicles (Wi-UAV), pp. 1 – 6, Atlanta, USA, December 2013.

- Ghasem Naddafzadeh Shirazi, Michael Botros Shenouda, and Lutz Lampe, "Second Order Cone Programming for Sensor Network Localization with Anchor Position Uncertainty", in IEEE 8th Workshop on Positioning Navigation and Communication (WPNC), pp. 51 – 55, Dresden, Germany, April 2011.

I hereby acknowledge the contribution by Dr. Michael Botros Shenouda, who was a post-doctoral fellow in the Department of Electrical and Computer Engineering at UBC in 2011, and helped me to understand the concept of the second order cone programming and to formulate the sensor localization problem.

Publications Related to Chapter 4

- Ghasem Naddafzadeh Shirazi, Lutz Lampe, Gustav Vos, and Steve Bennett,"Coverage Enhancement Techniques for Machine-to-Machine Communications over LTE", submitted.

- Ghasem Naddafzadeh Shirazi, Lutz Lampe, Gustav Vos, and Steve Bennett, "Enhancement for LTE Communication Systems", United States Patent App.#14/046733, International App.#PCT/CA2013/050749, Sierra Wireless Inc. (Filed October 4, 2013).

Chapter 4 is based on our research conducted in collaboration with Sierra Wireless [1] as a 4-term MITACS-Accelerate[2] internship program (July 2012-November 2013) for "designing low-cost machine-to-machine (M2M) devices for long-term evolution (LTE) networks". I would like to thank and acknowledge the help of Gustav Vos and Steve Bennett from Sierra Wireless, who have provided continuous support and feedback in this project, in particular with regard to the problem formulation and relevance for ongoing standardization efforts in the third generation partnership project (3GPP).

We have acquired the necessary disclosure permissions from Sierra Wireless for what appears in Chapter 4 in accordance with the UBC Mitacs-Accelerate Internship terms and Non-Disclosure Agreements[3]. The intelectual property and results of this project are owned by Sierra Wireless, including but not limited to the filed US and international patents listed above

[1] Sierra Wireless (Head Office) is at 13811 Wireless Way, Richmond, British Columbia, Canada, V6V 3A4, Tel: 604.231.1100 – See more at: `http://www.sierrawireless.com/`

[2] `http://www.mitacs.ca/accelerate`

[3] `http://www.mitacs.ca/sites/default/files/UBC-MitacsTerms-FINAL_June28_2011.pdf`

and technical documents (Tdocs) that appear on the 3GPP website[4].

[4] `http://www.3gpp.org/`

Table of Contents

List of Tables

List of Figures

List of Abbreviations

3GPP	Third Generation Partnership Project
BLER	Block Error Rate
BLUE	Best Linear Unbiased Estimator
CAT0	LTE Category 0 User Equipment
CE	Coverage Enhancement
CP	Cyclic Prefix
CRLB	Cramer-Rao Lower Bound
D-UMLJE	Distributed UMLJE
DL	Downlink
DMRS	Demodulation Reference Symbols
DR	Detection Requirement
EM	Expectation Maximization
EPA	Extended Pedestrian Channel Model Type-A
FCC	Federal Communications Commission

GLRT	Generalized Log-Likelihood Ratio Test
GPS	Global Positioning System
GSM	Global System for Mobile Communications
H2H	Human to Human Communication
HSPA	High Speed Packet Access
IFFT	Inverse Fast Fourier Transform
IoT	Internet of Things
IR-UWB	Impulse Radio Ultra Wideband
KKT	Karush Kuhn Tucker Optimality Conditions
LCM	Least Common Multiplier
LoS	Line of Sight
LP	Linear Programming
LTE	Long Term Evolution
LTE-A	Long Term Evolution-Advanced
M2M	Machine to Machine Communication
MAC	Medium Access Control
MB-OFDM	Multi Band Orthogonal Frequency Division Multiplexing

MDS	Multi-Dimensuinal Scaling
MERG	Minimum Energy Routing with Guaranteed Detection Requirements
MLB	Maximization of the Lifetime Upper-Bound
MSE	Mean Square Error
MTC	Machine-Type Communication
MTCN	Machine-Type Communication Network
ns	Nono Seconds
OFDM	Orthogonal Frequency Division Multiplexing
PAPR	Peak To Average Power Ratio
PBCH	Physical Broadcast Channel
PDCCH	Physical Downlink Control Channel
PDSCH	Physical Downlink Shared Channel
PRACH	Physical Random Access Channel
PRB	Physical Resource Block
PSD	Power Spectral Density
PUCCH	Physical Uplink control channel
PUSCH	Physical Uplink Shared Channel

Q-BLUE	Quasi-Best Linear Unbiased Estimator
QoS	Quality of Service
RAN TSG	Radio Access Network Technical Specification Group
RB	Resource Block
rBLER	Residual Block Error Rate
RE	Resource Element
RSDP	Robust SDP
RSOCP	Robust SOCP
RV	Redundancy Version
SC-FDMA	Single Carrier Frequency Division Multiple Access
SDP	Semidefinite Programming
SNR	Signal to Noise Ratio
SOCP	Second Order Cone Programming
TBS	Transport block Size
TH	Time Hopping
ToA	Time of Arrival
TTI	Transmission Time Interval
UE	User Equipment

UL	Uplink
UMLJE	UWB Maximum Lifetime for Joint Event Detection
UMTS	Universal Mobile Telecommunications System
URFP	UWB Maximum Rate Feasibility Problem
USN	Ultra Wideband Sensor Network
UWB	Ultra Wideband
WSN	Wireless Sensor Network

Acknowledgements

First of all, I would like to express my deepest gratitude to Professor Lutz Lampe for his invaluable academic and personal support during my PhD studies. His has taught me numerous concepts in the field of wireless communications and his advise has always directed my research towards success.

I would also like to thank Dr. Anand Oka from Microsoft for his teachings and support during my internship at BlackBerry. I also appreciate the help of Dr. Michael Botros Shenouda for his teachings on the concept of convex optimization.

I am thankful to Mr. Gusav Vos and Mr. Steve Bennett from Sierra Wireless who have provided their valuable and frequent feedback on our project for low-cost machine-type communication design over LTE. I am also grateful to MITACS for funding this part of my research through the Accelerate internship program.

Last but not least, I am appreciative of all my great friends at UBC and ECE's Data Communication Lab., Dr. Ehsan Mohammadi Zahrani, Javad Hajipour, Hao Ma, and Narjes Torabi to name a few, and especially my wife, Mrs. Fariba Aalamifar, who is the biggest inspiration in my academic and personal life.

Dedication

In the name of God, the compassionate, the merciful.

To Fariba, my beloved wife; and to my dear parents.

Chapter 1

Introduction

Wireless sensor networks (WSNs) are systems used for detecting events and gathering information from an area of interest in many different application domains, from home and industry automation, to healthcare and transportation, to environmental monitoring for social safety and security. Wireless sensors operate on small batteries with limited energy and it is usually impossible to provide external sources of energy. A sensor network should be able to operate days, months, or even years without requiring human assistance for inserting new sensors or replacing their batteries.

Sensors are typically deployed in large amounts in random locations. A broad range of WSN applications, for example detection and tracking of events and targets, require accurate location information of sensors to perform well. Despite this fact, for preserving their low cost, it is unlikely that they are equipped with complex self-localization units such as global positioning system (GPS). Therefore, WSNs should employ localization algorithms for obtaining location estimates. This is usually accomplished by collecting the ranging information between nearby sensors. Once all the sensors in the network are localized, they can also find the most energy-efficient routes to transmit their information to the data center (also known as the

sink) so that they can last longer [1]. Hence, two preeminent optimization problems in WSNs are accurate localization from ranging information, and lifetime maximization based on adjusting the transmission power and routes.

Wireless ultra wideband (UWB) technology enables transmission of signals over a very large communication bandwidth. For example, according to the United States' Federal Communications Commission (FCC), UWB transmissions occur over a bandwidth larger than 500 MHz or 20% of the total available bandwidth [2]. UWB devices typically utilize the spectrum in the 3.1-10.6 GHz range in a license-exempt fashion, adhering to the spectral density (PSD) emission regulations and possible further restrictions on their transmission activities. Due to the stealth-like operation of UWB radios enabled by the use of a large transmission bandwidth, UWB has a lower transmission power, and equivalently a longer operation time of the battery for a given data rate, compared to a narrowband system [3]. UWB signals also have a high temporal resolution which makes it possible to measure time of flight and thus find an accurate distance estimate between the transmitter and the receiver.

The above-mentioned properties of UWB are well-aligned with the low-transmission-power and location-awareness requirements of WSNs. These relations are investigated in detail in the first two parts of this thesis. Specifically, we present a UWB sensor network (USN) model and optimize its lifetime in Chapter 2. We then provide an optimization framework for WSN localization, which is also applicable to USNs, in Chapter 3.

1.1 Machines Operating as Sensors

With the advent of Internet of Things (IoT), the traditional sensors networks are being evolved to smarter entities with a higher degree of autonomy and information processing. This fact has given rise to the concept of machine-type communication (MTC), also known as machine to machine (M2M) communication, which has gained popularity in the past few years. MTC can be considered a generalization of traditional sensor networks in terms of their higher processing capabilities and covering in a broader range of applications[4, 5].

Different features of WSN and machine-type communication networks (MTCNs) are compared in Table 1.1. As can be seen, similar to a wireless sensor node, an MTC device can be used for automation, healthcare, transportation, and environment monitoring applications. In addition, MTC devices can be embedded to smart utility meters, electric vehicles, vending machines, point of sales terminals, etc., to accomplish a task related to a "business application" [5]. Similar to the traditional wireless sensor nodes, MTC devices usually have a simple design (low cost), transmit with a low power to conserve energy, and are typically deployed in large densities in an area of interest. Both wireless sensor nodes and MTC devices can be static or mobile. Although most of the WSN and M2M applications, such as event detection and smart metering, fit into the class of static networks, mobility can occur in for example, target tracking applications, or in the case of MTC, in electronic vehicle monitoring (charging control and billing [5]). The same argument holds for low versus high data rate, that is, most of

Table 1.1: Comparison between wireless sensor networks (WSNs) and machine-type communication networks (MTCNs). A **boldface** font is used to identify the typical values for each feature.

Feature	WSN	MTCN
Desired design cost and complexity	**Low**	**Low**
Density	**High**	**High**
Energy consumption	**Low**	**Low**
Mobility	**Zero**-High	**Zero**-High
Data rate	**Low**-High	**Low**-High
Processing capability	**Low**	**Low-Medium**
Common applications	**Monitoring**, **Automation**, **Healthcare**, **Transportation**	**Monitoring**, **Automation**, **Healthcare**, **Transportation**, **Smart metering**, **Electronic Vehicles**
Selected wireless technology in this thesis	**UWB**	**LTE**
Infrastructure	***Ad hoc***	**Cellular**

the WSN and M2M applications require low data rates, in contrast to few high-data rate applications, e.g. video surveillance. MTC devices may also have extra processing capabilities compared to the traditional wireless sensor nodes which in turn helps them in local decision making and requiring lower data rates.

M2M applications have grown tremendously in the past few years. It is predicted that the number of M2M connections reaches a quarter of a billion in the year of 2014 [6, 7], and that the global M2M market value doubles every three years [8]. This is a big incentive that drives the cellular operators to accommodate MTC in their networks. Long-term evolution (LTE) and LTE-advanced (LTE-A) are the latest cellular communication standards developed by the third generation partnership project (3GPP). Many cellular network operators have been migrating from GSM/HSPA, UMTS, and other legacy standards to LTE.

There exist, however, some important challenges for providing MTC in LTE. As explained above, MTC devices (user equipment (UE) in the LTE terminology) should be able to work without a need for human interaction, e.g. for maintenance, for a long duration. Moreover, the high density of MTC UEs should not lead to a substantially increased network cost for LTE operators (and consequently M2M customers). Hence, MTC UEs need to be designed with a low cost. Moreover, since in many M2M applications MTC UEs are located inside buildings or structures with large penetration losses and also unable to move, it is essential to enhance the MTC coverage so that they can access the network.

This is the subject of the third optimization problem in this thesis.

Specifically, in Chapter 4 we compare the coverage of different LTE uplink and downlink channels and identify the coverage gain required for MTC UEs in each of these channel, as reported in the 3GPP technical documents. We then focus on the channel with the worst coverage and propose a new transmission scheme which can provide the required gain for low cost MTC UEs.

1.2 Optimization Aspects

The algorithms that are developed in Chapters 2 and 3 of this thesis, respectively for lifetime maximization and sensor localization, take into account the specific characteristics and requirements of WSNs and USNs. In these two chapters, we use the following criteria to design our "efficient" solutions.

- **Scalability**: When the density of sensors becomes very large in the network, even a powerful central controller may be unable to solve the optimization problem. Therefore, a distributed algorithm should be devised to let the nodes individually solve small-size optimization problems based on the local information in their neighborhood. The global parameters are propagated in the network by iteratively solving such small distributed algorithms until all the nodes converge to the final optimum solution.

- **Low Complexity**: Due to the essentially limited resources available in wireless sensor nodes, we need to derive solutions that are simple to implement. In general, the solution to an optimization problem may

require a high computational power, and hence unsuitable for implementation on simple sensors. On the other hand, the family of linear programming (LP) [9] and convex optimizations [10] can be usually solved, and implemented on sensors, with a tractable complexity.

- **Robustness**: Because of the limited reliability of sensors and their simple design, algorithms devised for WSNs should take into account the underlying uncertainty in the system. The so called *robust* algorithms typically put a constraint on the problem so that the network can provide the desired performance, even when some of the nodes in the networks suddenly fail, or provide inaccurate input information.

The concepts of low complexity, scalability, and robustness will be defined more formally in the context of each optimization metric in Chapters 2 and 3.

When we propose our transmission scheme for coverage enhancement of low-cost MTC UEs in Chapter 4, we also provide scalability by allowing concurrent transmission of multiple MTC UEs. The low complexity criteria in this context is enforced by the LTE regulations to design low-cost MTC UEs. In addition, we take into account another criteria, namely **co-existence**, that is set by the LTE standard for MTC UEs. In fact, 3GPP asserts that the proposed coverage enhancement solutions for MTC UEs should require a minimal change to the current LTE standards, so that the MTC UEs can operate with no hindrance to the legacy LTE UEs. We also observe this requirement for our proposed solution in Chapter 4.

1.3 Thesis Outline and Main Contributions

The rest of this chapter provides an overview of the communication systems that will be used in our optimization frameworks in the later chapters. In particular, Section 1.4 provides background information on UWB communication (used for USNs in Chapter 2), and on LTE cellular systems (used for MTC networks in Chapter 4). The literature review regarding WSNs and MTC networks in the context of lifetime, localization, and coverage optimization problems will then be provided in Section 1.5.

The contents and interdependencies of the next chapters of this thesis are illustrated in Figure 1.1. As this figure shows, Chapter 2 provides a USN model which is dedicated to detection and reporting of multiple events. The lifetime of such networks is analyzed in detail and formulated as a convex function of the sensing rate and data flow in each UWB sensor. Then, based on the dual decomposition technique, a scalable distributed lifetime maximization solution is derived. Our main contribution in Chapter 2 is providing efficient (centralized and distributed) algorithms for maximizing the network lifetime by jointly considering the UWB physical layer, sensing and routing parameters, and detection requirement constraints.

Chapter 3 delves into the WSN localization problem and provides a suite of convex optimization formulations for achieving robust and distributed localization. Our main achievement in this chapter is developing a robust localization framework with the capability of balancing between localization accuracy and computational complexity, a very important prerequisite for implementing a localization algorithm on low cost sensors. At the end of

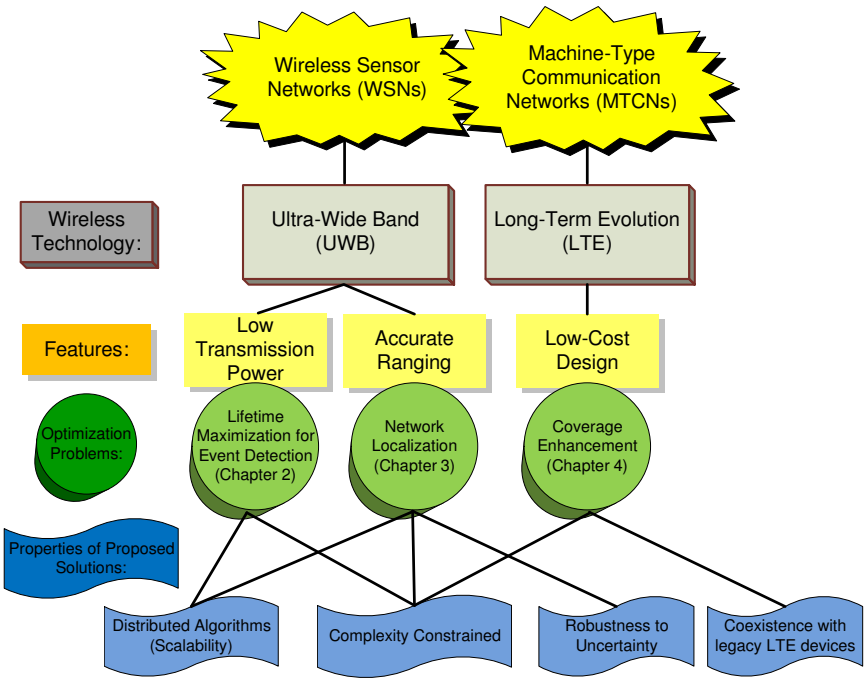

Figure 1.1: Thesis content and interdependencies between chapters. We focus on three main optimization problems related to WSN and MTC, two of which (lifetime and localization) are under the UWB sensor network framework, and the third one (coverage) relates to the LTE MTC. To model and solve each of these three optimization problems, scalability, low complexity, robustness, and coexistence criteria are taken into account.

this chapter, an extension to the mobile sensor networks is also presented.

Chapter 4 considers the coverage enhancement problem in MTC LTE networks and provides a transmission strategy which can significantly improve the coverage of the LTE uplink data channel, which is currently the LTE channel with the worst coverage. The novelty of the proposed coverage enhancement technique lies in its dynamically adjustable transmission size which is scalable to the number of active MTC UEs, and can be controlled

for the desired coverage gain. Moreover, it requires a minimal change in the current LTE standard. Finally, Chapter 5 presents the concluding remarks and avenues for future extension.

1.4 Background

This section provides an introduction to the basic mathematical models and transmission properties of ultra wideband (UWB) and long term evolution (LTE) wireless technologies. UWB and LTE are used in the next chapters as the underlying wireless technologies for the wireless sensor and machine type communication networks, respectively. More standardization details, comprehensive overviews and comparisons between UWB and LTE can be found in [11–13].

1.4.1 Ultra Wideband (UWB)

Large bandwidth required for UWB transmission can be realized using two distinct signalling methods, namely carrier-modulated and carrier-free signalling. Carrier-modulated UWB can be either based on the transmission with a single carrier over at least 500 MHz of bandwidth [14], or based on the multi-band orthogonal frequency division multiplexing (MB-OFDM) on the 14 bands defined in the 3.1-10.6 GHz spectrum [15]. High data rates (several hundred Mbps) can be achieved in both versions of carrier-modulated UWB over a short communication range (3-10 m).

On the other hand, impulse radio UWB (IR-UWB) transmits carrier-less "impulses" with a very short duration of a few nano seconds (ns)) [16].

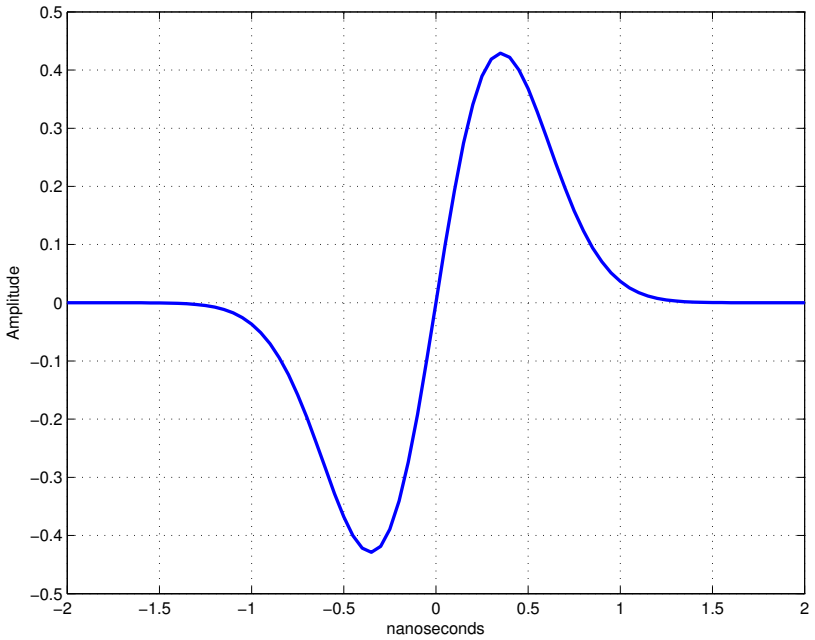

Figure 1.2: The first derivative of the Gaussian function known as the Gaussian Monocycle, can be used as an IR-UWB pulse. The pulse width parameter, t_w, in this example is 0.5 ns.

Figure 1.2 shows a possible shape of the impulse in time domain known as the Gaussian monocycle, which is basically the first derivative of the Gaussian function. Mathematically,

$$s_{\text{IR-UWB}}(t) = \frac{t}{t_w} \exp\left(-\left(\frac{t}{t_w}\right)^2\right), \tag{1.1}$$

where t_w is the pulse width parameter.

The short duration of pulse translates into the large signal bandwidth in IR-UWB. This enables low to moderately high data rates (e.g., several tens to a few hundreds of kbps) for low-power short-range transmission when

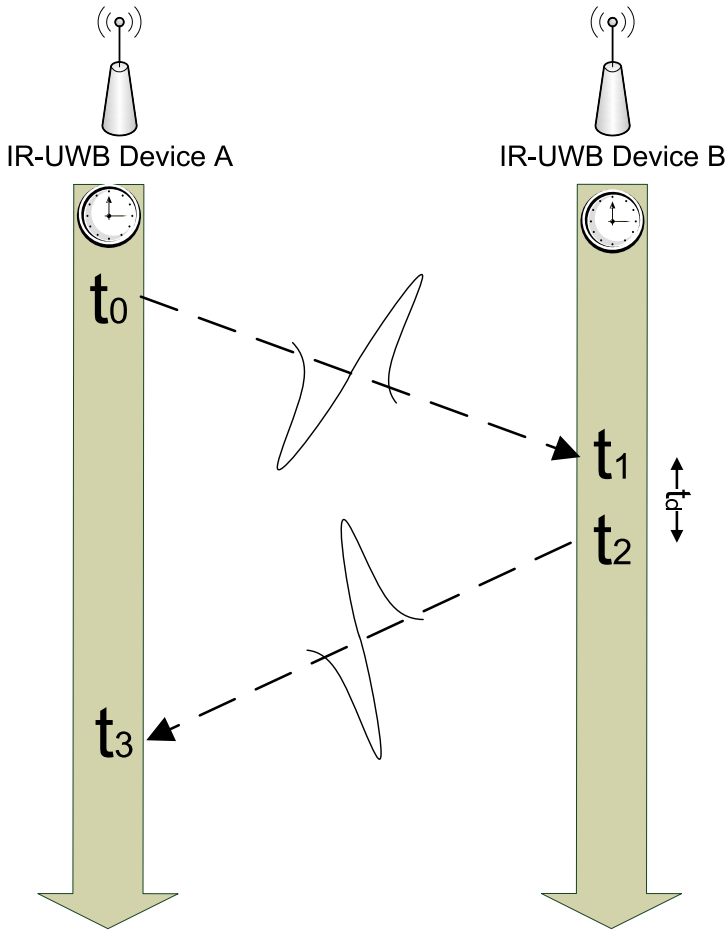

Figure 1.3: The concept of two-way ranging based on time of arrival (ToA) in IR-UWB. The pair-wise distance can be calculated by dividing the propagation time to the propagation speed.

combined with relatively simple receiver structures. But variants of IR-UWB can also be used for high data-rate. Moreover, the short pulse length leads a high temporal resolution, which mitigates the effect of fading and makes precise ranging possible. In particular, from the time of arrival (ToA) of the line-of-sight (LoS) signal path, the ranging information between the

nodes can be calculated, for example using the two-way ranging protocol [17, 18], as illustrated in Figure 1.3. As can be seen, the IR-UWB device A transmits an impulse to device B at time t_0, which is received and detected at time t_1. After a delay, t_d, which is known *a priori* to both sides, device B transmits an impulse to A which is detected at time t_3 at device A. Then, the A-B distance can be estimated as,

$$d_{AB} = \frac{t_3 - t_0 - t_d}{2c} \tag{1.2}$$

where c is the propagation speed. The two-way ranging mechanism enables IR-UWB nodes to obtain ranging information from their neighbours immediately after a round of hand-shaking. Besides the processing required at the receivers for signal detection and ToA estimating, the only side information needed for this calculation is the propagation speed of the UWB signal, c, which is equal to the speed of light and known. This makes IR-UWB an ideal technology for implementation of positioning systems [19, 20]. We focus on the impulse radio transmission mode for UWB in this thesis.

Since IR-UWB devices transmit with low power and low data rates over a wideband channel, it is not required to employ carrier sensing, power control, or other medium access control (MAC) protocols for such UWB systems [21]. Concurrent transmissions from multiple devices can be easily accommodated in the IR-UWB's MAC layer, for example by time hopping (TH). In TH, different nodes transmit their impulses at different time instances that are identified by their unique pseudo-random TH sequences. All of these properties make UWB radio an excellent choice for sensor networks,

where energy efficiency and operational simplicity is highly desirable. We can envision an application example, where nodes in an ultra wideband sensor network (USN) start their operation from a random placement, collect local ranging measurements from nearby nodes and perform self-localization with respect to other nodes in the network. Routes to send sensory data to the data collection center are then established such that the USN is able to continue its operation for a very long time.

1.4.2 Long-Term Evolution (LTE)

As a leading cellular technology, LTE offers a flexible communication architecture designed to provide communication at a lower cost per bit and to accommodate the continuous growth in wireless cellular demand, both in the number of connections and in the required data rate. Some of the key elements of LTE are the integration of applications into an all-IP architecture, spectral flexibility with signal bandwidths between 1.4 MHz and 20 MHz, and the use of orthogonal frequency division multiplexing (OFDM) for multiple access and high spectral efficiency [11].

1.4.2.1 LTE Structure

In LTE, OFDM and its precoded variant known as single carrier frequency division multiple access (SC-FDMA) are employed for the transmission of data. In OFDM, information bits are modulated on orthogonal subcarriers, as illustrated in the transmitter block diagram in Figure 1.4(a). An efficient implementation of OFDM is possible by taking the inverse fast Fourier transform (IFFT) of the input data, with the same size as the number of

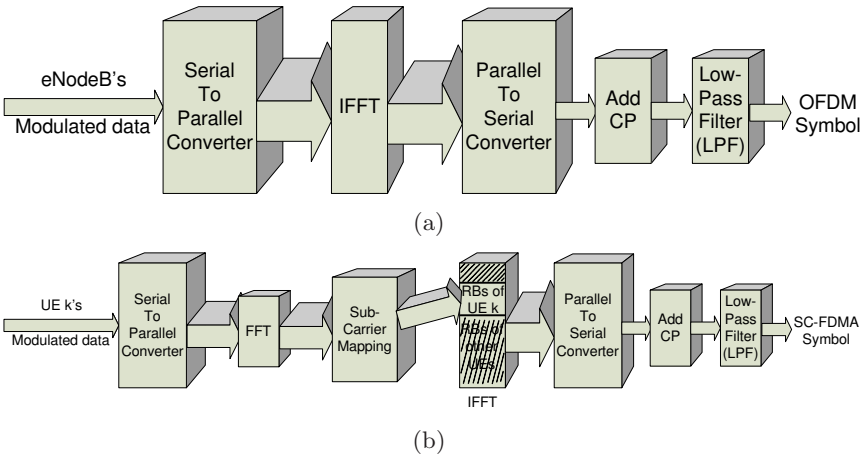

Figure 1.4: LTE transmission block diagrams, a) OFDM in downlink direction, b) SC-FDMA in uplink direction for UE k. eNodeB is the LTE term for a base station.

available subcarriers N_c, in order to map the symbols into their corresponding subcarriers [22, 23]. Mathematically,

$$s_{\text{OFDM}}(t) = \frac{1}{\sqrt{N_c}} \sum_{k=0}^{N_c-1} x_k \exp\left(j2\pi f_k t\right), \quad 0 \leq t < T_s \tag{1.3}$$

where x_k is the data, $T_s = 66.7\mu s$ is the OFDM symbol duration in LTE, and subcarriers with center frequencies f_k and uniform spacing of $f_{k-1} - f_k = \frac{1}{T_s} = 15$ kHz are used. Based on this, the atomic data unit in LTE, known as a resource element (RE), has a duration of $T_s = 66.7\mu s$ and a bandwidth of 15 kHz. A grid of 7×12 REs, in the time-frequency domain, is known as the LTE resource block (RB), which forms the basic unit commonly used in the LTE standard for scheduling and resource allocation of the devices. Considering the guard bands in frequency and cyclic prefix (CP) in time, an RB occupies 200 kHz over half a millisecond, which is also the duration of

Table 1.2: Number of RBs per time slot for different LTE system bandwidths

System Bandwidth (MHz)	1.4	2.5	5.0	10.0	15.0	20.0
Number of RBs per time slot	6	12	25	50	75	100

an LTE time slot. One LTE subframe, also known as the data transmission time interval (TTI), consists of two time slots (1 ms), and 10 consecutive subframes form a radio frame. Depending on the total bandwidth, the number of RBs in a time slot can be obtained from Table 1.2 [24].

SC-FDMA is used in uplink LTE transmission, as illustrated in Figure 1.4(b). SC-FDMA is implemented by performing a partial FFT prior to the actual OFDM mapping in the IFFT block, forming a "single-carrier" signal. The main advantage of a single-carrier transmission is the lower peak to average power ratio (PAPR) compared to the (multi-carrier) OFDM transmission. Low PAPR is a highly desirable property in uplink LTE, because it simplifies the design of power amplifiers and leads to the development of more cost-effective UEs [11]. In SC-FDMA, each UE maps its symbols on distinct subcarriers by using Fourier coefficients different from other UEs. The subcarriers which are assigned to a UE are usually selected consecutive to each other, which further reduces the cost of the FFT operation and sub-carrier mapping in SC-FDMA.

1.5 Literature Review

Before proceeding to the technical chapters, we present a synopsis of the existing literature on wireless sensor and machine-type communication net-

works in this section. The studies that are closely related to our work will be highlighted again in each individual chapter with more technical details.

We start by reviewing the studies on WSNs and USNs in Section 1.5.1. A detailed literature review on the lifetime maximization and location estimation problems is then provided in Sections 1.5.2, and 1.5.3, respectively. The works that consider LTE-based MTC and address its coverage enhancement problem are finally reviewed in Section 1.5.4.

1.5.1 Wireless Sensor Networks

Thanks to the advances in the design of low cost sensors, WSNs are now widely used in many applications including manufacturing automation [25, 26], smart home design for entertainment [27], healthcare [28], and safety [29]. There has been a considerable volume of research in the last decade on the optimization of different aspects of WSNs, for example lifetime maximization (cf. Section 1.5.2), accurate localization (cf. Section 1.5.3), congestion control, coverage enhancement, and quality of service (QoS)-aware scheduling [1, 30–35].

1.5.1.1 Ultra Wideband Sensor Networks

IR-UWB transmission was proposed by Scholtz and Win in 1998 [16]. In IR-UWB, low data rate communication in short range is possible with a very low transmission power. Furthermore, the use of TH [36] allows a very simple MAC without a need for power control or carrier sensing [21, 37–39]. Performing localization in USNs is also very effective due to the high resolution multipath components in the IR-UWB signal. Accordingly, the use of

IR-UWB as the physical layer of WSN devices has been promoted in several studies [19, 20, 40–46]. Zhang *et al.* [41] provide a comparison between the performance of narrowband WSNs and USNs, and conclude that UWB is a better choice for many sensor applications due to high interference resilience, low transceiver complexity, low transmission power, and localization accuracy. A practical USN architecture for outdoor applications is presented by Oppermann *et al.* in [40]. This model supports low data rate (around 10 kbps) transmission of a few thousands of UWB sensors through multi-hop communication. Based on this framework, a USN were deployed in a ski field for the localization and tracking purposes. Similarly, IR-UWB is used in [42] for developing a real-time target-tracking and accident-warning system for underground construction sites. Melodia and Akyildiz utilize TH-IR-UWB towards the design of a QoS-aware USN for multimedia applications [43].

1.5.2 Lifetime Maximization in Wireless Sensor Networks

Energy efficiency is probably the most important challenge in WSN design due to the limited capacity of sensor batteries [47, 48]. Sleep mechanisms can provide longer sensor lifetime [49], however, care must be taken not to make the network disconnected [50]. Several node placement and clustering methods have been proposed in the literature to account for coverage and adjusting the sleep duration [51–54].

The WSN lifetime maximization through flow control has been thoroughly investigated in the literature [55–60]. The lifetime can be defined as the time at which the first, or a specific percentage of sensors deplete their batteries [55–57] and/or the network becomes disconnected [61]. A

more application-oriented definition, however, is given in terms of the *network lifetime*, which is defined as the total time interval during which the network as a whole is able to accomplish the required objective [58–60] even if some sensors are already disconnected, or if a disconnected topology in a multi-sink architecture occurs [62–64].

Chang and Tassiulas [55] investigate the minimum energy routing through the lowest cost paths from sensors to the sink, where the cost is defined as the sum of energy consumed for transmission and reception of data packets. Wang *et al.* [56] provide a cross-layer convex optimization framework based on tuning the physical-layer, MAC and routing parameters in order to maximize the lifetime in different network topologies. They derive the Karush-Kuhn-Tucker (KKT) optimality conditions in the general case, and give closed-form solutions for the 3 and 4-node networks.

Direct formulation of lifetime maximization commonly leads to a centralized optimization problem [55, 60]. In order to convert the centralized optimization into smaller distributed sub-problems, dual decomposition techniques on the original convex problem can be employed. For example, Madan and Lall [65] decompose the standard lifetime maximization problem using the dual function and Lagrange multipliers on the energy and flow constraints. In the distributed methods, nodes are required to exchange the Lagrange multipliers and local flow and lifetime parameters with their neighbors and update them iteratively until converging to the near-optimal solution. Similarly, Xi and Yeh [57] investigate a node-based cross-layer optimization and derive the optimality conditions based on a general link cost function, and present a distributed power control and routing opti-

mization to account for scalability to the network size. This distributed algorithm can be solved in each node by an iterative algorithm based on gradient projection, with a guaranteed convergence to the optimal solution with a few control message exchange between neighboring sensor nodes. In order to make the dual function differentiable, regularization techniques are sometimes applied to the objectives. For example, [66] further changes the objective to optimize a weighted sum of lifetime and the routing cost.

Usually, the bottleneck nodes, i.e. sensors which are closer to the sink, should forward more data traffic than the other nodes, and are more likely to die first. To mitigate the effect of this problem, the use of multi-commodity flows in the network can help to balance the traffic over the sensor nodes [60, 65], and consequently achieve a longer lifetime. Furthermore, Blough and Santi [59] argue that a longer lifetime can be achieved by enforcing cooperation between nodes, for example by adjusting their sleep schedules or participating in data aggregation. In data aggregation, each sensor merges the received data from other sensors with its local measurements according to the correlation between them. This results in a longer network lifetime due to reduced volume of exchanged data packets [67, 68].

1.5.2.1 Energy Efficient Event Detection

A common class of WSN applications for data collection is event detection, for example in radar, sonar and ultrasound surveillance systems [69, 70], for disaster monitoring and emergency response [71], for example tsunami and earthquake alarm systems [72], farm protection [73], habitat monitoring [74], and for patient monitoring in health-care facilities [75, 76].

Energy efficient routing strategies in WSN specific to event detection have been investigated in [69] and [70]. Yang *et al.*[69] consider active radar-like sensors responsible for detecting the presence of an object, and use the Neyman-Pearson hypothesis test [77, 78] to design their decision variables. They use a Lagrangian relaxation technique to maximize a lower bound for lifetime. In another work, Li and AlRegib [70] derive an upper bound for lifetime as a function of the number of bits used at a node for representing its measurements. This enables nodes to tradeoff accuracy of the reported measurement with energy consumption for communication. Their approach is based on decoupling the problem of quantization from the routing problem. Specifically, each node first minimizes a local cost function to decide on the number of bits that it will generate for detecting an event. Then a linear program is solved to obtain the optimal routes and flows of the entire network. The decoupling significantly decreases the complexity of the problem. The algorithms proposed in [69] and [70] provide useful solutions for the energy efficiency problem under event detection requirements.

There are a number of related literature on USNs for event detection. For example, Bai *et al.* [79] propose and compare the performance of different distributed detection techniques in UWB sensor networks under energy constraints. However, only the UWB physical layer is considered in this study and routing layer optimization is left unhandled. Xu *et al.* [80] provide some upper bounds on the operational lifetime of a general UWB sensor network, and Shi and Hou [81] investigate the UWB maximum rate feasibility problem. They solve this non-linear problem using a linearization relaxation technique and devise a heuristic for connecting the source nodes to the sink.

None of these works consider the exact lifetime maximization of USNs for a given detection requirement.

In Chapter 2, we provide centralized and distributed lifetime maximization frameworks for an event-detection USN, and compare their performance to the algorithms proposed in [69, 70], and [81].

1.5.3 Sensor Network Localization

The availability of accurate information about the location of nodes is essential in many sensor network applications, for example target tracking and detection, cooperative sensing, and energy-efficient routing [82–85].

The localization problem and its properties, such as computational complexity and unique localizability have been investigated in recent studies, e.g. [86–89]. A common approach for sensor localization is to utilize the (noisy) ranging information between sensor nodes and anchor nodes, i.e. nodes with *a priori* known location, in order to estimate the sensor positions. This ranging information is obtained for nodes which are in the communication range of each other by measuring received signal strength [90, 91], angle of arrival [92], or ToA [93, 94]. In general, $D+1$ "anchor nodes", defined as the nodes with known positions, can triangulate a node in a D-dimensional space. Moreover, the availability of more anchors increases the localization accuracy at the cost of more computational complexity.

It is well-known that the sensor localization problem in its general form, due to the presence of measurement noise, is very difficult to solve. In fact, the exact solution of the localization problem with noisy measurements has a high computational complexity and belongs to the NP-hard class of al-

gorithms [95]. A number of approaches have been proposed to reduce the complexity of the localization problem in the general case. These methods can be categorized as non-parametric [96, 97] and parametric [98–104] class of algorithms. The non-parametric methods such as [96, 97] commonly perform localization based on correlating the received signals to a set of *signatures* which are collected from different location and distance configurations. On the other hand, the parametric approaches are based on an underlying assumption on the signal propagation and thus may suffer from the modeling mismatch, but they do not require offline data collection.

An example of the parametric approach is the multi-dimensional scaling approach (MDS-MAP) by Shang *et al.* [98], which constructs an approximate map of the network based on the shortest-path distance information between the nodes, and then applies MDS to the map in order to find the relative locations of the nodes. The weighted least square method can be also used for obtaining approximate closed-form location estimates [104], but this method relies on the availability of a good initial estimate.

Another common parametric approach to the localization problem is to relax the original problem to a convex formulation which can be efficiently solved using algorithms such as interior point methods [10]. The two main convex relaxation techniques that have been considered for the sensor localization problem are second order cone programming (SOCP) [105, 106], and semidefinite programming (SDP) [107–109]. Authors in [107] use SDP to determine and localize the subset of nodes which are uniquely localizable in the absence of noise. It is shown that if the network is uniquely localizable, SDP can verify and provide the exact solution in a polynomial time. How-

ever, both SDP and SOCP provide suboptimal solutions in the presence of noise.

Most sensor localization algorithms assume accurate anchor positions in order to estimate the location of the rest of the sensor nodes. However, in many scenarios anchor positions may not be accurately known. This uncertainty in turn significantly affects the quality of the estimated sensor positions. Robust sensor localization under anchor position uncertainty is studied in [110], where a convex relaxation based on SDP is developed. More specifically, a maximum likelihood criterion consisting of two parts is optimized. The first term reflects the likelihood of measurements, which is common in the robust and non-robust optimization. The second term is the likelihood of anchor positions, which forces the problem to find a reliable solution despite any errors in the initial measurement(s) of the anchor positions.

Another important issue for the localization problem is the scalability to larger networks. In fact, when the number of nodes in the network is large, the centralized formulations of MDS-MAP, SDP and SOCP include many optimization variables and constraints, and therefore, solving them entails a high computational complexity. A three-phase distributed refinement algorithm is proposed for the SOCP [105] and a distributed MDS approach is proposed in [111] which uses the local ranging information in the sensors to calculate their locations. A distributed version of SDP is also proposed in [109], which can localize large networks by solving SDP on small clusters of nodes. If the anchors are not distributed uniformly, this method requires intelligent clustering to accurately localize nodes that

are connected to only a few anchors (usually at the network boundaries). A different approach for reducing the complexity of SDP is known as the edge-based method [110, 112, 113], which further relaxes SDP by breaking a large constraint into smaller ones at the cost of reduced localization accuracy. Edge-based SDP methods can be also solved in a distributed manner [114]. In this paper we provide a new distributed algorithm based on SOCP. Different from the distributed SDP algorithm proposed in [109], it does not require clustering. It is faster compared to the edge-based SDP methods [114], and also leads to a more accurate localization when compared to the existing distributed robust approaches [105].

Chapter 3 extends the works in [106, 107, 110], and provides more technical details on the properties and relations of robust localization based on SDP and SOCP techniques .

1.5.3.1 Localization in Mobile Sensor Networks

Mobile sensor networks consist of a group of mobile nodes (robots, unmanned vehicles, sensors, cellphones, etc.) which dynamically change their locations, sometimes by posing into a desired formation, to cooperatively accomplish different tasks such as sensing or event detection [115]. Therefore, localization and tracking are the two inherent challenges in the mobile sensor networks. Localization and tracking of nodes in mobile sensor networks can be accomplished with the help of sequential Monte Carlo methods, Bayesian or particle filtering [116–119]. In these tasks, one of the main challenges is the ambiguity of the initial sensor locations. A solution to this problem is to perform a *robust* localization prior to (as in [120]) or jointly with (as

in [118, 121]) the main tracking algorithm. Such approaches may suffer from the high complexity of localization algorithms in a large network, and thus convex relaxation techniques may be required for generating a simpler solution, yet with an acceptable accuracy.

Formation control, i.e. creating and maintaining a desired shape is an essential part of many cooperative robot systems [122, 123]. In [122], authors use a (non-robust) convex optimization to minimize the total node traveled distances for forming a desired topology with or without vehicle motion constraints. Their convex relaxation is based on second order cone programming (SOCP), which is known to have a low complexity (e.g. compared to semidefinite convex relaxation) and be scalable to the large network size. Due to this property, it is shown in [122] that the SOCP optimization is able to control the robot movements to the optimal direction in real-time and with an acceptable accuracy, if the exact initial locations of the nodes are known. In practice, however, the initial location uncertainty of the mobile robots necessitates design of a robust SOCP algorithm for this task, as will be explained in Section 3.5.

1.5.4 Machine-Type Communication over LTE

The inherent differences between the operation of M2M and human-to-human (H2H) wireless communication devices and systems, such as higher device density and smaller message lengths for M2M communication, calls for modifications and optimizations in the physical and higher layers of MTC [124]. Reference [125] investigates the benefits of optimizing the MTC network for mobility. Environment-aware design of M2M networks for green

communication [126] and secure communication [127] have also been considered in the literature.

In recent years, the idea of using cellular technologies for providing reliable MTC-based services to customers has attracted the attention of many network operators around the globe. Among different cellular technologies, long-term evolution (LTE) leads the way towards regulating MTCNs due to its promising role in the future of cellular communication [5, 11]. To this end, 3GPP thrives to develop an optimized MTC-enabled LTE architectures in the near future [7].

MTC devices may belong to different access classes of the LTE cell based on their features, such as low mobility, small data transmission, secure connection, and location-specific trigger [128]. Moreover, the high density of MTC devices makes it difficult for the LTE base station (known as the eNodeB) to perform access management. In this regard, several device clustering algorithms have been proposed in the literature [129, 130]. In [130, 131], simple and cooperative access management schemes for high-density M2M networks with QoS guarantees have been proposed. Under their model, MTC devices work in clusters and the eNodeB assigns resources to the clusters based on their arrival rate, and deterministic or statistical packet jitter requirements. Also, a non-cooperative game theory framework for distributed rate and admission control in the context of multimedia sharing has been proposed in [132].

In [133], it is argued that the current QoS classes for H2H communication, which are typically delay requirements, are not suitable for the MTC devices, because of the different nature of their application. They propose

and analyze new QoS categories for M2M devices based on accuracy, priority, and real-time requirements. In order to enhance the functionality of densely-deployed M2M devices in the LTE uplink random access channel, different intelligent random access algorithms can be employed [134–136]. It is also essential to ensure the active MTC devices, which have data to transmit, can be covered over the entire cell area. The next section gives an overview of coverage enhancement literature in LTE-based MTC networks.

1.5.4.1 Coverage Enhancement for MTC over LTE

In June 2013, a new coverage enhancement (CE) study item, for LTE in general, has been approved in the 3GPP radio access network technical specification group (RAN TSG) [137]. This study aims at identifying the (uplink and downlink) LTE channels which have a worse coverage, and to find solutions for improving their coverage. By balancing the level of coverage among different LTE channels, the UEs can have a more reliable communication at the cell edge.

A need for CE is intensified in MTCNs, since different from H2H cellular communication, MTC UEs are often immobile and located inside buildings which suffer from high penetration loss. The 3GPP work item [138], which has also been initiated in June 2013, considers the CE specifically for MTC. The methods that are currently being reviewed in this work item include the simplifications of the structure of control messages, repetition of data, PSD boosting, and a relaxed false-alarm mode for the contention-based access of MTC UEs [139]. In addition, as an alternative to the default centralized mode of operation, some studies propose that when MTC UEs are in low cov-

erage in an LTE cell, they can form a mesh so that the packets from farther nodes can be relayed to the eNodeB with the help of closer nodes [140–142]. We propose a novel CE method based on the data repetition technique in Chapter 4.

Chapter 2

Lifetime Maximization for UWB Sensor Networks

In the first technical chapter of our thesis, we address the energy efficiency aspect of WSNs, which is one the most important challenge in designing a WSN. In this chapter we consider a specific, yet commonly-used, class of UWB sensor networks, namely USNs used for event detection. For accomplishing an event detection task, UWB sensor nodes should observe the status of one or more events at known locations and report their observations (measurements) to a fusion center (sink) through multihop routing. At the sink, a decision about the event status is made using the received measurement results from reporting sensors.

We aim at optimizing the routing of measurement data from nodes to the sink such as to maximize the operational lifetime of the WSN. Here, the operational lifetime is defined as the time from the beginning of operation of the WSN until the WSN is unable to perform its task, i.e., until given detection requirements (DRs) cannot be met any more. Our method jointly optimizes routes to detect multiple events, which avoids the overuse of individual sensor nodes in multiple paths known to decrease operational lifetime.

Furthermore, nodes send their measurements with different precisions to the sink. For example, a node with a larger/smaller amount of remaining energy represents its measurement with larger/smaller number of bits. By considering this degree of freedom in our model, nodes can easily trade off accuracy with energy consumption, leading to an overall increase in network lifetime. The optimization problem is formulated as a convex program, and numerical results for selected network examples show that the lifetime achieved with this program are considerably increased compared to those obtained with different routing schemes proposed in the literature, such as the minimum energy routing with guaranteed detection requirements (MERG) [69], the maximization of the lifetime upper-bound (MLB) [70], and the UWB maximum rate feasibility problem (URFP) [81].

We show that our model improves these works by considering a more general framework as well as providing more effective techniques for maximizing the lifetime. Specifically, we consider and maximize *exact* network lifetime subject to DRs, compared to the optimization of lower and upper bounds on lifetime in [69] and [70]. We also improve upon [69] by considering variable generation rates and balancing them based on the sensor's location and available energy. In addition, we overcome the well-known *bottleneck node* problem, i.e., fast depletion of a node with a higher amount of flow compared to other nodes, by jointly optimizing the routes for all event locations, such that the flows can be balanced among different paths to prolong lifetime. A distributed method is also proposed as a solution that shares the computational load for optimization among sensors and only requires local communication. This distributed method extends the dual decomposition

method [65, 66] by taking into account the DRs.

This chapter is organized as follows. The event detection system model and assumptions made are described in detail in Section 2.1. The optimization framework for UWB-based sensor network lifetime maximization is presented in Section 2.2, and its distributed version is explained in Section 2.3. The performance of the proposed method is then evaluated and compared by means of simulations in Section 2.4.

2.1 Event Detection System Model

We consider a multiple-event detection UWB-based sensor network, as illustrated in Figure 2.1. In this network, N sensors s_i, $i = 1, \ldots, N$, should sense the K events e_k, $k = 1, \ldots, K$, and report their measurements to the sink o. The sensors s_i are placed at locations (x_i, y_i), and events e_k are expected to occur at locations (x'_k, y'_k). Throughout this chapter, we assume that sensors know their locations, for example by employing the localization methods that will be explained in Chapter 3. Let d_{ij} denote the Euclidean distance between s_i and s_j. Each node s_i can transmit to or receive from the nodes in its communication range D, i.e., its neighbours $\mathcal{N}_i = \{s_j : d_{ij} \leq D\}$. Details about the sensing model are provided in Section 2.1.1. After sensing the events, the measured data is routed to the sink via multipath routing as explained in Section 2.1.3. Energy consumption at the nodes for data transmission and data flow in the links are determined by the UWB-specific transmission and link capacity models, as will be described in Section 2.1.2.

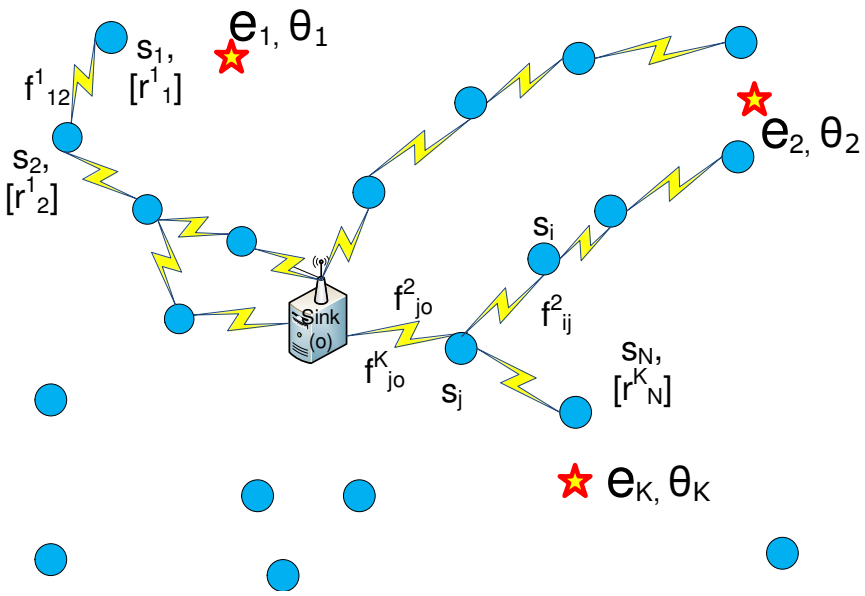

Figure 2.1: Illustration of the UWB-based sensor network for event detection. N UWB-enabled nodes (circles, s_i, $i = 1, \ldots, N$) are located around a sink (square, o). They measure data from K events (stars, e_k, $k = 1, \ldots, K$ with parameters θ_k), quantize the measurements into b_i^k bits, and report it to the sink, where f_{ij}^k denotes the data flow from s_i to s_j for reporting the event e_k.

2.1.1 Sensing Model

Consider the task of sensing in the network for gathering information about a possible event at a given location. Figure 2.2 illustrates the sensing model for an event e_k in such a network. The presence of the event e_k is indicated by the parameter θ_k, which is observed by the sensors. Let H_1^k and H_0^k, $k = 1, \cdots, K$, indicate the presence and absence of e_k, respectively. Under

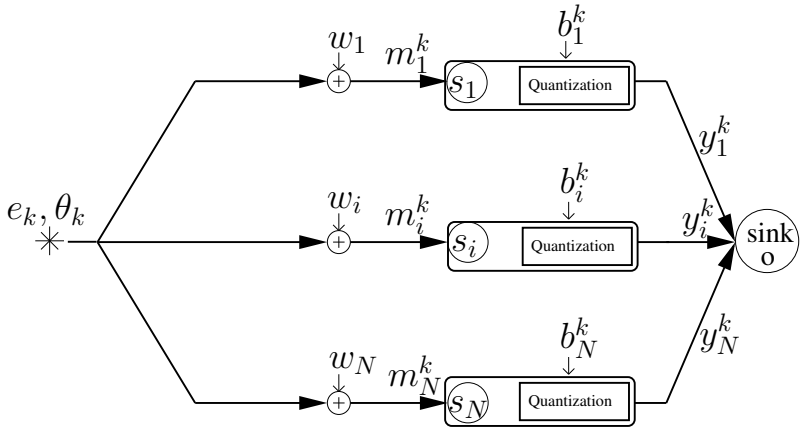

Figure 2.2: Sensing model under presence of e_k.

this model, the measured signal at sensor s_i is given by

$$m_i^k = \begin{cases} w_i, & H_0^k, \\ \theta_k + w_i, & H_1^k, \end{cases} \tag{2.1}$$

where w_i is Gaussian measurement noise with variance σ_i^2. We assume that the events occur at locations which are far from each other relative to the communication range D. Therefore, in (2.1) it is implied that each sensor observes at most one event (cf. also [75, 143]). Furthermore, note that known attenuation of observations can be easily handled by the sensing model in (2.1). Specifically, denoting the attenuation between s_i and e_k by a_i^k, the model

$$m_i'^k = a_i^k \theta_k + w_i' \tag{2.2}$$

with noise variance $\sigma_i'^2$ reduces to (2.1) by letting $m_i^k = m_i'^k/a_i^k$ and $\sigma_i^2 = \sigma_i'^2/(a_i^k)^2$ [70, 144]. We would also like to point out that (2.1) includes the active sensing framework of [69] as a special case, where sensors should send signals to the location of e_k with the sensing energy E_s and measure the reflected signal. In fact, (2.2) can be specified to the active sensing model by applying the deterministic value $\theta_k = \sqrt{E_s}$ and setting $a_i^k = \sqrt{\beta_{ik}}$, where β_{ik} is the path loss coefficient between e_k and s_i. Note, however, that in the general model (2.1) the value of θ_k is unknown, and the sensors are required to estimate it when e_k is present (H_1^k).

We further assume that the measurement m_i^k is quantized into $b_i^k \in \{1, 2, \ldots, b_{\max}\}$ bits, i.e., s_i sends only b_i^k bits for the measurement m_i^k to the sink. The quantization interval, $\mathcal{M}_R = [-M, M]$, with a fixed known $M > 0$ which is determined based on the effective signal range that sensors can observe [70, 145]. In order to provide an unbiased estimate for θ_k, we use the probabilistic quantization scheme from [145], where $\mathcal{M}_R$ is divided into $2^{b_i^k}$ equal intervals of length $\Delta_i^k = \frac{2M}{2^{b_i^k}}$, and the measurement $n\Delta_i^k \leq m_i^k \leq (n+1)\Delta_i^k$ is mapped to its quantization $y_i^k \doteq \mathcal{Q}(m_i^k)$ using the probabilities

$$\begin{aligned} P(y_i^k = n\Delta_i^k) &= 1 - \frac{m_i^k - n\Delta_i^k}{\Delta_i^k} \\ P\left(y_i^k = (n+1)\Delta_i^k\right) &= 1 - P(y_i^k = n\Delta_i^k)\ . \end{aligned} \tag{2.3}$$

The quantization error variance for this method is given by

$$\varrho_i^k(b_i^k) = \frac{M^2}{(2^{b_i^k} - 1)^2}\ . \tag{2.4}$$

A larger value of b_i^k leads a smaller quantization error variance $\varrho_i^k(b_i^k)$ and thus provides a higher accuracy of detection, but at the cost of consuming more energy and bandwidth for transmitting more data bits to the sink. For brevity of notation, we define

$$\pi_i^k \doteq \sigma_i^2 + \varrho_i^k(b_i^k) \tag{2.5}$$

as effective measurement variance and omit the explicit dependence of π_i^k on b_i^k.

We assume that each sensor performs sensing at regular intervals of length T_s. Accordingly, we define the *generation rate* of node s_i for event e_k as

$$r_i^k \doteq b_i^k / T_s \ . \tag{2.6}$$

Clearly, a node can tradeoff between accuracy and energy consumption by varying its generation rate.

As it is shown in [70, 145], the quantized measurements of y_i^k, $i = 1, \ldots, N$, generated by mapping (2.3) enable an unbiased estimation of θ_k under hypothesis H_1^k. The corresponding quasi-best linear unbiased estimator (Q-BLUE) of θ_k is specified as

$$\overline{\theta}_k = \left(\sum_{i=1}^{N} \frac{1}{\sigma_i^2 + \varrho_i^k(b_i^k)} \right)^{-1} \sum_{i=1}^{N} \frac{y_i^k}{\sigma_i^2 + \varrho_i^k(b_i^k)} \ . \tag{2.7}$$

This is essentially the same as the BLUE estimator given un-quantized data, except that the quantization variance $\varrho_i^k(b_i^k)$ is added to the noise variance σ_i^2.

We assume that the sensing interval T_s is chosen such that the value of θ_k is changing much slower than the sensing rate. Under this assumption, the filtered estimate

$$\hat{\theta}_k(\ell) = \delta\,\hat{\theta}_k(\ell-1) + (1-\delta)\,\overline{\theta}_k, \tag{2.8}$$

is used for determining the likelihood of hypothesis H_1^k in the current sensing interval ℓ, where $\hat{\theta}_k(\ell-1)$ is the estimate from the previous interval $\ell-1$ and $\delta < 1$ is a forgetting factor to account for dynamics of θ_k. For brevity, we omit the interval index ℓ in the following and denote the updated estimate by $\hat{\theta}_k$.

Given the described estimation procedure, deciding between H_0^k and H_1^k is performed using the generalized log-likelihood ratio test (GLRT) [78, 146]

$$L^k \underset{H_0^k}{\overset{H_1^k}{\gtrless}} T_0^k\ , \tag{2.9}$$

where L_k is given by

$$L^k = \log \frac{\Pr(H_1^k | y_1^k, \cdots, y_N^k, \hat{\theta}_k)}{\Pr(H_0^k | y_1^k, \cdots, y_N^k)}\ . \tag{2.10}$$

Here, the threshold T_0^k is determined by the DRs. More details about the detection procedure will be provided in Section 2.2.

2.1.2 Transmission Model

Transmission of quantized measurements is performed using a TH-IR-UWB physical layer. As stated earlier, TH-IR-UWB requires a very low transmis-

sion power. In addition, it is fairly robust to interference when time hopping codes are used for the transmission of UWB pulses. Based on these properties, it is shown in [39] that power control is not required and each UWB node should transmit with the maximum permissible power. Motivated by this result, we assume that all sensors transmit with a fixed transmission power P_{tx}. Furthermore, we make use of the low spectral efficiency property of TH-IR-UWB and approximate the link capacity as a linear function of SINR [147]. That is, we express the maximum achievable rate C_{ij} for transmission from s_i to s_j as

$$C_{ij} = \frac{W}{\ln 2}\ \mu_{ij}\ , \tag{2.11}$$

where W is the bandwidth and μ_{ij} denotes the SINR for this link. The latter is given by

$$\mu_{ij} = \frac{P_{tx}\ \alpha_{ij}}{\sigma_j^2 + \chi \sum_{l \in \mathcal{N}_j \setminus \{i\}} I_l^{tx} P_{tx}\ \alpha_{lj}}, \tag{2.12}$$

where I_l^{tx} determines if node l is a potential interferer, i.e., $I_l^{tx} = 1$ if s_l is transmitting, and $I_l^{tx} = 0$ otherwise. The parameter χ is a constant depending on the autocorrelation of the UWB pulse, and α_{ij} denotes the path gain between nodes s_i and s_j. For the latter, we adopt the double-slope UWB channel model developed during IEEE 802.15.4a standardization

[18, 148], according to which

$$\alpha_{ij}(d_{ij}) = \begin{cases} g - 10\gamma_1 \log_{10}(d_{ij}) & d_{ij} \leq d_0, \\ & \text{(in dB)}\ , \\ c_0 - 10\gamma_2 \log_{10}(\frac{d_{ij}}{d_0}) & d_{ij} > d_0, \end{cases} \tag{2.13}$$

where g is the gain for the unit distance, c_0 is the gain for the reference distance d_0, and γ_1, γ_2 are the path-loss exponents. The SINR term in (2.12) along with the path gain model (2.13) are used in this paper for computing the link capacities. We note, however, that other channel models could be used in our optimization framework.

The indicator terms I_l^{tx} in (2.12) are determined by the scheduling of transmissions in the network. The joint scheduling and routing problem in UWB has been investigated in [39, 81, 147]. In these studies, it is shown that finding the optimal scheduling policy to achieve a given objective, such as minimum power consumption or maximum throughput, is in general NP-hard to solve, and different techniques for finding an approximate solution are suggested. The simpler interference-free scheduling, in which separate subbands or time slots are assigned to links that would otherwise cause interference to each other, is often assumed when lifetime maximization is done at the routing layer [65, 69, 70]. In this case, the second term in the denominator of SINR (2.12) would vanish and a larger capacity would be obtained, at the cost of synchronizing the nodes and providing orthogonal resources (time, frequency, etc.). Since the UWB PHY provides robustness

to interference (see (2.12)), carefully designed interference-free scheduling is not required. However, since including the exact effect of the scheduling policy significantly increases the complexity of optimizing the routing layer [39, 81, 147], in this work we resort to consider two extreme cases. The first is the capacity lower bound C_{ij}^{L} assuming maximum interference according to $I_l^{tx} = 1$, $\forall l \in \mathcal{N}_j$, and the second is the capacity upper bound C_{ij}^{U} assuming $I_l^{tx} = 0$, $\forall l \in \mathcal{N}_j$ in (2.12). This simplification allows us (i) to provide a simplified model for lifetime optimization in USNs, (ii) to fairly compare the proposed framework to the existing literature which implicitly uses the scheduling with no interference (i.e., C_{ij}^{U}) [69, 70], and (iii) to adapt the distributed routing framework [65] to the problem at hand.

Finally, we consider dynamic channel coding [37, 41, 43]. This technique adaptively adjusts the channel code rate according to the level of interference. This allows us to express the energy consumed for the transmission of one bit from s_i to s_j as

$$E_{tx} = \frac{P_{tx}}{C_{ij}} \, . \tag{2.14}$$

2.1.3 Routing

Let f_{ij}^k be the data flow from s_i to s_j for event e_k. Then, the flow conservation constraints are given by

$$r_i^k + \sum_{j \in \mathcal{N}_i} f_{ji}^k - \sum_{j \in \mathcal{N}_i} f_{ij}^k = 0, \quad \forall i, k. \tag{2.15}$$

Since all the flow is absorbed by the sink, the flow conservation is valid for the sink node by defining

$$r_o^k = -\sum_{i=1}^{N} r_i^k, \tag{2.16}$$

and noting that $f_{oi}^k = 0$, $\forall i, k$.

It is worth mentioning that the fraction of time taken for the transmission of each flow is f_{ji}^k / C_{ij}. Thus, a feasible scheduling can be obtained for the high interference case if

$$\sum_i \sum_j \sum_k \frac{f_{ij}^k}{C_{ij}^{\mathrm{L}}} \leq T_s \ . \tag{2.17}$$

This is also a sufficient condition for the existence of a feasible schedule in the interference-free with the capacity upper bound C_{ij}^{U}.

2.1.4 The Optimization Procedure

Based on the sensing, transmission, scheduling, and routing models explained above, a centralized and a distributed optimization of sensor rates r_i^k and flows f_{ij}^k are devised in the next two sections. Figure 2.3 shows a flowchart of the proposed centralized and distributed algorithms. As can be seen, in both methods the sink performs the GLRT to decide for H_0^k or H_1^k, and updates the estimate for θ_k if the event e_k is deemed present. In the centralized scheme, the sink also optimizes all routing variables and generation rates. Since the optimization of these parameters depends on the estimate $\hat{\theta}_k$ of θ_k, as will be explained in Section 2.2, the sink needs to repeat the optimization whenever the current estimate is notably different

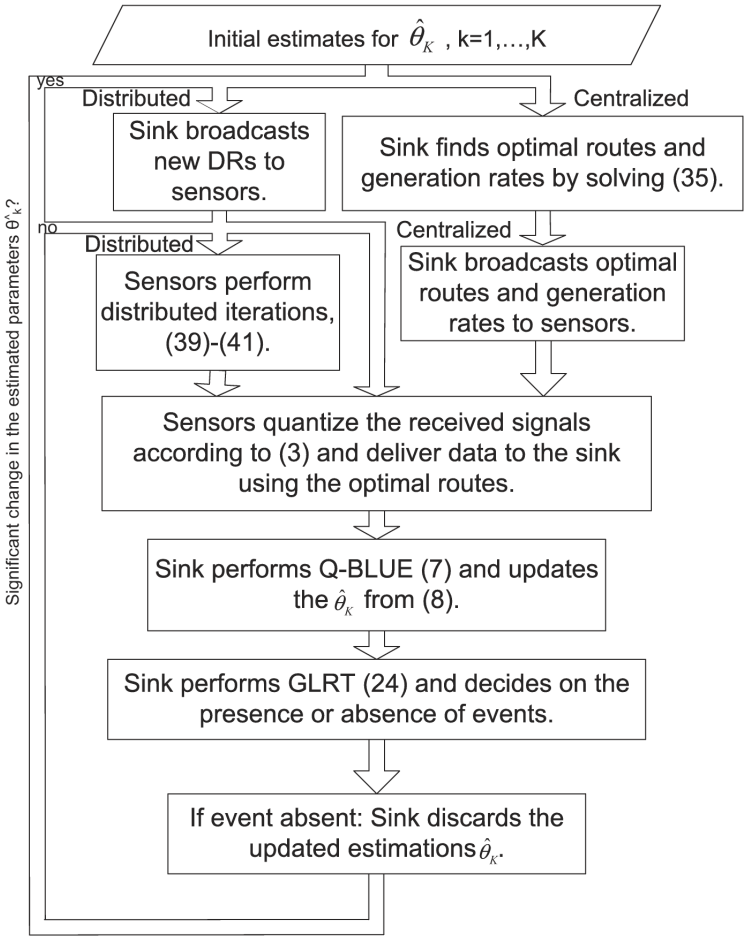

Figure 2.3: Flowchart of the proposed centralized and distributed lifetime maximization algorithms.

from the estimate used previously for optimization. Since we assume that θ_k is changing slowly compared to T_s, the optimization by the sink is performed infrequently. Furthermore, since no *a priori* model for the dynamics of θ_k is assumed to be known, the optimization by the sink needs to be performed in a myopic fashion. The routing and generation rate optimizations in the distributed scheme are performed locally in each sensor, and the optimized local variables only need to be exchanged among the neighboring nodes. However, the sink needs to broadcast the estimates $\hat{\theta}_k$ in the network when notable changes of these estimates occur.

In the next section, we present the centralized UWB maximum lifetime for joint event-detection (UMLJE) algorithm. Its distributed version, referred to as D-UMLJE, is developed in Section 2.3.

2.2 UWB Maximum Lifetime for Joint Event Detection (UMLJE)

In UMLJE, the sink determines the generation rates and routing flows such that network lifetime is maximized and the DRs are satisfied. In this section, we first make the implementation of the GRLT from (2.10) explicit. Then we formalize the DRs as functions of generation rates and map them to equivalent convex constraints. Using these constraints, we devise a convex program for the lifetime maximization problem. For the derivation of the GLRT and DRs we closely follow [69], but we note that [69] did not consider quantization of measurements at sensor nodes.

2.2.1 Closed-Form Expression for the GLRT

In order to obtain a closed-form expression for the GLRT, we approximate y_i^k as a Gaussian distributed random variable with variance π_i^k and mean 0, if H_0^k, and mean $\hat{\theta}_k$, if H_1^k, where $\hat{\theta}_k$ is the current estimation for θ_k given by (2.8). Then, according to the sensing model from Section 2.1.1, the generalized likelihood ratio L^k in (2.10) can be approximated as

$$L^k = \sum_{i=1}^{N} \frac{1}{2\pi_i^k} \left(2\hat{\theta}_k y_i^k - \hat{\theta}_k^2 \right). \tag{2.18}$$

Therefore, the hypothesis test (2.9) follows as

$$\sum_{i=1}^{N} \frac{\hat{\theta}_k y_i^k}{\pi_i^k} \underset{H_0^k}{\overset{H_1^k}{\gtrless}} T_0^k + \sum_{i=1}^{N} \frac{\hat{\theta}_k^2}{2\pi_i^k}. \tag{2.19}$$

It is convenient to make the following definitions:

$$\psi_i^k \doteq \frac{\hat{\theta}_k^2}{\pi_i^k} \tag{2.20}$$

$$\psi^k \doteq \sum_i \psi_i^k \tag{2.21}$$

$$h^k \doteq \sum_{i=1}^{N} \frac{\hat{\theta}_k y_i^k}{\pi_i^k} \tag{2.22}$$

$$T_1^k \doteq \left(T_0^k + \frac{1}{2} \sum_{i=1}^{N} \psi_i^k \right). \tag{2.23}$$

Then, the GLRT (2.19) can be expressed in the compact form

$$h^k \underset{H_0^k}{\overset{H_1^k}{\gtrless}} T_1^k. \tag{2.24}$$

2.2.2 Detection Requirements

The DRs for event-detection applications are given in terms of the probability of detection

$$p_d^k \doteq \Pr(L^k > T_0^k | H_1^k), \tag{2.25}$$

if event e_k is present (hypothesis H_1^k) and the probability of false alarm

$$p_f^k \doteq \Pr(L^k > T_0^k | H_0^k), \tag{2.26}$$

if e_k is absent (hypothesis H_0^k). Specifically, we focus on the Neyman-Pearson detection model [69, 77], where $p_f^k = \nu^k$ and $p_d^k \geq \eta^k$ should be satisfied for some thresholds ν^k and η^k. That is, the threshold T_0^k in (2.9) is obtained by solving $p_f^k = \nu^k$ [78]. In the following, we elaborate on this relationship, which also relates the DR parameters ν^k and η^k to the sensor generation rates r_i^k.

The random variable h^k defined in (2.22) has the variance ψ^k, and zero mean, if H_0^k, and mean $\frac{\hat{\theta}_k \theta_k}{\pi_i^k}$, if H_1^k. Since $\hat{\theta}_k$ approximates θ_k, we assume that $E(h^k | H_1^k) \simeq \psi^k$. Denoting by φ the cumulative distribution function (cdf) of the "standard" h^k, i.e., when its mean and variance are adjusted to 0 and 1, respectively, and using (2.24) in (2.26), the false alarm probability can be expressed as

$$p_f^k = 1 - \varphi\left(\frac{T_1^k - 0}{\sqrt{\psi^k}}\right) . \tag{2.27}$$

Since φ is not a one-to-one function due to the quantization step, we first need to define its inverse in an unambiguous manner. Let for values of $\{x_0 < x_1 < \cdots < x_{n+1}\}$, $\{p_0 = 0 < p_1 < \cdots < p_n = 1\}$ be the set of values

that $\varphi(x)$ can take, i.e., $x_i \leq x < x_{i+1} \Leftrightarrow \varphi(x) = p_i$. For $p_i \leq p < p_{i+1}$ we define two inverse functions, $\varphi_{\downarrow}^{-1}(p) \doteq x_i$ and $\varphi_{\uparrow}^{-1}(p) \doteq x_{i+1}$. Then, setting $p_f^k = \nu^k$ leads to the detection threshold

$$T_1^k = \sqrt{\psi^k}\varphi_{\uparrow}^{-1}\left(1-\nu^k\right) , \tag{2.28}$$

where the use of $\varphi_{\uparrow}$ causes the achieved false alarm probability not to be larger than the desired ν^k. Similarly, from the demanded detection accuracy $p_d^k \geq \eta^k$ it follows that

$$1 - \varphi\left(\frac{T_1^k - \psi^k}{\sqrt{\psi^k}}\right) \geq \eta^k . \tag{2.29}$$

This implies that in order to meet the DR constraints, the following condition should be satisfied:

$$\psi^k \geq \xi_k^2 \doteq \left(\varphi_{\uparrow}^{-1}(1-\nu^k) - \varphi_{\downarrow}^{-1}(1-\eta^k)\right)^2 , \tag{2.30}$$

where the use of $\varphi_{\downarrow}$ results in an achieved detection probability which is never smaller than η^k. The expression in (2.30), through (2.20), (2.21), (2.5), and (2.6), links the generation rates r_i^k to the DRs.

Finally, we show that for any given ξ_k^2, the expression in (2.30) can also be written as an equivalent constraint.

Proposition 2.1. *Define*

$$\rho^k \doteq \left(\sum_{i=1}^{N} \frac{1}{\pi_i^k}\right)^{-1} , \quad \zeta^k \doteq \frac{\hat{\theta}_k^2}{\xi_k^2}. \tag{2.31}$$

Then, the DR constraint in (2.30) *can be equivalently written as*

$$\rho^k \leq \zeta^k \ . \tag{2.32}$$

Proof. Introducing the definitions (2.20), (2.21), and (2.31) into the inequality (2.30), we obtain

$$\rho^k = \left(\sum_{i=1}^{N} \frac{1}{\pi_i^k} \right)^{-1} = \left(\sum_{i=1}^{N} \frac{\psi_i^k}{\hat{\theta}_k^2} \right)^{-1} = \frac{\hat{\theta}_k^2}{\psi_k} \leq \frac{\hat{\theta}_k^2}{\xi_k^2} = \zeta^k \ .$$

□

Proposition 2.1 states that the constraints (2.30) and (2.32) can be equivalently used to account for the DRs. Note that any value of ζ^k can be mapped to specific DRs at a given event signal-to-noise ratio (SNR),i.e., θ_k^2/σ_i^2. As the DRs become stricter, ζ^k becomes smaller and hence sensors need to generate more bits per measurement in order to reduce ρ^k and satisfy (2.32).

While constraints (2.30) and (2.32) can be used interchangeably, it turns out that unlike (2.30), the expression (2.32) leads to a convex formulation of the DRs in the generation rates [149]. This can be verified by computing the Hessian matrix of ρ^k with respect to variables r_i^k and noting that it is positive definite for $r_i^k \geq \kappa_0$, where $\kappa_0 > 0$ is a small threshold. It is also worth mentioning that ρ^k represents an upper bound on the mean square error (MSE) of the Q-BLUE estimation in (2.7) [70, 145].

2.2.3 Operational Lifetime

We are interested in finding the maximum time during which the network is able to detect given events with the required detection probabilities, which we define as the operational lifetime of the network.

Let t_i denote the operational lifetime of node s_i during which it is able to perform sensing and routing for the events before its energy E_i is depleted. We can express t_i as

$$t_i = \frac{E_i}{\sum_k \left(I_{ik}^s \frac{E_s}{T_s} + \sum_j f_{ji}^k E_{rx} + \sum_j f_{ij}^k (E_p + E_{tx}) \right)} , \tag{2.33}$$

where E_s, E_{rx}, and E_p is the energy consumed for sensing, receiving a bit, and processing a bit, respectively. In (2.33), $I_{ik}^s = 1$ only if s_i performs sensing for the event e_k, and the terms in the denominator correspond to the energy consumed for sensing, receiving, and transmitting data, respectively, in each sensing interval. The operational lifetime of the network T is then defined as the minimum lifetime among the nodes:

$$T \doteq \min_i t_i \, . \tag{2.34}$$

Defining the inverse of the lifetime, $q \doteq \frac{1}{T}$, lifetime maximization can be written as the following optimization problem:

$$\min_{q, r_i^k, f_{ij}^k} \quad q \qquad \text{subject to} \tag{2.35a}$$

$$r_i^k + \sum_j f_{ji}^k - \sum_j f_{ij}^k = 0 \ , \forall i, k \tag{2.35b}$$

$$\sum_k \left(I_{ik}^s \frac{E_s}{T_s} + \sum_j f_{ji}^k E_{rx} + \sum_j f_{ij}^k (E_p + E_{tx}) \right) \leq q E_i \ , \forall i \tag{2.35c}$$

$$\left(\sum_{i=1}^{N} \frac{1}{\sigma_i^2 + \frac{M^2}{(2^{r_i^k}-1)^2}} \right)^{-1} \leq \frac{\hat{\theta}_k^2}{\left(\varphi_\uparrow^{-1}(1-\nu^k) - \varphi_\downarrow^{-1}(1-\eta^k) \right)^2} \ , \forall k \tag{2.35d}$$

$$0 \leq r_i^k \leq \frac{b_{\max}}{T_s}, \forall i, k \tag{2.35e}$$

$$0 \leq q, \tag{2.35f}$$

$$0 \leq f_{ij}^k, \forall i, j, k. \tag{2.35g}$$

In (2.35), the constraint (2.35b) ensures flow conservation, and the constraint (2.35c) gives the local energy consumption in the nodes based on (2.33). Note that in each node, the total energy consumption for detecting, sensing, and reporting of all events is jointly considered. Since this constraint also considers the total flow for multiple events, the optimal solution will efficiently avoid the bottleneck situations which would occur if single event detection methods like [69, 70] were applied. Consequently, the optimal solution will balance the energy consumption for sensing and communicating among the UWB-enabled sensors to achieve the highest operational lifetime. In addition, the DR constraint (2.35d) ensures that the DRs in (2.30) are satisfied as well. Numerical evidence and quantitative results of these properties are provided in Section 2.4, specifically, in Figures 2.4, 2.6, and 2.8. Finally, the last three constraints give the range of variables. While (2.35d) is written in terms of optimization variables, for brevity, we will use the compact form (2.32) in the following.

Furthermore, note that in the optimization (2.35), we consider continu-

ous variables r_i^k. From the solution, we obtain b_i^k by rounding to the nearest integer. Consequently, all the constraints except (2.35d) are linear and simple to handle for optimization routines. These constraints are also typically considered in existing lifetime maximization frameworks such as [55, 65]. Moreover, the DR constraint (2.35d), which is unique to our problem, is also convex in the variables r_i^k. Hence, (2.35) is a convex optimization problem and can efficiently be solved by standard methods. Since the DR constraint (2.35d) depends on the value of $\hat{\theta}_k$, a new optimization should be performed by the sink if these parameters have notably changed over time.

2.3 Extension to Distributed Optimization (D-UMLJE)

In this section, we devise a distributed version of UMLJE, which we refer to as D-UMLJE. To this end, we apply a dual decomposition method similar to the one from [65] and [150], which decomposes problem (2.35) into local subproblems by means of Lagrangian relaxation. These problems are solved by exchanging Lagrange multipliers between nodes and updating the variables based on the subgradient method. This process is continued until the variables converge to their global optimal point, i.e., when the subgradient method is unable to improve the current values of the local variables.

2.3.1 Distributed UMLJE (D-UMLJE)

To explain this in more detail, we start with the regularized objective

$$J_{\text{reg}} = q^2 + \epsilon \sum_{i,j,k} (f_{ij}^k)^2 \ , \tag{2.36}$$

where ϵ is the regularization weight. Note that the all terms in the objective function are differentiable. The Lagrangian relaxation can then be used to obtain the following regularized decomposition of the original problem in (2.35):

$$\begin{aligned}
\min_{q, r_i^k, f_{ij}^k} \quad & q^2 + \epsilon \sum_{i,j,k} (f_{ij}^k)^2 + \sum_{k=1}^{K} \omega^k (\rho^k - \zeta^k) \\
& + \sum_{i,k} \lambda_i^k \left(-r_i^k - \sum_j f_{ji}^k + \sum_j f_{ij}^k \right) \\
& + \sum_i \tau_i \left(\sum_k \left(I_{ik}^s \frac{E_s}{T_s} + \sum_j f_{ji}^k E_{rx} \sum_j f_{ij}^k (E_p + E_{tx}) \right) - q E_i \right)
\end{aligned} \tag{2.37a}$$

$$\text{subject to} \quad 0 \le r_i^k \le \frac{b_{\max}}{T_s}, \quad \forall i, k \tag{2.37b}$$

$$0 \le q, \tag{2.37c}$$

$$0 \le f_{ij}^k \ , \quad \forall i, j, k. \tag{2.37d}$$

where Lagrange multipliers λ_i^k, τ_i, and ω^k correspond to constraints (2.35b), (2.35c), and (2.35d) of the original problem, respectively. Problem (2.37) is analogous to the distributed problem in [65, Sec. IV.C], but here the variables ω^k enable us to account for the DR constraints. Note that the

objective (2.37a) is locally separable over flow variables f_{ij}^k. In other words, nodes can optimize the flow variables by exchanging the Lagrange multipliers λ_i^k and τ_i only between their neighbors. However, this fact does not hold for the variables q and ρ^k, and the Lagrange multipliers ω^k. Hence, problem (2.37) is a *partially separable distributed optimization* [65]. In order to map (2.37) to its fully distributed equivalent, we need to define local variables q_i and ρ_i^k and solve the following optimization:

$$\begin{aligned}
\min_{q_i, r_i^k, f_{ij}^k} \quad & \sum_i q_i^2 + \epsilon \sum_{i,j,k} (f_{ij}^k)^2 + \sum_{i,k} \omega_i^k (\rho_i^k - \zeta^k) \\
& + \sum_{i,k} \lambda_i^k \left(-r_i^k - \sum_j f_{ji}^k + \sum_j f_{ij}^k \right) \\
& + \sum_i \tau_i \left(\sum_k \left(I_{ik}^s \frac{E_s}{T_s} + \sum_j f_{ji}^k E_{rx} \sum_j f_{ij}^k (E_p + E_{tx}) \right) \right. \\
& \left. - q_i E_i \right) \\
& + \sum_{i,j} \Lambda_{ij} (q_i - q_j) + \sum_{i,j,k} \Upsilon_{ij}^k (\rho_i^k - \rho_j^k) && \text{(2.38a)} \\
\text{subject to} \quad & 0 \le r_i^k \le \frac{b_{\max}}{T_s}, \qquad \forall i, k && \text{(2.38b)} \\
& 0 \le q_i, \qquad \forall i, && \text{(2.38c)} \\
& 0 \le f_{ij}^k, \qquad \forall i, j, k, && \text{(2.38d)}
\end{aligned}$$

where the objective is summed over the newly-defined local variables, and the last two terms in the objective are inserted in order to force the local variables q_i and ρ_i^k to be equal to their global value. After this modification, every single term in the objective (2.38a) is separable over all variables q_i,

r_i^k, f_{ij}^k and Lagrange multipliers λ_i^k, τ_i, ω_i^k, Λ_{ij}, Υ_{ij}^k. However, note that the value of ζ^k, which is independent of local variables, needs to be broadcasted to all nodes whenever a significant change in $\hat{\theta}^k$ is observed, and therefore D-UMLJE is not fully distributed in the strict sense. But since D-UMLJE is distributed as far as the solution of the optimization problem is concerned, we refer to D-UMLJE as a distributed solution similar to [65].

The distributed problem (2.38) is solved using the subgradient method. At each iteration, the sensor s_i solves the localized part of (2.38) with only the terms involving its own variables using the current values of Lagrangian multipliers obtained from the previous iteration. Mathematically, at iteration ℓ

$$\begin{aligned}
q_i(\ell) &= \underset{0\le q_i\le Q}{\operatorname{argmin}} \left(q_i^2 - q_i \left(E_i\tau_i + \sum_{j\in\mathcal{N}_i} (\Lambda_{ij} - \Lambda_{ji}) \right) \right), \quad \forall i, \\
f_{ij}^k(\ell) &= \underset{0\le f_{ij}^k}{\operatorname{argmin}}\, \epsilon \sum_{k=1}^{K} (f_{ij}^k)^2 + \sum_{k=1}^{K} f_{ij}^k \left(\left(\lambda_i^k - \lambda_j^k \right) \right. \\
&+ \left. \tau_i(E_p + E_{tx}) + \tau_j E_{rx} \right), \quad \forall i,j \in \mathcal{N}_i, \\
r_i^k(\ell) &= \underset{0\le r_i^k\le \frac{b_{\max}}{T_s}}{\operatorname{argmin}} \left(\rho_i^k \left(\omega_i^k + \sum_{j\in\mathcal{N}_i} \left(\Upsilon_{ij}^k - \Upsilon_{ji}^k \right) \right) \right. \\
&- \left. r_i^k \lambda_i^k \right), \quad \forall i,k,
\end{aligned} \tag{2.39}$$

where Q is a loose upper bound for q_i and all the terms in right hand side are from iteration $\ell-1$. Also, according to the definition of ρ^k in (2.31), the values of $\rho_i^k(\ell)$ are updated as

$$\rho_i^k(\ell) = \left(\frac{1}{\rho_i^k(\ell-1)} - \frac{1}{\pi_i^k(\ell-1)} + \frac{1}{\pi_i^k(\ell)} \right)^{-1}, \tag{2.40}$$

where $\pi_i^k(\ell-1)$ and $\pi_i^k(\ell)$ are the variances corresponding to $r_i^k(\ell-1)$ and $r_i^k(\ell)$ defined in (2.5). We observe that optimization over q_i, f_{ij}^k, and r_i^k takes place separately. In addition, the optimization for q_i and f_{ij}^k are in the form of a quadratic functions, for which closed-form solutions exist.

Finally, the update rules for Lagrange multipliers based on the subgradient method are given by

$$\begin{aligned}
\omega_i^k(\ell) &= \left(\omega_i^k(\ell-1) + u(\ell-1)\left(\zeta^k - \rho_i^k\right)\right)_+, \\
\lambda_i^k(\ell) &= \lambda_i^k(\ell-1) + u(\ell-1)\left(r_i^k + \sum_j f_{ji}^k - \sum_j f_{ij}^k\right), \\
\tau_i(\ell) &= \left(\tau_i(\ell-1) + u(\ell-1)\left(q_i E_i - \sum_k \left(I_{ik}^s \frac{E_s}{T_s}\right.\right.\right. \\
&- \left.\left.\left. \sum_j f_{ji}^k E_{rx} - \sum_j f_{ij}^k (E_p + E_{tx})\right)\right)\right)_+, \\
\Lambda_{ij}(\ell) &= \Lambda_{ij}(\ell-1) + u(\ell-1)\left(q_i - q_j\right), \\
\Upsilon_{ij}^k(\ell) &= \Upsilon_{ij}^k(\ell-1) + u(\ell-1)\left(\rho_i^k - \rho_j^k\right),
\end{aligned} \tag{2.41}$$

where $u(\ell)$ is a decreasing function of ℓ, and $(.)_+$ maps the negative values to 0 [10, 65]. Note that the Lagrange multipliers are updated using the results of optimizations in (2.39) at the same iteration. The convergence of the above-mentioned subgradient method to the optimal solution of the problem (2.38) can be shown using the same arguments as [65]. Furthermore, strong duality holds between the UMLJE (2.35) and the un-regularized D-UMLJE (i.e., (2.38) with $\epsilon = 0$). Hence, choosing a small regularization weight ϵ allows us to closely approximate the optimal solution of the UMLJE. (See

[65, Sections IV and V] and references therein for further details.)

2.3.2 Discussion

2.3.2.1 Overhead Comparison

As stated earlier, both UMLJE and D-UMLJE schemes incur signalling overhead for exchanging the information with the sink or their neighboring nodes. The major overhead in UMLJE comes from the initial collection of SINR values in the sink. Also, the optimized data need to be sent by the sink to each node. Hence, we have $O(\Gamma)$ two-way transmissions between nodes and sink per node, where Γ is the average network depth, i.e., the average number of hops that a node needs for connecting to the sink. On the other hand, D-UMLJE only requires $O(E)$ communications per node per iteration for exchanging optimization variables, where E is the average number of neighbors of a node in the network. For a fixed density, Γ grows with network size N, but E is independent of N, which renders D-UMLJE scalable with regards to message exchange for optimization, and thus better suited than UMLJE for larger networks. However, denser topologies would lead to an increased packet exchange between neighbors for local optimization in D-UMLJE. Finally, as mentioned above, K variables ζ^k in D-UMLJE and the optimization results in UMLJE need to be broadcasted by the sink.

With regards to computational complexity, the problem (2.35) is more computationally-involved than each round of the distributed optimizations (2.39)-(2.41). Specifically, solving the convex optimization (2.35) in a centralized manner has a computational complexity of $O(N^3)$, while the com-

plexity of each distributed update iteration is $O(1)$ at every node. Our simulations indicate that the number of iterations needed for D-UMLJE to converge is typically $O(N)$. Hence, unless the sink has considerably more computational resources than the other sensor nodes, D-UMLJE is preferable in terms of complexity.

2.3.2.2 Dynamics of θ^k

If no prior knowledge is available, $\hat{\theta}^k$ can be initialized arbitrarily. (For the numerical results reported in the next section, we initialize it as 0). Through the choice of the forgetting factor δ, we can trade-off speed of convergence towards the true value θ^k and steady-state accuracy of the estimate. However, an uninformed initialization of $\hat{\theta}^k$ is only needed at a first acquisition, then this parameter can be tracked. This also means that δ could be chosen smaller during acquisition, and then larger in the tracking phase. Since updates of the estimate of θ^k also lead to broadcasts from the sink for updating ζ^k in D-UMLJE and of optimization results in UMLJE, there is a tradeoff between tracking accuracy of θ^k and energy consumption for communicating parameter updates. The coherence time of θ^k should also be larger than the time needed for the iterations in D-UMLJE convergence. Assuming that the values of θ^k remain constant during at least one sampling interval, D-UMLJE should converge within a fraction of T_s. Since the iterations involve one-hop communication, the $O(N)$ iterations needed for D-UMLJE convergence are fast, and this assumption is practical for a properly chosen value of T_s based on the event type and the network size.

2.4 Performance Evaluation

In this section, we examine the performance of the proposed UMLJE and D-UMLJE approaches and compare them with previously proposed maximum lifetime and event detection methods, namely, MERG [69, Alg. 2], MLB [70], and URFP [81, Figure 2]. Recall that MERG finds the minimum energy routes that satisfy the DRs. The best route is obtained by maximizing a lower bound for lifetime. URFP connects the source nodes to the sink through the links with the highest data rates. Finally, MLB tries to maximize an upper bound for lifetime by decoupling the quantization and routing problems. Since the decoupled routing problem in MLB is identical to the routing problem in URFP, MLB and URFP use the same set of routes. We also note that for URFP and MERG, there is no notion of quantization bits b_i^k, and we equally divide the required bits between the nodes in the sensing range of an event. In the simulations, we always apply the interference-free scheduling to MERG, MLB and URFP.

Table 2.1 summarizes the parameters used for the simulations. For the UWB channel model, the non-line-of-sight (NLOS) indoor office environment is assumed [148]. The energy consumption parameters are chosen according to a typical UWB device [41, 151]. In the simulations, the number of nodes varies from $N = 10$ to $N = 50$ for detecting $K = 2$ events. Unless otherwise specified, all sensors are assumed to experience the same noise variance, and the default detection requirements are set to $\eta^k = 0.90$ and $\nu^k = 0.10$. We assume that the parameters θ_k remain constant with an SNR of $\frac{\theta_k^2}{\sigma_i^2} = 37.0$ dB $\forall i, k$, and are perfectly estimated, i.e., $\hat{\theta}_k = \theta_k$,

Table 2.1: Simulation Parameters for Lifetime Maximization

Parameter	Value	Parameter	Value
γ_1	2.0	γ_2	3.07
d_0	4 m	g	-60 dB
G	1	D	12 m
P_{tx}	-14.3 dBm	T_s	1 Sec.
E_{rx}	2.5 nJ/bit	E_p	10 pJ/bit
E_i	10 J	E_s	10 nJ
W	1.0 GHz	σ_i^2	-84 dBm
K	2 - 5	N	10 - 50
δ	0.9	χ	0.08
Simulation runs	100	$b_{\max}$	12 bits
ϵ	$\max\{0.1, \exp(\frac{-\ell}{10})\}$	$u(\ell)$	$\max\{0.01, \frac{0.5}{\sqrt{\ell}}\}$
$\frac{M^2}{\sigma^2}$	50.0 dB	$\frac{\theta^2}{\sigma^2}$	37.0 dB

$k = 1, \ldots, K$.

2.4.1 A Sample Scenario

We first consider an example with $N = 25$ nodes and $K = 2$ events shown in Figure 2.4. In this figure, sensor nodes are represented by circles, and

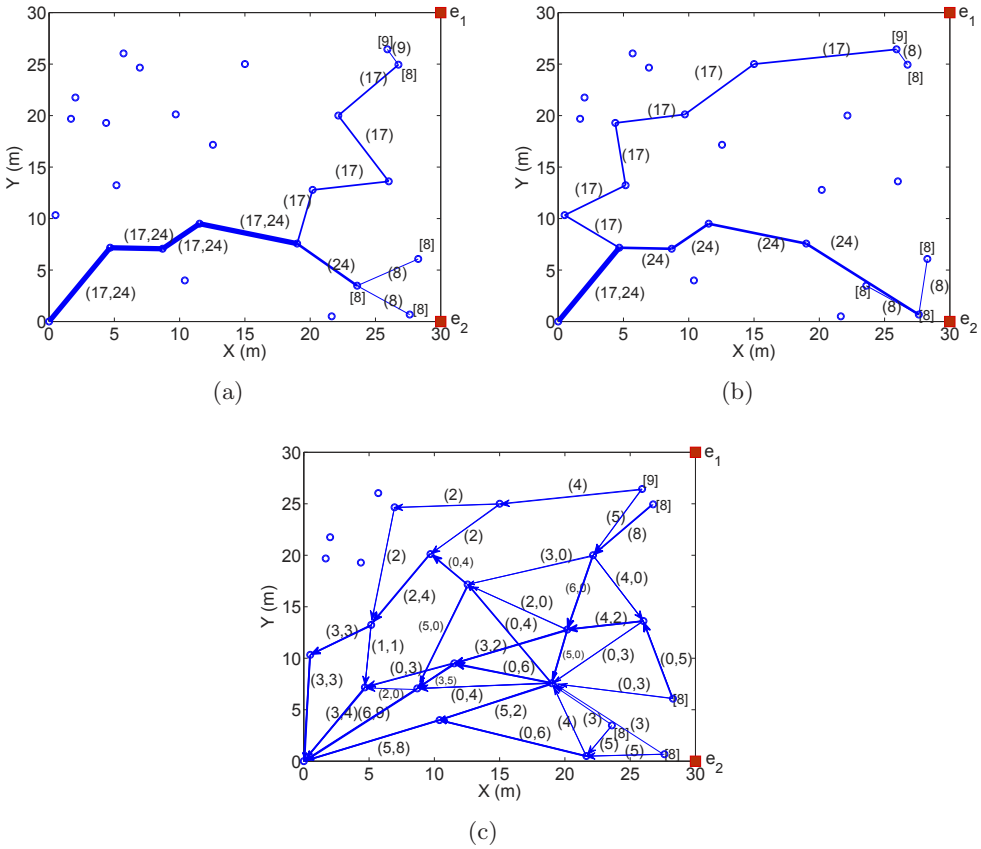

Figure 2.4: Comparison between routes (a) URFP, (b) MERG, and (c) UMLJE. $N = 25$ sensor nodes (circles) detecting $K = 2$ events e_1, e_2 (squares) with DRs $\nu^k = 0.03, \eta^k = 0.97$. The MLB approach in the homogeneous networks chooses the same routes as URFP. The sink is located at (0,0), and the squares at (30,0) and (30,30) represent the location of events. The numbers in brackets show the optimal number of quantization bits b_i^k at each node and the numbers in the parentheses show the amount of flow in the link for each event. Each line's thickness is proportional to the amount of flow on the corresponding link. In (c), arrows are used for indicating the flow directions in the network.

the events, which are located at the right corners, are identified by the squares. The sink is located at the lower left corner. For this example,

we apply the interference-free scheduling with detection requirements of ($\eta^k = 0.97,\ \nu^k = 0.03$). The set of routes found by URFP, MERG, and the proposed UMLJE are shown in Figures 2.4(a), 2.4(b), and 2.4(c), respectively. As stated previously, URFP routes also represent the MLB routes. The numbers in the brackets in Figure 2.4 show the number of quantization bits b_i^k at each node and the numbers in the parentheses show the amount of flow in the link for each event. Each line's thickness is proportional to the amount of flow on the corresponding link. In Figure 2.4(c), arrows are used for indicating the direction of flows in the network.

As can be seen from Figure 2.4(c), the total flow for jointly detecting e_1 and e_2 is completely distributed between the nodes in the network core, i.e., the nodes in the transmission range of the sink. Specifically, in UMLJE there are 4 nodes that transmit to the sink, while in Figures 2.4(a) and 2.4(b) only 1 node transmits to the sink. The balance of flows in the network core causes this nodes to run out of energy almost at the same time, and thus avoids the bottleneck problem. Note that, following the arrows in Figure 2.4(c), it can be observed that UMLJE directs a fair proportion of flow generated from e_1 downwards, in order to balance the flow between the three core nodes that carry traffic from this part of the network. Note that in UMLJE, the number of quantization bits for estimating an event may vary among sensors. This is because UMLJE jointly optimizes the quantization and routing problems, hence quantization bits are adjusted according to the optimal routes. On the other hand, MLB decouples the quantization problem and thus the quantization bit assignments are independent of the routes. Since the network is homogeneous, i.e., noise variances are the same,

MLB assigns the same number of quantization bits to different sensors.

2.4.2 Lifetime Comparison

Figure 2.5 compares the maximum lifetime obtained from UMLJE and D-UMLJE with $K = 2$ events when the number of nodes vary from 10 to 20 under the interference-free scheduling C^{U}. In D-UMLJE, a node stops its local updates if for all variables the difference between the updated and previous value is less than 0.1% in ten consecutive iterations. This stopping criterion could be relaxed for an earlier stop, and to tradeoff complexity and energy consumption for optimization with performance and lifetime for event detection. As can be seen, the optimal value of D-UMLJE is very close to that for UMLJE. This fact is expected due to the strong duality between UMLJE and un-regularized D-UMLJE [65]. The small gap is due to the regularization weight. Hence, we provide a powerful lifetime maximization solution that can be implemented in a distributed manner.

It is worth mentioning that the absolute values of the reported lifetime in Figure 2.5 and other figures in this section are based on the parameters listed in Table 2.1, in particular the sensing interval of $T_s = 1$ second and the initial available energy of $E_i = 10$ Joules at the sensor batteries. These values are provided as an example for the purpose of performance comparison, and vary when the parameters are adjusted depending on the application. For example, changing the sensing interval to 1 hour provides a gain of 3600 in the lifetime. There are also other parallel approaches that can be employed to further improve the lifetime, for example, by providing sleeping mechanisms for the sensors [49], and/or by energy harvesting from

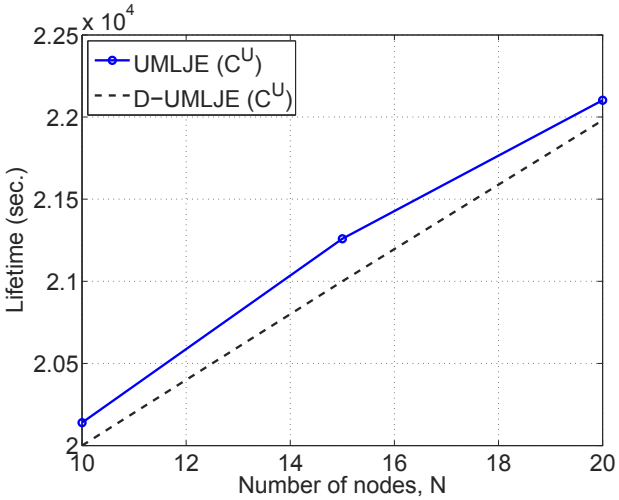

Figure 2.5: Network lifetime of UMLJE and D-UMLJE as a function of number of nodes for $K = 2$ events.

the environment [152]. UMLJE and D-UMLJE can also support these extensions by solving a new optimization based on the updated set of active sensors, and/or their updated values of E_i.

For network sizes of 10 to 50 nodes, we compare the performance of D-UMLJE with URFP (also MLB) and MERG in Figure 2.6. In this figure, the lifetime of D-UMLJE with both lower and upper bounds of link capacities $(C^{\mathrm{L}}, C^{\mathrm{U}})$ are shown. We observe from Figure 2.6 that the lifetime obtained using D-UMLJE is significantly improved by increasing the number of nodes and thus node density, since in a network with larger number of nodes, the optimization is able to find more paths towards the sink and balance energy consumption among them. On the other hand, MERG fails to grab this opportunity, since after satisfying the DRs, MERG always chooses a minimum energy route regardless of its load, which is clearly not a lifetime-optimal

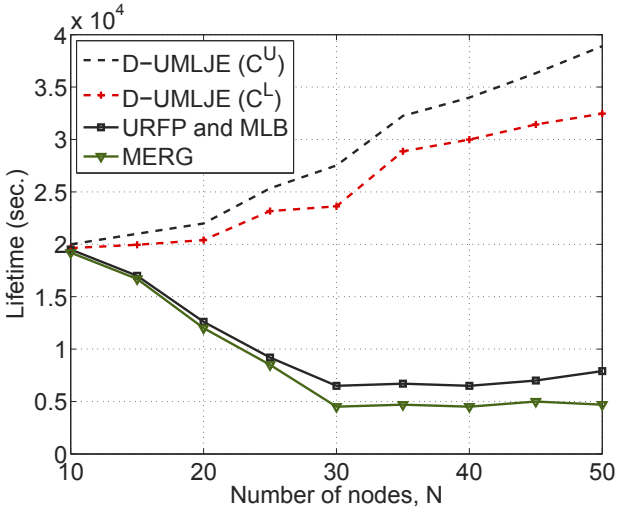

Figure 2.6: Network lifetime of MERG, URFP and D-UMLJE as a function of network size N for $K = 2$ events.

approach in the presence of multiple events. Although the lifetime in URFP (also MLB) is slightly improved by increasing N from 40 to 50, the overall lifetime is significantly lower than that for D-UMLJE due to the fact that URFP sacrifices the lifetime by finding the routes with higher capacities. This also shows the disadvantage of MLB, which tries to maximize a loose upper bound on lifetime based on the MSE requirements.

It can also be seen from Figure 2.6 that the lifetime of the proposed method with interference-free scheduling (C^{U}) is larger than that for maximum interference scenario (C^{L}), since in the latter the consumed transmission energy per bit is higher.

Figure 2.7 compares the lifetime of D-UMLJE, URFP (also MLB), and MERG for different DRs ζ^k in a network with $N = 25$ nodes and $K = 2$ events under interference-free scheduling. Note that, as explained in Sec-

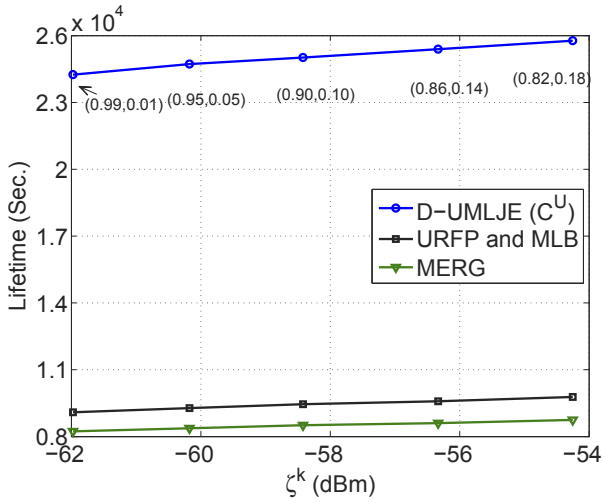

Figure 2.7: Network lifetime as a function of DRs for $N = 25$ nodes and $K = 2$ events. A smaller value of ζ^k corresponds to a stricter DR, which is shown as (η^k, ν^k) for each point.

tion 2.2.2, any value of ζ^k can be mapped to a specific DR at a given event SNR based on (2.31). These corresponding values for each ζ^k are also shown in this figure. Note that a larger ζ^k corresponds to a looser DR and hence a smaller generation rate. Therefore, lifetime increases as ζ^k increases. As can be further seen from Figure 2.7, for a given DR, the lifetimes of URFP, MLB, and MERG are significantly lower than that for D-UMLJE. This shows that D-UMLJE is able to find the best routing and quantization strategy for the given DR.

Figure 2.8 shows the detection rate achieved in a network. The detection rate should ideally match to the desired η^k assigned in the optimization, but because of the quantization of observation variables, it deviates from its ideal value. As can be seen in Figure 2.8, the achieved detection rate in our simulations is larger than the assigned value of η^k and is very close to η^k for

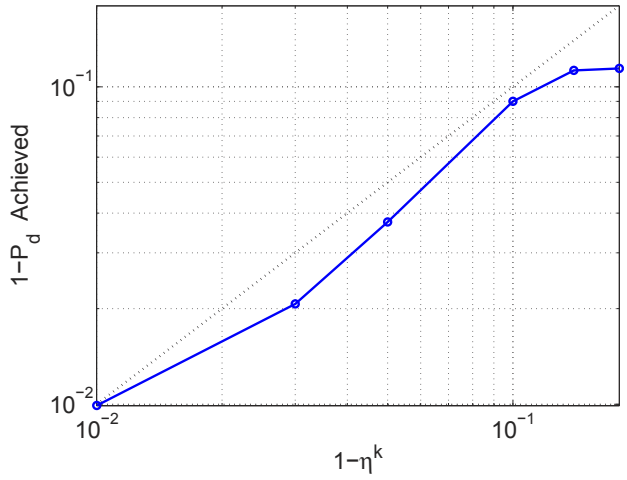

Figure 2.8: Achieved detection rate as a function of the desired detection probability η^k. Dotted line shows the 45° line for reference.

higher values, because more bits are used for reporting an event, and thus the Gaussian approximation is tighter.

2.4.3 Convergence of D-UMLJE

In this section, we present some simulation results to illustrate the convergence properties of D-UMLJE. Considering network of sizes of $N = 10$, 25, and 50, and $K = 2$ events, we plot the variables q_i and ρ_i^k, normalized to their final values, as a function of the iteration number in Figure 2.9. Figure 2.9(a) shows the evolution of q_i for two selected sensors for each network size, and Figure 2.9(b) provides plots of ρ_i^k for one selected sensor for each network size. As can be seen, ρ_i^k generally converges faster than q_i. In particular, after about 100 iterations, the values for ρ_i^k are practically converged to their final value, regardless of the network size. This is because the variables ρ_i^k are only updated by the nodes in the sensing range of e_k, and thus

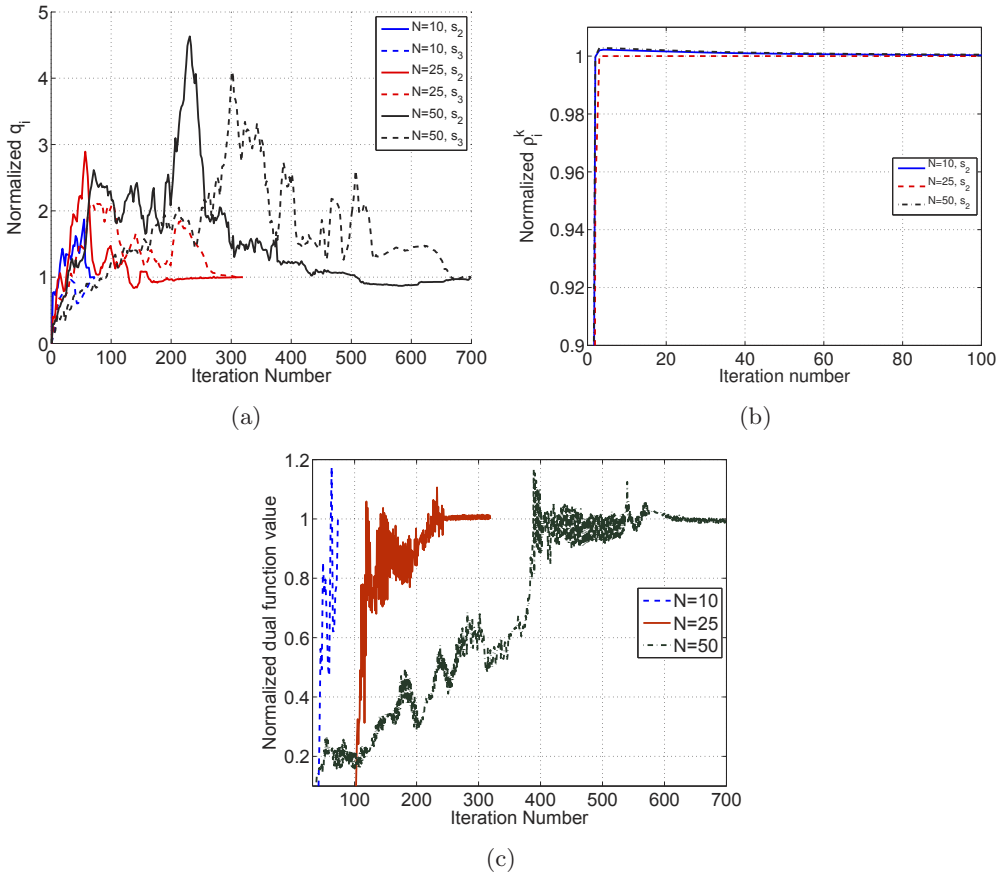

Figure 2.9: Convergence of (a) q_i, (b) ρ_i^k, and (c) value of dual function in sample networks of sizes $N = 10, 25, 50$, and with $K = 2$. The values are normalized to their optimal value.

there is no scalability issue with regards to network size N. Compared to this, the convergence of q_i requires a larger number of iterations and the convergence time increases with network size. Balancing the network traffic by adjusting the local variables q_i through local message passing eventually involves an information exchange throughout the entire network.

Figure 2.9(c) shows the convergence of the dual value (2.38a) normalized

to its optimal for three scenarios of network sizes of $N = 10$, 25, and 50. As can be seen, the convergence is fairly fast, i.e. nodes can find a solution close to the optimal one after few iterations. As expected, more number of iterations is needed for convergence in larger networks. Figures 2.9(a) to 2.9(c) also indicate that, since only local communications are performed in each iteration, the time needed for the convergence of the dual function and variables would be less than the coherence time of the events.

2.5 Conclusions

We have investigated the optimization of operational lifetime in event detection sensor networks using UWB communication. The specific sensor network task considered assumed sensing events with known locations under given detection requirements. We have assumed UWB signal properties and a simple MAC layer (no power control, random access), and we have considered variable generation bit rates at the sensors, which made it possible to tradeoff detection accuracy with energy consumption for transmission. Given this setup, we have formulated a convex optimization problem, which can be solved using standard methods at a central node, preferably the network sink. Moreover, we have provided a distributed method, which shares the computational load among the network nodes and requires mostly local communication among neighboring nodes. Numerical results show that our UWB-based maximum-lifetime joint event detection (UMLJE) approach and its distributed version are able to efficiently find the routes for maximum operational lifetime and achieve significant performance gains over

previously proposed methods.

Chapter 3

Robust Localization in Wireless Sensor Networks

After considering the lifetime maximization in Chapter 2, we now focus on the WSN localization problem. The location estimates obtained from the formulations in this chapter are a pre-requisite for many WSN enhancements, including the algorithms presented in Chapter 2.

As explained in Section 1.4.1, ranging information can be easily obtained in USNs using a two-way ranging technique between two nearby UWB sensors (see Figure 1.3 and Equation (1.2) for details). These ranging measurements can then be passed to a localization algorithm in order to determine the location of sensors [153]. Hence, the algorithms presented in this chapter for a general WSN model are also applicable to the USN model used in Chapter 2.

Node localization is in general a difficult task in WSNs in which the ranging measurements are subject to errors and anchor positions are subject to uncertainty. In this chapter, the *robust* localization problem is formulated using the maximum likelihood criterion under an unbounded uncertainty model for the anchor positions. To overcome the non-convexity of the result-

ing optimization problem, convex relaxations leading to either semi-definite programming (SDP) [110] or second order cone programming (SOCP) [106] can be obtained.

The comprehensive study by Tseng [106] investigates the SOCP and SDP formulations for the localization problem and studies several interesting properties, such as the relation of the SOCP and SDP solutions to the convex hull of anchors, conditions on uniqueness of the solutions, characterizing the optimal objective values, and how to make the formulations distributed. Tseng further shows that there is a tradeoff between SDP and SOCP in terms of complexity and localization accuracy. While SDP provides a tighter relaxation and hence results in a better localization accuracy compared to SOCP, SOCP has a lower computational complexity and takes a shorter time to solve. The lower complexity of SOCP is because for a given problem, the number and size of variables and constraints required for solving SOCP are smaller than those required for solving SDP. This tradeoff motivates the design of mixed SDP-SOCP algorithms which benefit from the better accuracy of SDP and the lower complexity of SOCP.

This chapter essentially follows the model in the SDP localization [110] and provides robust SOCP algorithms with significantly lower computational complexities compared to their SDP counterpart. In doing so, our work specifically extends [106, 107, 110] by exploring tradeoffs between the *robust* versions of SDP and SOCP. Based on this extension, a mixed robust SDP-SOCP localization framework is proposed which benefits from the better accuracy of SDP and the lower complexity of SOCP. Since the centralized optimization involves a high computational complexity in large networks,

we also derive the distributed implementation of the proposed robust SOCP convex relaxation. Moreover, we propose an iterative optimization based on the expectation maximization (EM) algorithm for the cases where anchor uncertainty parameters are unavailable. An analysis is performed in order to identify the set of nodes which are accurately positioned using robust SOCP, and to establish a relation between the solution of the proposed robust SOCP optimization and the existing robust optimization using SDP. Finally, we utilize the properties of robust SOCP localization towards mobile sensor network applications, such as formation control and detection of boundary trespassing.

The rest of this chapter is organized as follows. The SOCP formulation with unbounded anchor position uncertainty and its unambiguous localizability property are presented respectively in Sections 3.1 and 3.2. We then show the relation between robust SOCP formulation and robust SDP and propose a localization method based on mixing these two methods in Section 3.3. In Section 3.4, the robust SOCP formulation is extended to its distributed form, and an EM method for the case of unknown uncertainty covariance is proposed. We then present another extension of SOCP for mobile sensor network applications in Section 3.5. Extensive simulations are finally presented in Section 3.6 to confirm that the robust SOCP and mixed robust SDP-SOCP provide tradeoffs between localization accuracy and computational complexity that render them attractive solutions, especially in networks with a large number of nodes.

3.1 Sensor Localization Framework

We consider a sensor network that consists of a set of anchors, $\mathcal{N}_a$, and a set of general sensor nodes $\mathcal{N}_s$. We denote $\mathcal{N} = \mathcal{N}_s \cup \mathcal{N}_a$ as the set of all nodes in the network, and $\boldsymbol{x}_i^o$ as the vector that contains the actual coordinates of a node $i \in \mathcal{N}$. Furthermore, we denote the number of anchors by $k \doteq |\mathcal{N}_a|$ and the total number of nodes by $m \doteq |\mathcal{N}|$. Although we assume two-dimensional coordinates in this paper, the extension to higher dimensions is straightforward.

The sensor network can be represented by an undirected graph $\mathcal{G} = (\mathcal{N}, \mathcal{E})$, where $\mathcal{N}$ is the set of all sensors as defined above, and $\mathcal{E}$ is the set of links. A link $(i, j) \in \mathcal{E}$ if nodes i, j are neighbors, i.e. they are in the communication range, R_c, of each other: $d_{ij}^o \doteq \|\boldsymbol{x}_i^o - \boldsymbol{x}_j^o\| \leq R_c$. Similar to [110], we assume that $\mathcal{E}$ does not include anchor-anchor links. Because of errors in the ranging measurements, the estimated distance between nodes i and j can be written as

$$d_{ij} = d_{ij}^o + e_{ij}. \tag{3.1}$$

The measurement error e_{ij} is modeled as a zero-mean Gaussian random variable with variance σ_{ij}^2 [110]. We denote $\mathcal{D}$ as the set of all available noisy measurements

$$\mathcal{D} = \{d_{ij} |\ (i, j) \in \mathcal{E}\}.$$

3.1.1 Localization with Perfectly Known Anchor Positions

Let us first assume a sensor network in which the anchor positions are perfectly known. Given the anchor positions $\boldsymbol{x}_i^o$, $i \in \mathcal{N}_a$, and the set of noisy

measurements $\mathcal{D}$, the goal of node localization is to obtain estimates of general sensor node positions, $\boldsymbol{x}_i,\ i \in \mathcal{N}_s$, that minimize the sum of squared measurement errors based on the maximum likelihood criterion:

$$\min_{\boldsymbol{x}_i, i\in\mathcal{N}_s} \quad \sum_{(i,j)\in\mathcal{E}} \left(\|\boldsymbol{x}_i - \boldsymbol{x}_j\| - d_{ij} \right)^2 . \tag{3.2}$$

Since this optimization problem is non-convex and in its general form NP-hard to solve [88], convex SOCP and SDP relaxation techniques have been applied to (3.2) and its variants in [105, 106, 108–110, 114].

3.1.2 Localization with Anchor Position Uncertainty

In practice, perfect knowledge of anchor positions may not be available. In many scenarios, the anchor positions are obtained using global positioning system (GPS) and thus subject to estimation errors, which usually are modeled as Gaussian random variables [104, 110, 154, 155][5]. Accordingly, the uncertain anchor positions are given by

$$\boldsymbol{a}_i = \boldsymbol{x}_i^o + \boldsymbol{w}_i, \quad i \in \mathcal{N}_a, \tag{3.3}$$

where the position uncertainty of the i^{th} anchor, $\boldsymbol{w}_i$, is a zero-mean Gaussian random vector with covariance matrix $\boldsymbol{\Psi}_i$.

Using the anchor position uncertainty model in (3.3), our goal is to obtain a *robust* counterpart of the localization problem in (3.2) that explicitly takes

[5]For example, the GPS performance standard [155, Section A.5.4] argues that the long-term user ranging errors can be reasonably approximated by a zero-mean normal distribution.

into account the uncertainty in the anchor positions. We note that the robust problem involves the refinement of the anchor positions. Following [110], we consider a maximum likelihood estimation (MLE) approach for $\boldsymbol{x}_i^o,\ i \in \mathcal{N}$, and examine the probability

$$\begin{aligned} P\left(\mathcal{D}, \{\boldsymbol{a}_i\} \,|\, \{\boldsymbol{x}_i\}\right) &= P\left(\mathcal{D}|\, \{\boldsymbol{x}_i\}\right) \quad \times P\left(\{\boldsymbol{a}_i\} \,|\, \{\boldsymbol{x}_i\}\right) \\ &= \prod_{(i,j)\in\mathcal{E}} \frac{1}{\sqrt{2\pi}\sigma_{ij}} \exp\left(\frac{-\left(\ \|\boldsymbol{x}_i - \boldsymbol{x}_j\| - d_{ij}\ \right)^2}{2\sigma_{ij}^2}\right) \\ &\times \prod_{i\in\mathcal{N}_a} \frac{1}{\sqrt{2\pi\,|\boldsymbol{\Psi}_i|}} \exp\left(\frac{-\left(\boldsymbol{a}_i - \boldsymbol{x}_i\right)^T \boldsymbol{\Psi}_i{}^{-1} \left(\boldsymbol{a}_i - \boldsymbol{x}_i\right)}{2}\right) \end{aligned} \tag{3.4}$$

By taking the logarithm of (3.4), the robust localization problem can be written as

$$\min_{\boldsymbol{x}_i,\ i\in\mathcal{N}} \sum_{(i,j)\in\mathcal{E}} \frac{\left(\ \|\boldsymbol{x}_i - \boldsymbol{x}_j\| - d_{ij}\ \right)^2}{\sigma_{ij}^2} + \sum_{i\in\mathcal{N}_a} (\boldsymbol{a}_i - \boldsymbol{x}_i)^T \boldsymbol{\Psi}_i{}^{-1} (\boldsymbol{a}_i - \boldsymbol{x}_i). \tag{3.5}$$

Similar to the optimization problem in (3.2), the robust localization problem (3.5) is non-convex. To obtain an SOCP relaxation of (3.5), we first write the optimization problem in the following equivalent form:

$$\min_{\{\boldsymbol{x}_i\},\{t_{ij}\},\{s_i\}} \quad \sum_{(i,j)\in\mathcal{E}} t_{ij}^2 + \sum_{i\in\mathcal{N}_a} s_i^2 \tag{3.6a}$$

$$\text{subject to} \quad g_{ij}\,|\|\boldsymbol{x}_i - \boldsymbol{x}_j\| - d_{ij}| \le t_{ij}, \quad (i,j) \in \mathcal{E}, \tag{3.6b}$$

$$\|\boldsymbol{\Psi}_i^{-1/2}(\boldsymbol{a}_i - \boldsymbol{x}_i)\| \le s_i, \quad i \in \mathcal{N}_a, \tag{3.6c}$$

where $g_{ij} \doteq \frac{1}{\sigma_{ij}}$. By defining a vector $\boldsymbol{u}$ as the concatenation of variables in

the objective, i.e.,

$$\boldsymbol{u} \doteq [t_{ij} \ (i,j) \in \mathcal{E}, \ s_i \ i \in \mathcal{N}_a] \,,$$

we can write (3.6) as the following equivalent epigraph form:

$$v_{\text{socp}} \doteq \min_{\{\boldsymbol{x}_i\},\boldsymbol{u},\{q_{ij}\},v} \quad v \tag{3.7a}$$

$$\text{subject to} \quad \|\boldsymbol{u}\| \leq v, \tag{3.7b}$$

$$g_{ij} \, |q_{ij} - d_{ij}| \leq t_{ij}, \quad (i,j) \in \mathcal{E}, \tag{3.7c}$$

$$\|\boldsymbol{\Psi}_i^{-1/2}(\boldsymbol{a}_i - \boldsymbol{x}_i)\| \leq s_i, \quad i \in \mathcal{N}_a, \tag{3.7d}$$

$$\|\boldsymbol{x}_i - \boldsymbol{x}_j\| = q_{ij}, \quad (i,j) \in \mathcal{E}. \tag{3.7e}$$

Finally, a convex SOCP relaxation of the robust localization problem in (3.7) can be obtained by relaxing the equality constraint (3.7e) to inequality

$$\|\boldsymbol{x}_i - \boldsymbol{x}_j\| \leq q_{ij}, \quad (i,j) \in \mathcal{E}. \tag{3.8}$$

Substituting (3.7e) with (3.8) results in a standard SOCP program which can be solved using an interior point algorithm [10].

In the special case of perfectly known anchor positions, i.e. $\boldsymbol{x}_i = \boldsymbol{a}_i = \boldsymbol{x}_i^o, \ i \in \mathcal{N}_a$, (3.7) reduces[6] to the standard SOCP formulation in [106]. The bounded uncertainty model in [114] is another special case of (3.7) by setting $\boldsymbol{\Psi}_i = \boldsymbol{I}_2$ and $s_i = \delta$, where δ is the given uncertainty bound. Also note that SOCP location estimates always lie within the convex hull of the anchor positions, which is not in general true for the SDP solution [106]. It is also

[6] We should point out that the objective function of SOCP relaxation in (3.5) follows the MLE approach [110] and is slightly different from that of [114].

worth mentioning that the sensors in (3.7) can be viewed as anchors with no prior information.

3.2 Unambiguously Localizable Nodes

Having formulated the robust SOCP localization problem (3.7), in this section we provide necessary and sufficient conditions for identifying the set of uniquely localizable nodes in the robust SOCP case.

A node i is called *unambiguously localizable* if the minimum value of (3.7) is achieved for only a unique value of $\boldsymbol{x}_i$. In other words, unambiguous localizability of a sensor node i means that its estimated location is invariant over all solutions, which is in fact a property of the convex optimization that is being used. Note that this definition is different from the definition of "unique localizability" from the viewpoint of network rigidity in the absence of noise, for example in [87, 88]. Here, the term unambiguously localizable refers to the set of nodes whose estimated locations are *invariant over all solutions of the robust SOCP problem* (3.7) [106, 107].

Let $\mathcal{B} = \{(i,j) \in \mathcal{E} \text{ s.t. } \|\boldsymbol{x}_i - \boldsymbol{x}_j\| = q_{ij}\}$ be the set of links which satisfy the SOCP relaxed constraint (3.8) with equality for every relative interior solution[7] to the robust SOCP problem. We hereafter refer to the links in $\mathcal{B}$ as *tight links*, and to the corresponding nodes as *tightly-connected* nodes. We also denote the convex hull of anchors as $\mathcal{C}\{\mathcal{N}_a\}$, or more generally the convex hull of a set of points $\mathcal{S}$ as $\mathcal{C}\{\mathcal{S}\}$. The set of tightly-connected nodes

[7] A relative interior solution lies inside the relative interior of the solution set. In our case, all solutions which satisfy the remaining constraints corresponding to $\mathcal{E} - \mathcal{B}$ with strict inequality are relative interior solutions.

is denoted by $\mathcal{M}$.

Tight links are essentially indicators of less uncertainty in the optimization problem, since the optimization has found a unique optimal value for their corresponding nodes. In fact, Tseng [106] shows that the tightly-connected nodes are accurately localized in the sense that their localization error is less than the square root of their average link measurement errors. Furthermore, it is mathematically proved that, for the case of perfectly known anchor positions, the set of unambiguously-localizable nodes are exactly those which are tightly-connected. In other words, the optimization solution for not tightly-connected nodes is not unique. In these situations, the localization algorithm can return any of the solutions, for example (and as in our simulations) the analytic center solution which corresponds to the center of the solution set. Mathematically, the product of all slack variables corresponding to non-tight constraints is maximized at the analytic center solution. Geometrically, the analytic center solution has the maximum "distance" to the solution set boundaries. The nodes which are not tightly-connected, and hence their location estimates are not unique, can be further re-localized using the combined method presented in Section 3.3.2 for more accuracy.

In order to extend the above-mentioned relation between uniqueness of the solution and tightly-connected nodes to the robust case, we note that in the robust SOCP the i^{th} anchor position can vary in an area around $\boldsymbol{a}_i$ and the proof of [106] for unambiguous localization does not directly apply. In fact, here we first need to establish that all of the anchors are unambiguously localizable.

Proposition 3.1. *a) All anchors are unambiguously localizable in* (3.7)*.*
b) A sensor node i is unambiguously localizable in (3.7) *if and only if it is tightly-connected, i.e., $\boldsymbol{x}_i$ is invariant over all solutions $\Leftrightarrow i \in \mathcal{M}$.*
c) At the analytic center solution, the estimated location of all nodes lie inside the convex hull of the estimated anchor locations, i.e., all nodes on the convex hull of the analytic center solution are anchors.

Proof. See Appendix A. □

Proposition 3.1a) states that solving (3.7) leads to an unambiguous location for anchors. This is due to the availability of a prior on the anchor positions. In fact, if we also had a prior of the same form for sensors, $\boldsymbol{\Psi}_i^{-1/2}(\boldsymbol{a}_i - \boldsymbol{x}_i),\ i \in \mathcal{N}_s$, then all sensors would have been unambiguously localizable as well. This property follows from the fact that the point at which the contour defined by the convex prior touches the convex solution set of $\boldsymbol{x}_i,\ i \in \mathcal{N}_s$, is unique [10]. In other words, adding the information $\boldsymbol{a}_i, \boldsymbol{\Psi}_i,\ i \in \mathcal{N}_s$ to the problem leads to the selection of a unique solution for $\boldsymbol{x}_i,\ i \in \mathcal{N}_s$, which has the smallest Mahalanobis distance[8] to $\boldsymbol{a}_i$, with regard to $\boldsymbol{\Psi}_i$. Part b) shows that the the set of tight nodes in the robust SOCP have similar properties to those in the original SOCP. An important corollary from combining parts b) and c) is that the sensor nodes that lie outside the convex hull of the anchors are not tightly-connected. Moreover, part c) provides a useful characteristic for the analytic center solution of robust SOCP which is not in general true for its SDP counterpart.

[8]The Mahalanobis distance of $\boldsymbol{x}_i$ from $\boldsymbol{a}_i$ with regard to the covariance matrix $\boldsymbol{\Psi}_i$ is defined as $\|\boldsymbol{\Psi}_i^{-1/2}(\boldsymbol{a}_i - \boldsymbol{x}_i)\|$.

3.3 Tradeoffs between Accuracy and Complexity

In this section, we first analyze the relation between (3.7) and the existing robust SDP formulation [110] in Section 3.3.1, and then devise an optimization problem for mixing the robust SOCP and SDP in Section 3.3.2 which enables a flexible tradeoff between accuracy and complexity.

3.3.1 Relation of Robust SOCP and Robust SDP Relaxations

In general, SOCP is a special case of SDP, in the sense that we can always find an equivalent SDP for a given SOCP formulation [156]. The reverse does not always hold, and hence we may be able to find an SDP formulation for a problem which provides a tighter relaxation compared to the SOCP. For the non-robust localization problem, this relation is studied in [106], where it is shown that the set of all possible solutions obtained from the (tighter) SDP relaxation is a subset of all possible solutions that can be obtained by SOCP. In this section we show a similar relation between the robust formulation of SOCP (3.7) and the robust SDP in [110].

Introducing $\boldsymbol{X}$ as a $2 \times m$ matrix whose i^{th} column is set to $\boldsymbol{x_i}$, $\boldsymbol{Y} = \begin{bmatrix} \boldsymbol{X}^T\boldsymbol{X} & \boldsymbol{X}^T \\ \boldsymbol{X} & \boldsymbol{I}_2 \end{bmatrix}$, $\gamma_{ij} = \|\boldsymbol{x}_i - \boldsymbol{x}_j\|^2$, and $\boldsymbol{\Xi}_i = \boldsymbol{x}_i\boldsymbol{x}_i^T$, and applying the SDP relaxations [110] obtains the following robust SDP formulation:

$$\begin{aligned} v_{\text{sdp}} \doteq \min_{\boldsymbol{X},\boldsymbol{Y},\{\boldsymbol{\Xi}_i\},\{\gamma_{ij}\},\{r_{ij}\}} & \sum_{(i,j)\in\mathcal{E}} g_{ij}^2 \left(\gamma_{ij} - 2d_{ij}r_{ij}\right) \\ & + \sum_{i\in\mathcal{N}_a} \left(\mathbf{tr}\left(\boldsymbol{\Psi}_i^{-1}\boldsymbol{\Xi}_i\right) - 2\boldsymbol{a}_i^T\boldsymbol{\Psi}_i^{-1}\boldsymbol{x}_i\right) \end{aligned} \tag{3.9a}$$

$$\text{subject to} \quad \gamma_{ij} = y_{ii} + y_{jj} - y_{ij} - y_{ji}, \quad (i,j) \in \mathcal{E}, \tag{3.9b}$$

$$r_{ij}^2 \leq \gamma_{ij}, \quad (i,j) \in \mathcal{E}, \tag{3.9c}$$

$$\mathbf{tr}(\boldsymbol{\Xi}_i) = y_{ii}, \quad i \in \mathcal{N}_a, \tag{3.9d}$$

$$\boldsymbol{x}_i = \left[y_{im+1}\ y_{im+2}\right]^T, \quad i \in \mathcal{N}, \tag{3.9e}$$

$$\begin{bmatrix} y_{m+1m+1} & y_{m+1m+2} \\ y_{m+2m+1} & y_{m+2m+2} \end{bmatrix} = \boldsymbol{I}_2, \tag{3.9f}$$

$$\begin{bmatrix} \boldsymbol{\Xi}_i & \boldsymbol{x}_i \\ \boldsymbol{x}_i^T & 1 \end{bmatrix} \succeq \mathbf{0}_3, \qquad i \in \mathcal{N}_a, \tag{3.9g}$$

$$\boldsymbol{Y} \succeq \mathbf{0}_{m+2}, \tag{3.9h}$$

where $\mathbf{tr}(.)$ is the trace of a matrix, '$\succeq \mathbf{0}_n$' stands for positive semidefiniteness of an $n \times n$ matrix, and y_{ij} denotes the element in the i^{th} row and j^{th} column of $\boldsymbol{Y}$. The objective (3.9a) is obtained by removing the constant term

$$v_0 \doteq \sum_{(i,j)\in\mathcal{E}} g_{ij}^2 d_{ij}^2 + \sum_{i\in\mathcal{N}_a} \boldsymbol{a}_i^T \boldsymbol{\Psi}_i^{-1} \boldsymbol{a}_i, \tag{3.10}$$

from the log-likelihood (3.5). The following proposition, whose proof is provided in Appendix B, explains in detail the relation between robust SOCP (3.7) and robust SDP (3.9) feasible sets.

Proposition 3.2. *Let* $S_{\text{sdp}} = \{\boldsymbol{X}, \boldsymbol{Y}, \{\boldsymbol{\Xi}_i\}, \{\gamma_{ij}\}, \{r_{ij}\}\}$ *be a feasible solution for robust SDP constraints* (3.9b)-(3.9h)*. Then, the set of variables*

$S_{\text{socp}} = \{\{\boldsymbol{x}_i'\}, \{q_{ij}\}, \{t_{ij}\}, \{s_i\}, v\}$ *defined as*

$$\begin{aligned}
\boldsymbol{x}_i' &= \boldsymbol{x}_i, \\
q_{ij} &= \sqrt{\gamma_{ij}}, \quad (i,j) \in \mathcal{E}, \\
t_{ij} &= g_{ij}\left|q_{ij} - d_{ij}\right| = g_{ij}\left|\sqrt{\gamma_{ij}} - d_{ij}\right|, \quad (i,j) \in \mathcal{E}, \\
\boldsymbol{M}_i &= \boldsymbol{\Xi}_i + \boldsymbol{a}_i\boldsymbol{a}_i^T - \boldsymbol{a}_i\boldsymbol{x}_i^T - \boldsymbol{x}_i\boldsymbol{a}_i^T, \quad i \in \mathcal{N}_a, \\
s_i &= \left(\boldsymbol{tr}\left(\boldsymbol{\Psi}_i^{-1}\boldsymbol{M}_i\right)\right)^{\frac{1}{2}}, \quad i \in \mathcal{N}_a, \\
v &= \left(\sum_{(i,j)\in\mathcal{E}} t_{ij}^2 + \sum_{i\in\mathcal{N}_a} s_i^2\right)^{\frac{1}{2}},
\end{aligned} \tag{3.11}$$

forms a feasible solution for the robust SOCP constraints (3.7b)-(3.7d) *and* (3.8)*. Furthermore, there exists a robust SDP formulation equivalent to* (3.9) *whose optimum value is* $v'_{sdp} = \sqrt{v_{sdp} + v_0}$ *and this adjusted optimum value is always greater than or equal to the robust SOCPs optimum value* (3.7a)*, i.e.,*

$$v_{socp} \leq \sqrt{v_{sdp} + v_0}, \tag{3.12}$$

where v_0 *is defined in* (3.10)*.*

Proof. See Appendix B. □

Proposition 3.2 states that the robust SDP solution set is contained in the robust SOCP solution set if (3.12) holds with equality. Note that the equivalent SDP formulation in Proposition 3.2 is obtained by applying the mapping $\boldsymbol{\Xi}_i \rightarrow \boldsymbol{M}_i$ in (3.11) to (3.9), as explained in Appendix B. The main importance of this proposition is that it extends the results of [106] for the non-robust case to the robust case. In general, robust SDP provides

a tighter relaxation for the localization problem compared to robust SOCP.

We close this section by noting that the authors in [110] have calculated the Cramer-Rao lower bound (CRLB) for robust localization problem. Since the CRLB is independent of the solution being used and we have the same noise model as [110], the same formulation can be used here. Specifically, the CRLBs for the location variables are given by the corresponding diagonal elements of the inverse of the Fisher information matrix

$$\begin{aligned} \boldsymbol{F}_{(2m\times 2m)} &= \boldsymbol{H}_a \ \mathbf{blkdiag}^{-1}(\{\boldsymbol{\Psi}_i,\ i\in\mathcal{N}_a\})\ \boldsymbol{H}_a^T \\ &+ \boldsymbol{H}_s \ \mathbf{diag}^{-1}(\{\sigma_{ij}^2,\ (i,j)\in\mathcal{E}\})\ \boldsymbol{H}_s^T, \end{aligned} \tag{3.13}$$

where $\boldsymbol{H}_{a,\ (2m\times 2k)} \doteq [\boldsymbol{I}_{(2k)}\ \mathbf{0}_{(2k\times 2m-2k)}]^T$, and

$$\begin{aligned} \boldsymbol{H}_{s,\ (2m\times 2|\mathcal{E}|)} \doteq \mathbf{cat}(\{[\ \ 0\ldots\ \underbrace{(\boldsymbol{x}_i^o-\boldsymbol{x}_j^o)^T/d_{ij}^o}_{(2i-1)\text{st and } 2i\text{th element}}\ \ldots \\ 0\ldots\ \underbrace{(\boldsymbol{x}_j^o-\boldsymbol{x}_i^o)^T/d_{ij}^o}_{(2j-1)\text{st and } 2j\text{th element}}\ \ldots 0]^T,\ (i,j)\in\mathcal{E}\}). \end{aligned}$$

That is, each column of $\boldsymbol{H}_s$ contains only 2 non-zero elements corresponding to an edge, and $\mathbf{0}$, $\mathbf{diag}(.)$, $\mathbf{blkdiag}(.)$, and $\mathbf{cat}(.)$ denote all-zero, diagonal, block diagonal, and column-wise-concatenated matrices, respectively.

3.3.2 Combination of Robust SOCP and SDP

As suggested by Tseng [106], the SOCP and SDP problems can be mixed in order to provide an accuracy-complexity tradeoff for the localization problem. Such a combination is possible by dividing the set of nodes into two

sets $\mathcal{N}_{\text{socp}}$ and $\mathcal{N}_{\text{sdp}}$ and running SOCP and SDP for these sets with the corresponding ranging information, respectively. Specifically, we have

$$\begin{aligned}
\min_{\substack{\boldsymbol{X},\boldsymbol{Y},\{\boldsymbol{\Xi}_i\},\{\gamma_{ij}\},\\ \{r_{ij}\},\{\boldsymbol{x}_i\},\boldsymbol{u},\{q_{ij}\},v}} \quad & v \quad + \quad \sum_{(i,j)\in\mathcal{E}_{\text{sdp}}} g_{ij}^2\left(\gamma_{ij} - 2d_{ij}r_{ij}\right) \\
& + \quad \sum_{i\in\mathcal{N}_{a,\text{sdp}}} \left(\mathbf{tr}\left(\boldsymbol{\Psi}_i^{-1}\boldsymbol{\Xi}_i\right) - 2\boldsymbol{a}_i^T\boldsymbol{\Psi}_i^{-1}\boldsymbol{x}_i\right) \qquad (3.14)\\
\text{subject to} \quad & \text{(3.9b)-(3.9h) for } \mathcal{N}_{\text{sdp}},\mathcal{E}_{\text{sdp}},\mathcal{D}_{\text{sdp}},\\
& \text{(3.7b)-(3.7d) and (3.8) for } \mathcal{N}_{\text{socp}},\mathcal{E}_{\text{socp}},\mathcal{D}_{\text{socp}},
\end{aligned}$$

where subscripts 'sdp' and 'socp' on $\mathcal{N},\mathcal{E},\mathcal{D}$ indicate the sets of nodes, links and ranging measurements belonging to SDP and SOCP sub problems, respectively. Note that in general there is no reason to force completely separate problem sets, i.e. one can have $\mathcal{N}_{\text{socp}} \cap \mathcal{N}_{\text{sdp}} \neq \emptyset$.

The main task here is to efficiently assign the nodes to these two problem sets so that the overall performance, which can be a function of both computational complexity and localization accuracy, is optimized. Here we propose a simple hybrid algorithm which is faster than robust SDP and provides a better accuracy compared to robust SOCP.

- Step 1: Solve robust SOCP problem (3.7) for the set of all sensors and anchors $\mathcal{N}_{\text{socp}} = \mathcal{N}$.

- Step 2: Let $\mathcal{B}$ be the set of tight links in the SOCP solution as defined in Section 3.2. Then, construct $\mathcal{N}_{\text{sdp}} = \{i \text{ s. t. } \forall(i,j) \in \mathcal{E} : (i,j) \notin \mathcal{B}\} \cup \mathcal{N}_a$. In other words, the robust SDP is solved over the subset of

nodes without tight links, as well as anchors.

Note that the method in (3.14) is more general than the idea proposed in [106], in the sense that we allow combined optimizations where $\mathcal{N}_{\text{sdp}} \cap \mathcal{N}_{\text{socp}} \neq \emptyset$. In fact, what is novel about the proposed combined method is that we use the SOCP result over $\mathcal{N}_{\text{socp}} = \mathcal{N}$ to determine $\mathcal{N}_{\text{sdp}}$. We should also mention that for sparse networks, a subset of tight nodes can be kept for step 2 to avoid graph disconnectivity [157]. This technique is however not used in our simulations for the combination algorithm since we have considered sufficiently dense topologies.

3.4 Extensions of the SOCP Formulation

In this section we provide different extensions to the SOCP formulation in (3.7) We first give a distributed version of the problem (Section 3.4.1) and compare the complexity of different centralized and distributed localization methods (Section 3.4.2). Then, we consider the case that the covariance matrices of the uncertainty model, $\mathbf{\Psi}_i$, are unknown, and propose an EM algorithm to iteratively estimate these parameters (Section 3.4.3). Finally, we mention a gradient-based refinement algorithm which can be applied to the results obtained by the robust SOCP or SDP methods in order to reduce their positioning error (Section 3.4.4).

3.4.1 Distributed SOCP-based Robust Localization Algorithm

Another attractive feature of the SOCP relaxation for the robust localization problem is its potential for distributed implementation, which allows the optimization problem to be divided into a number of smaller sub problems that can be solved locally at each node. These sub problems will depend on the position of the neighboring nodes. Hence, after the step of solving the sub problems locally, the nodes exchange the estimates of their positions with neighbor nodes.

A distributed algorithm was proposed for network localization with perfectly known anchor positions in [105]. In this case, the local sub problems are solved only at the general sensor nodes and not at the anchors. We generalize this distributed algorithm to the robust localization problem with uncertain anchor positions. Consider the robust localization problem in (3.5). It can be written as

$$\min_{\boldsymbol{x}_i, i\in\mathcal{N}} \sum_{(i,j)\in\mathcal{E}} g_{ij}^2 \left(q_{ij} - d_{ij}\right)^2 + \sum_{i\in\mathcal{N}_a} (\boldsymbol{a}_i - \boldsymbol{x}_i)^T {\boldsymbol{\Psi}_i}^{-1} (\boldsymbol{a}_i - \boldsymbol{x}_i) \tag{3.15a}$$

$$\text{subject to} \quad \|\boldsymbol{x}_i - \boldsymbol{x}_j\| = q_{ij}, \quad (i,j) \in \mathcal{E}, \tag{3.15b}$$

where constraint (3.15b) can be replaced by an inequality constraint for the SOCP relaxation. Using the barrier function approach, cf. [105, 114, 158], the relaxed constrained problem can be approximated as the following

unconstrained problem:

$$\min_{\boldsymbol{x}_i, i\in\mathcal{N}, q_{ij}, (i,j)\in\mathcal{E}} \sum_{(i,j)\in\mathcal{E}} g_{ij}^2 \left(q_{ij} - d_{ij}\right)^2 + \sum_{i\in\mathcal{N}_a} (\boldsymbol{a}_i - \boldsymbol{x}_i)^T {\boldsymbol{\Psi}_i}^{-1} (\boldsymbol{a}_i - \boldsymbol{x}_i) + \sum_{(i,j)\in\mathcal{E}} B(\|\boldsymbol{x}_i - \boldsymbol{x}_j\|^2 - q_{ij}^2), \tag{3.16a}$$

where $B(.)$ is a properly chosen barrier function, such as the *logarithmic barrier* function $B(z) = -\frac{1}{c}\log(-z)$ for a large constant $c \gg 1$. Now, the problem in (3.16) is partially separable and each term in the summation can be minimized independently at each node i using only information about the positions $\boldsymbol{x}_j$ and ranging information d_{ij} of the set of its neighbor nodes, $\mathcal{K}_i$ [105]. Using an approach similar to the one used in the previous section, we can formulate the local sub problems to be solved at each anchor or general sensor node. Specifically, for each general node $i \in \mathcal{N}_s$, the local sub problem can be approximated by iteratively solving[9]

$$\min_{\boldsymbol{x}_i, t_{ij}, q_{ij}, v_i,} \quad v_i \tag{3.17a}$$

$$\text{subject to} \quad \|\boldsymbol{u}_{t,i}\| \leq v_i, \tag{3.17b}$$

$$g_{ij}\,|q_{ij} - d_{ij}| \leq t_{ij}, \quad j \in \mathcal{K}_i, \tag{3.17c}$$

$$\|\boldsymbol{x}_i - \boldsymbol{x}_j\| \leq q_{ij}, \quad j \in \mathcal{K}_i, \tag{3.17d}$$

where $\boldsymbol{u}_{t,i} \doteq [t_{ij}\ j \in \mathcal{K}_i]$. Moreover, for each anchor node $i \in \mathcal{N}_a$, the local

[9] In general, there is no analytical proof that iteratively solving (3.17), (3.18) converges to the optimal solution of (3.7) [159], but this is usually the case in the simulations.

sub problem can be approximated by solving

$$\min_{\boldsymbol{x}_i, t_{ij}, q_{ij}, s_i, v_i} \quad v_i \tag{3.18a}$$

$$\text{subject to} \quad \|\boldsymbol{u}_{t,s,i}\| \leq v_i, \tag{3.18b}$$

$$\|\boldsymbol{\Psi}_i^{-1/2}(\boldsymbol{a}_i - \boldsymbol{x}_i)\| \leq s_i, \tag{3.18c}$$

$$g_{ij}\,|q_{ij} - d_{ij}| \leq t_{ij}, \quad j \in \mathcal{K}_i, \tag{3.18d}$$

$$\|\boldsymbol{x}_i - \boldsymbol{x}_j\| \leq q_{ij}, \quad j \in \mathcal{K}_i, \tag{3.18e}$$

where $\boldsymbol{u}_{t,s,i} \doteq [t_{ij}\ j \in \mathcal{K}_i,\ s_i]$. We observe that the local sub problem of each anchor is different from that of a general sensor node due to the robust formulation of the problem. However, these two formulations can be unified in the same way as the centralized version, i.e. by adding priors for sensors.

In an attempt to treat the case of uncertain anchor positions, the distributed algorithm for the case of known anchor positions in [105] suggested including the anchors in solving local sub problems. In their method, the sensors first perform a local SOCP phase to find their locations assuming perfect anchor positions. Then, the anchors use these estimations to refine their location information. In the third phase, the general sensors run a new round of local SOCP based on the refined location of anchors. However, the sub problems at sensors are run without taking into account the anchor uncertainty, and the sub problems at anchors are run without taking into account the prior information. Hence, a better performance of the proposed distributed robust approach is expected, as will be demonstrated in Section 3.6.

As the final remark, we should note that the combined robust SOCP and SDP in Section 3.3.2 can be made distributed. In fact, the SOCP part of the proposed hybrid method (3.14) can be solved in a distributed manner using (3.17) and (3.18) above, and the SDP part can be also solved by following the existing distributed SDP methods e.g. [109]. However, distributed SDP would require clustering for a good accuracy and can still have a higher complexity in a highly-connected network. Hence, we focus on the distributed robust SOCP in our simulations and provide results only for the centralized combined method. When more accuracy is desired for the boundary nodes, the proposed distributed SOCP may be replaced by the distributed SDP with appropriate clustering methods and/or heuristic anchor refinements at the cost of a higher complexity.

3.4.2 Complexity Analysis

Table 3.1 shows the number of variables and constraints for robust and non-robust versions of SDP and SOCP in terms of number of optimization variables, and equality and inequality constraints. Also, the number of variables and constraints for the robust edge-based SDP (ESDP) [110] and SOCP (ESOCP) [114] are shown. Since the complexity is an increasing function of both number and size of the constraints, for an easier comparison we also show a combined metric for constraints which is the product of their size and their number in the last column. In this table, $|\mathcal{K}_i|$ denotes the number of neighbours of node i, and $|\mathcal{E}|$ is the number of links in the graph.

Table 3.1: Complexity of robust and non-robust SDP and SOCP.

Method	Variables	Equality constraints and their size	Inequality constraints and their size	Total Constraints (Number × Size)
Standard SOCP [106]	$2\|\mathcal{E}\| + \|\mathcal{N}\| - \|\mathcal{N}_a\|$ +1	0	$\|\mathcal{E}\|$ of size 2, $\|\mathcal{E}\|$ of size 3, and 1 of size $\|\mathcal{E}\| + 1$	$6\|\mathcal{E}\|$+1
Robust SOCP (3.7)	$2\|\mathcal{E}\| + \|\mathcal{N}\| + \|\mathcal{N}_a\|$ +1	0	$\|\mathcal{E}\| + \|\mathcal{N}_a\|$ of size 2, $\|\mathcal{E}\|$ of size 3, and	$6\|\mathcal{E}\|$+3$\|\mathcal{N}_a\|$+1

Continued on next page

Method	Variables	Equality constraints and their size	Inequality constraints and their size	Total Constraints (Number × Size)
			1 of size $\|\mathcal{E}\| + \|\mathcal{N}_a\| + 1$	
Distributed Robust SOCP Sensors (3.17)	$2\|\mathcal{K}_i\| + 2$	0	$\|\mathcal{K}_i\|$ of size 2, $\|\mathcal{K}_i\|$ of size 3, and 1 of size $\|\mathcal{K}_i\| + 1$	6 $\|\mathcal{K}_i\|$+1

Continued on next page

Method	Variables	Equality constraints and their size	Inequality constraints and their size	Total Constraints (Number × Size)
Anchors (3.18)	$2\|\mathcal{K}_i\|+3$	0	$\|\mathcal{K}_i\|+1$ of size 2, $\|\mathcal{K}_i\|$ of size 3, and 1 of size $\|\mathcal{K}_i\|+2$	6 $\|\mathcal{K}_i\|$+3
Distributed Robust ESOCP [114], each node	$2\|\mathcal{K}_i\|+3$	0	2 of size 3,$\|\mathcal{K}_i\|$ of size 4, and 1 of size $\|\mathcal{K}_i\|+2$	5 $\|\mathcal{K}_i\|$ +8

Continued on next page

Method	Variables	Equality constraints and their size	Inequality constraints and their size	Total Constraints (Number × Size)
Standard SDP [108]	$2\,\lvert\mathcal{E}\rvert$ $+(\lvert\mathcal{N}\rvert - \lvert\mathcal{N}_a\rvert)^2$ $+(\lvert\mathcal{N}\rvert - \lvert\mathcal{N}_a\rvert)$	1 of size 2, $\lvert\mathcal{E}\rvert$ of size 5, and $\lvert\mathcal{N}\rvert - \lvert\mathcal{N}_a\rvert$ of size 3	$\lvert\mathcal{E}\rvert$ of size 2, and 1 of size $\lvert\mathcal{N}\rvert + 2$	$7\lvert\mathcal{E}\rvert + 4\,\lvert\mathcal{N}\rvert$ - 3 $\lvert\mathcal{N}_a\rvert$ +2
Robust SDP (3.9) [110]	$2\,\lvert\mathcal{E}\rvert$ $+(\lvert\mathcal{N}\rvert + 2)^2$ $+4\,\lvert\mathcal{N}_a\rvert + \lvert\mathcal{N}\rvert$	1 of size 2, $\lvert\mathcal{E}\rvert$ of size 5, and $\lvert\mathcal{N}\rvert + \lvert\mathcal{N}_a\rvert$ of size 3	$\lvert\mathcal{E}\rvert$ of size 2, $\lvert\mathcal{N}_a\rvert$ of size 3, and 1 of size $\lvert\mathcal{N}\rvert + 2$	$7\,\lvert\mathcal{E}\rvert + 4\,\lvert\mathcal{N}\rvert$ + 6 $\lvert\mathcal{N}_a\rvert$ + 4

Continued on next page

Method	Variables	Equality constraints and their size	Inequality constraints and their size	Total Constraints (Number × Size)
Robust ESDP [110]	$2\,\lvert\mathcal{E}\rvert$ $+(\lvert\mathcal{N}\rvert+2)^2$ $+4\,\lvert\mathcal{N}_a\rvert+\lvert\mathcal{N}\rvert$	$\lvert\mathcal{E}\rvert$ of size 5, and $\lvert\mathcal{N}_a\rvert$ of size 3	$\lvert\mathcal{E}\rvert$ of size 2, $\lvert\mathcal{N}_a\rvert$ of size 3, and $\lvert\mathcal{E}\rvert$ of size 4	$11\,\lvert\mathcal{E}\rvert + 6\,\lvert\mathcal{N}_a\rvert$

As can be seen from Table 3.1, the robust SDP approach (3.9) which considers anchor uncertainty [110], has $2\,|\mathcal{E}| + (|\mathcal{N}| + 2)^2 + 4\,|\mathcal{N}_a| + |\mathcal{N}|$ variables, while the proposed robust SOCP in (3.7) has only $2\,|\mathcal{E}| + |\mathcal{N}| + |\mathcal{N}_a| + 1$ variables. Since typically we have $|\mathcal{E}| = \Omega(|\mathcal{N}|)$ [106], the number of variables grow linearly with the number of nodes ($\Omega(|\mathcal{N}|)$) compared to a quadratic growth ($\Omega(|\mathcal{N}|^2)$) for robust SDP [106, 108]. This enables SOCP to solve large problems with e.g. $|\mathcal{N}| > 200$ nodes.

In general, interior point methods can solve SOCP more efficiently than SDP. According to [160], each iteration of SOCP entails a cubic computational complexity ($O(|\mathcal{N}|^3)$), while this is quartic ($O(|\mathcal{N}|^4)$) for SDP. The numbers of variables and constraints in the second and sixth rows of Table 3.1 also show that when the network is sparse, the complexity is significantly lower for robust SOCP (RSOCP) compared to robust SDP (RSDP). In the other extreme case of a highly dense network, i.e. $|\mathcal{E}| = \Omega(|\mathcal{N}|^2)$, the number of RSOCP variables become asymptotically similar to those of RSDP, but the constraint metric still remains smaller by an asymptotic factor of 6 to 7.

It can be also observed from Table 3.1 that the distributed SOCP (3.17) reduces the number of variables and constraints to the order of the number of neighbouring nodes (node connectivity). Specifically, we have $|\mathcal{N}_s|$ distributed general node sub problems (3.17) with $2|\mathcal{K}_i| + 2$ variables and the constraint metric of $6|\mathcal{K}_i| + 1$; and $|\mathcal{N}_a|$ anchor sub problems (3.18) with $2|\mathcal{K}_i| + 3$ variables and the constraint metric of $6|\mathcal{K}_i| + 3$. Since these small sub problems are solved in parallel at different nodes, the distributed robust SOCP is scalable to the network size. This fact also holds for the robust

ESOCP [114], which has almost similar number of variables and constraint metric to our method. We also observe that the robust SOCP has a smaller number of variables and constraint metric compared to the robust ESDP.

3.4.3 An Expectation Maximization (EM) Approach for Gaussian Uncertainty with Unknown Covariance

We have formulated the robust SOCP (3.7) for anchor position uncertainties assuming known covariances, $\mathbf{\Psi}_i$, $i \in \mathcal{N}_a$. In practice, however, the sensors' knowledge about the anchor position errors may be limited, and thus the covariance matrices might be unknown. In this case, given $n_{\mathrm{m}} \geq 2$ measurements $\{\boldsymbol{a}_{i,1}, \ldots, \boldsymbol{a}_{i,n_{\mathrm{m}}}\}$ are available, we can iteratively estimate $\mathbf{\Psi}_i$ by the EM method as explained in the following. The n_{m} measurements can be obtained prior to the start of the robust localization by inquiring the underlying anchor location provider, e.g. GPS, cellular towers or buoys [110].

The log-likelihood of the observed data given the current anchor location and covariance matrix approximations, $\mathbf{\Psi}_i$, can be written as

$$\begin{aligned} L_i &\doteq \log P\left(\{\boldsymbol{a}_{i,n}\} \,|\mathbf{\Psi}_i, \boldsymbol{x}_i\right) = \\ &- \frac{n_{\mathrm{m}}}{2} \log\left(2\pi \left|{\mathbf{\Psi}_i}^{-1}\right|\right) - \frac{1}{2} \sum_{n=1}^{n_{\mathrm{m}}} \left(\boldsymbol{a}_{i,n} - \boldsymbol{x}_i\right)^T {\mathbf{\Psi}_i}^{-1} \left(\boldsymbol{a}_{i,n} - \boldsymbol{x}_i\right) \end{aligned} \quad (3.19)$$

In the EM algorithm, the complete log-likelihood is first computed for a given set of observations (E step), and then the parameters are maximized based on this expression (M step). These steps are iteratively executed until they converge to a local optimum point for the likelihood.

The E step: Let $\mathbf{\Psi}_i^{\ell}$ be the estimated covariance matrix of $\boldsymbol{w}_i$ at it-

eration ℓ. The expectation of the complete log-likelihhod function can be written as

$$Q_i(\boldsymbol{\Psi}_i, \boldsymbol{\Psi}_i^\ell) \doteq \mathbb{E}_{\boldsymbol{x}_i|\{\boldsymbol{a}_{i,n}\},\boldsymbol{\Psi}_i^\ell} \left\{ \log P\left(\boldsymbol{x}_i, \{\boldsymbol{a}_{i,n}\} | \boldsymbol{\Psi}_i^\ell\right) \right\} \tag{3.20}$$

In order to calculate the expectation in (3.20), a probability distribution of $\boldsymbol{x}_i$ given $\boldsymbol{a}_{i,n}$ and $\boldsymbol{\Psi}_i^\ell$ is needed. However, such a distribution might in general be difficult to find since in our problem $\boldsymbol{x}_i$ also depends on the distance measurements in $\mathcal{D}$. In order to simplify the problem, we propose that this distribution can be approximated as $\delta(\boldsymbol{x}_i - \boldsymbol{x}_i^{\ell+1})$, where δ is the Dirac delta function and $\boldsymbol{x}_i^{\ell+1}$ is the anchor estimate obtained by running the robust SOCP optimization (3.7)[10].

Another possible simplification on (3.20) can be applied by writing the complete log-likelihood as

$$\log P\left(\boldsymbol{x}_i^{\ell+1}, \{\boldsymbol{a}_{i,n}\} | \boldsymbol{\Psi}_i^\ell\right) = \log P\left(\{\boldsymbol{a}_{i,n}\} | \boldsymbol{\Psi}_i, \boldsymbol{x}_i^{\ell+1}\right) + \log P(\boldsymbol{x}_i^{\ell+1} | \boldsymbol{\Psi}_i), \tag{3.21}$$

and noting that the term $P(\boldsymbol{x}_i^{\ell+1}|\boldsymbol{\Psi}_i)$ can be treated as a constant, since the covariance matrix does not reveal information about the mean. Therefore, we can use (3.19) as the likelihood in the maximization step.

The M step: The maximization step involves maximizing the Q-function after the above-mentioned E-step,

$$\boldsymbol{\Psi}_i^{\ell+1} = \arg\max_{\boldsymbol{\Psi}} Q_i = \arg\max_{\boldsymbol{\Psi}} \left(L_i | \boldsymbol{x}_i = \boldsymbol{x}_i^{\ell+1} \right) \tag{3.22}$$

[10]Note that RSOCP also requires a location estimate for anchors as input, and thus we pass our current estimates $\boldsymbol{x}_i^\ell$ as well as $\boldsymbol{\Psi}_i^\ell$ to RSOCP to obtain $\boldsymbol{x}_i^{\ell+1}$.

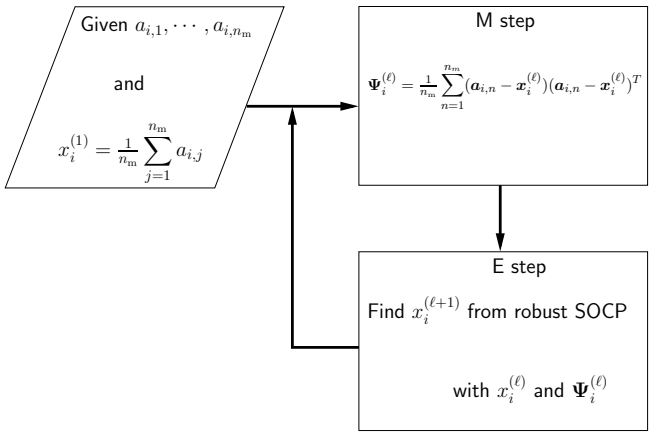

Figure 3.1: A schematic of the proposed EM algorithm. In each E step, a robust SOCP is executed and then the covariance is estimated in the M step.

This can be performed by taking the derivative of L_i with respect to $\boldsymbol{\Psi}_i$ and finding the corresponding root. This results in

$$\boldsymbol{\Psi}_i^{\ell+1} = \frac{1}{n_{\mathrm{m}}} \sum_{n=1}^{n_{\mathrm{m}}} (\boldsymbol{a}_{i,n} - \boldsymbol{x}_i) (\boldsymbol{a}_{i,n} - \boldsymbol{x}_i)^T , \tag{3.23}$$

where $\boldsymbol{x}_i$ is the expected location of $\boldsymbol{a}_i$ which is obtained from the robust SOCP algorithm in the E step.

We stop the EM algorithm at iteration ℓ_0 when $L_i^{\ell_0+1} - L_i^{\ell_0} < \epsilon = 0.1$, where the log-likelihood L_i for each EM iteration is obtained from (3.19). Furthermore, the EM complexity can be approximated as O(ℓ_0 O(RSOCP)), where O(RSOCP) is the RSOCP complexity from Table 3.1. Figure 3.1 shows the flowchart of the EM algorithm. As can be seen, the robust SOCP iteratively calculates new the anchor position estimations in the E step, which is utilized in the M step (3.23) for finding a better approximation

for $\mathbf{\Psi}_i$. The iterations continue until the values of L_i converge to a local optimum point. As it is typical in EM, random restart points for $\mathbf{\Psi}_i^0$ can be considered to find different local optima and choose the best. We will use the sample covariance of measurements as the initial value of $\mathbf{\Psi}_i^0$. It is interesting to note that the proposed EM algorithm can be also viewed as an offline decision feedback method for estimating the covariance [161].

3.4.4 Gradient Descent Refinement Method

It is worth pointing out that an iterative gradient-descent (GD) method can be employed in order to further refine the results obtained by the robust SDP or SOCP convex optimizations [108, Sec. V]. In each iteration ℓ of the GD method, the location of a sensor node is updated[11] by moving in the opposite direction of the gradient. Specifically, let

$$f(\boldsymbol{x}_i^\ell) = \sum_{j \in \mathcal{K}_i,} g_{ij}^2 \left(\|\boldsymbol{x}_i^\ell - \boldsymbol{x}_j^\ell\| - d_{ij} \right)^2$$

be the local value of objective for sensor i, i.e. the summation of terms in (3.5) which depend on $\boldsymbol{x}_i$, at iteration ℓ. Then,

$$\boldsymbol{x}_i^{\ell+1} = \boldsymbol{x}_i^\ell - \alpha \frac{\partial f(\boldsymbol{x}_i^\ell)}{\partial \boldsymbol{x}_i^\ell}, \quad i \in \mathcal{N}_s$$

where α is the step size, and the gradient is given by,

$$\frac{\partial f(\boldsymbol{x}_i^\ell)}{\partial \boldsymbol{x}_i^\ell} = \sum_{j \in \mathcal{K}_i,} 2 g_{ij}^2 (\boldsymbol{x}_i^\ell - \boldsymbol{x}_j^\ell)(1 - \frac{d_{ij}}{\|\boldsymbol{x}_i^\ell - \boldsymbol{x}_j^\ell\|}).$$

[11] For simplicity, anchors are excluded from the GD refinement.

It is shown in [108] that GD can refine the location of sensor nodes found by the convex optimization. However, GD fails to provide a good solution if a good initial solution is unavailable.

3.5 Robust Localization in Mobile Sensor Networks

In this section we extend our robust SOCP solution to improve the localization and tracking accuracy of *mobile* sensor networks. These extensions follow from interesting properties of the robust SOCP proved in Proposition 3.1, which further give rise to the following properties:

Property 1: All nodes are estimated within the convex hull of their neighbours. This fact follows from the proof of Proposition 3.1 c) and suggests that the localization error of a node is also a function of its neighbor's errors. If the neighbours have a high localization error, the surrounding convex hull is looser and thus the node may have a high error as well. On the other hand, a node which is estimated within a convex hull of its tight neighbours is expected to have a small localization error. We will see in Section 3.5.1 that this fact can help achieving a higher accuracy in formation control.

Property 2: According to the same proposition, the estimated location of all nodes are inside the convex hull of anchors, denoted by $\mathcal{C}$, at the solution of RSOCP. More generally and less rigorously, it is observed in the simulations that the nodes which are actually inside the convex hull, especially those in the center of convex hull, have a high probability of

being tightly-connected. This is also supported by our simulations and we express it as a general rule of thumb without providing a mathematical proof. Section 3.5.2 uses this observation for detecting boundary trespassing in a mobile sensor network.

We now focus on two specific applications for mobile sensor networks, namely formation control and tracking the nodes on the boundaries, and use the properties which are specific to SOCP in order to adjust and predict the location of nodes for a better localization and tracking accuracy. We perform several numerical simulations to confirm the effectiveness of our heuristic algorithms.

3.5.1 Robust Formation Control

We now consider a mobile network in which mobile sensors should achieve a desired formation after a sequence of coordinated movements. Here, the aim is controlling the movement of sensor nodes rather than detecting it. The core part of formation control, **form**, is the SOCP formulation (8) in [122] in which a shape is defined by a linear constraint $Ax = 0$ and the objective is to minimize the total traveled distance. Note that the definition of a shape by this constraint allows for 4 degrees of freedom, namely 2-D translation, scale and rotation. Additional constraints for forcing a specific translation, scale and rotation are also derived in [122]. In this formation control setting, it is highly desirable that the nodes are initially unambiguously-localizable [115, 122]. In order to do so, we provide the following solution.

3.5.1.1 The Tightening Procedure

We now show that our robust SOCP can be used for providing an unambiguous localization with low complexity. Specifically, we use the Property 1 in the previous section to direct a sensor node i which is ambiguously localized, or equivalently $i \notin \mathcal{M}(t)$, to a location which has a better chance of being unambiguously localized.

We propose a heuristic movement to this end, in which every non-tight node moves towards the center mass of its unambiguously localized neighbors, while tight nodes remain at their place. Mathematically, node $i \notin \mathcal{M}(t)$ chooses its velocity vector as

$$\boldsymbol{v}_i(t+1) = \frac{1}{|\mathcal{J}_i(t)|\,\Delta t} \sum_{j \in \mathcal{J}_i(t)} \boldsymbol{x}_j(t) - \boldsymbol{x}_i(t), \tag{3.24}$$

where Δt is the time unit, and $\mathcal{J}_i(t) = \{j : (i,j) \in \mathcal{E} \text{ and } j \in \mathcal{M}(t)\}$ is the set of neighbor nodes of i which are tightly-connected[12] at time t. Note that if there is a limit for speed of movement, $v_{\max}$, then if $||\boldsymbol{v}_i(t+1)|| > v_{\max}$, the velocity vector in (3.24) should be further normalized as

$$\boldsymbol{v}_i(t+1) \leftarrow \frac{v_{\max}}{||\boldsymbol{v}_i(t+1)||} \boldsymbol{v}_i(t+1).$$

As we will see in the simulation results, this strategy is able to make almost all of the mobile sensors unambiguously localizable after only a few rounds of movements.

[12] In the special case when $|\mathcal{J}_i(t)| = 0$, i.e. node i does not have any tight neighbors, it can move towards the center of convex hull, i.e. by setting $\mathcal{J}_i(t) = \mathcal{C}(t)$.

3.5.2 Detecting Boundary Trespassing

Property 2 suggests that for a node whose actual location is outside the convex hull of anchors, the estimated location would be close to the boundaries of $\mathcal{C}(t)$. Therefore, it is reasonable to assume that if a sensor node is not tightly-connected and its estimated location is near the border of the convex hull, there is a high probability that the node is actually located outside the convex hull. This important observation about the SOCP solution implies that we can distinguish those nodes which enter or exit the convex hull of anchors in a mobile scenario. Specifically, a node is marked as "exiting" the convex hull at time t if

$$i \in \mathcal{M}(t-1) \text{ and } i \notin \mathcal{M}(t) \text{ and } \delta_i(t) \leq \epsilon_d,$$

where $\delta_i(t)$ is the minimum distance of a node's location estimates at time t from the edges of the current convex hull of anchors, $\mathcal{C}(t)$, and ϵ_d is a threshold chosen according to the desired false alarm and missed detection probability as a function of maximum speed. Similarly, a sensor is marked as "entering" the convex hull at time t if

$$i \notin \mathcal{M}(t-1) \text{ and } i \in \mathcal{M}(t) \text{ and } \delta_i(t) \leq \epsilon_d.$$

3.6 Performance Evaluation

In this section we examine the performance of the proposed localization methods by means of simulations. We use the `CVX` Matlab toolbox [162] for

solving the devised robust SOCP (RSOCP, (3.7)) and the benchmark robust SDP (RSDP, (3.9)) optimizations. The distributed method is considered only in the last sub-section. Simulations are performed on a computer with a 3.07 GHz processor and 8.0 GB of RAM. For the simulations, nodes are located in a 40 m $\times$ 40 m area. Unless specified otherwise for a simulation setting, the communication range R_c in each topology is adjusted based on $|\mathcal{N}|$ for obtaining the average connectivity of $\overline{|\mathcal{K}_i|} = 4$ in the network. We apply a fixed link error model with equal noise variances σ_{ij}^2 for all links $(i,j) \in \mathcal{E}$, and also a variable link error model where $\sigma_{ij}^2 = \sigma_d^2\, d_{ij}^2$, and σ_d^2 is the noise variance for the unit distance, i.e., a link with a longer distance has a larger noise variance [110]. We consider the positioning mean squared error (MSE) in dBm^2,

$$\eta = 10 \log_{10} \left(\frac{1}{|\mathcal{N}|} \sum_{i \in \mathcal{N}} \|\boldsymbol{x}_i - \boldsymbol{x}_i^o\|^2 \right),$$

as the performance criterion. A smaller positioning MSE indicates a better localization performance.

3.6.1 Performance of the Robust SOCP

Figure 3.2 shows the RSOCP and RSDP localization results for a sample scenario from [110] with $|\mathcal{N}_s| = 10$ general sensors and $|\mathcal{N}_a| = 8$ anchors and the communication range of $R_c = 25$ m ($\overline{|\mathcal{K}_i|} = 8.7$). Also, the noise variance parameter and the anchor uncertainty covariance matrix are set to $\sigma_d^2 = -20$ dBm^2 and $\boldsymbol{\Psi}_i = -10\boldsymbol{I}_2$ dBm^2, respectively. As can be seen, both robust methods are able to locate anchors and general sensors with

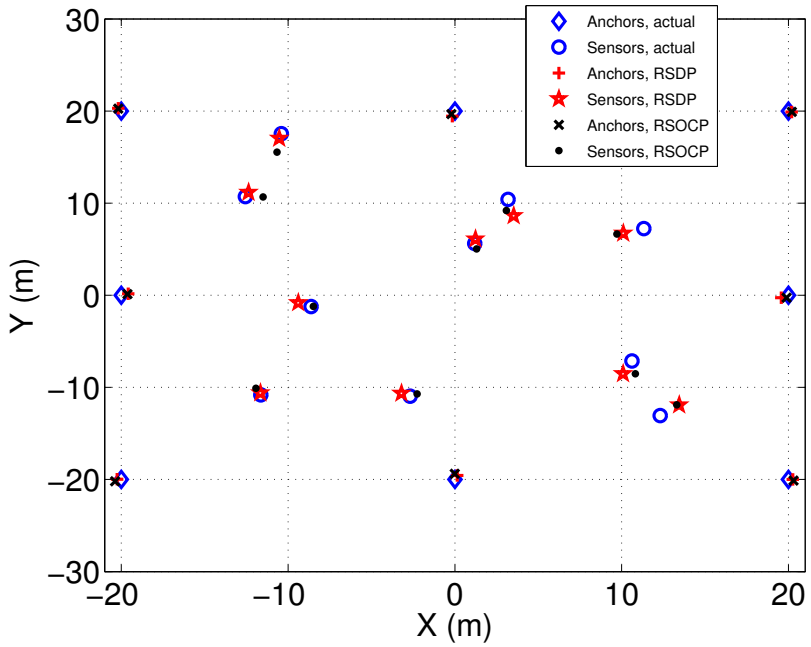

Figure 3.2: Location of nodes found by the RSDP and RSOCP relaxations for a sample scenario with $|\mathcal{N}_a| = 8$ anchors, $|\mathcal{N}_s| = 10$ general sensors, $R_c = 25$ m ($\overline{|\mathcal{K}_i|} = 8.7$), $\sigma_d^2 = -20$ dBm^2, and $\boldsymbol{\Psi}_i = -10\ \boldsymbol{I}_2$ dBm^2. The blue circles and diamonds represent the actual position of general nodes and anchors, respectively; the red asterisks and plus signs show the estimated locations of general nodes and anchors by RSDP, respectively; and the black dots and crosses show the estimated locations of general nodes and anchors by the proposed RSOCP (3.7), respectively.

a small error. For the nodes located close to the origin $(0, 0)$, the RSOCP estimations are slightly more accurate than those for RSDP. For the nodes closer to the perimeter, the RSOCP error increases and becomes larger than the RSDP error. This trend is consistent with the fact that the nodes located closer to the center of the anchors' convex hull are generally localized more accurately in RSOCP. Note that this property is because of the special structure in RSOCP optimization and is generally not true for RSDP. For

example, the minimum RSDP localization error in Figure 3.2 belongs to the node located at $(-11.6, -10.8)$ m, which is far from the origin. In this scenario, the total MSE for RSOCP is $\eta_{\text{RSOCP}} = 1.35$ dBm^2, which is somewhat higher than that for RSDP ($\eta_{\text{RSDP}} = 0.50$ dBm^2) due to the tighter relaxation by RSDP.

Table 3.2 shows the positioning MSE η, number of variables and constraints, and the CPU time spent in different robust optimizations methods for solving the network in Figure 3.2. As can be seen, SOCP-based methods are faster while SDP-based methods are more accurate. Note that although robust ESDP (RESDP, [110]) has more constraints than RSDP, it is faster because the constraint sizes, i.e. number of variables involved in each constraint, are smaller.

Figure 3.3 shows the average value of positioning MSE as a function of σ_{ij}^2, for RSOCP, RESDP, and RSDP in 1000 uniformly-random network topologies with $|\mathcal{N}_s| = 35$ sensors and $|\mathcal{N}_a| = 15$ anchors. In order to observe the effect of anchor position uncertainties on the performance, we also plot the MSE of the standard SOCP, which does not take into account the anchor position uncertainties [105, 106]. We also show the MSEs after performing 50 iterations of refinement using gradient descent (GD) with step size $\alpha = 10^{-4}$. Finally, the CRLB (3.13) is also shown. The value of σ_{ij}^2 varies from -35 to -5 dBm^2 and the uncertainty covariance is set to $\boldsymbol{\Psi}_i = -10\boldsymbol{I}_2$ dBm^2.

As can be seen, RSOCP outperforms the standard SOCP in terms of MSE. While RSDP performs better than RSOCP due to the tighter relaxation on the problem, we also observe that for lower values of noise (i.e. $\sigma_{ij}^2 \leq -20$ dBm^2), none of the convex relaxations can achieve the CRLB.

Table 3.2: Performance and complexity comparison of different robust localization methods for the network in Figure 3.2. CPU runtime is defined as the time spent for solving the `CVX` problem, and it is measured using Matlab's `tic` and `toc` commands.

Method	Positioning MSE, η (dBm^2)	Number of variables	Number of constraints	CPU runtime (Sec.)
Standard SOCP	1.84	151	141	1.80
RSOCP	1.35	167	149	2.00
RESDP	0.87	590	226	2.25
RSDP	0.50	590	176	2.74

This trend has also been observed in other SDP and SOCP-based localization methods, e.g., [110, Figure 5]. The gap between the CRLB and the MSE achieved by RSDP and RSOCP can be somewhat reduced by the GD method. Not surprisingly, the RESDP performance is in between those of RSOCP and RSDP. For larger values of noise, the MSEs of all robust methods converge to the CRLB performance limit.

Figure 3.4 shows the average value of η as a function of σ_d^2 with $|\mathcal{N}_s| = 18$ sensors and $|\mathcal{N}_a| = 12$ anchors for $\boldsymbol{\Psi}_i = \kappa_i^2 \boldsymbol{I}_2$ with $\kappa_i^2 = \{-10, 0, 10\}$ dBm^2. Also, 8 of the anchors are located at the corners similar to Figure 3.2. As expected, the positioning MSE is an increasing function of noise variance in all methods. The RSOCP performance is notably improved compared to the

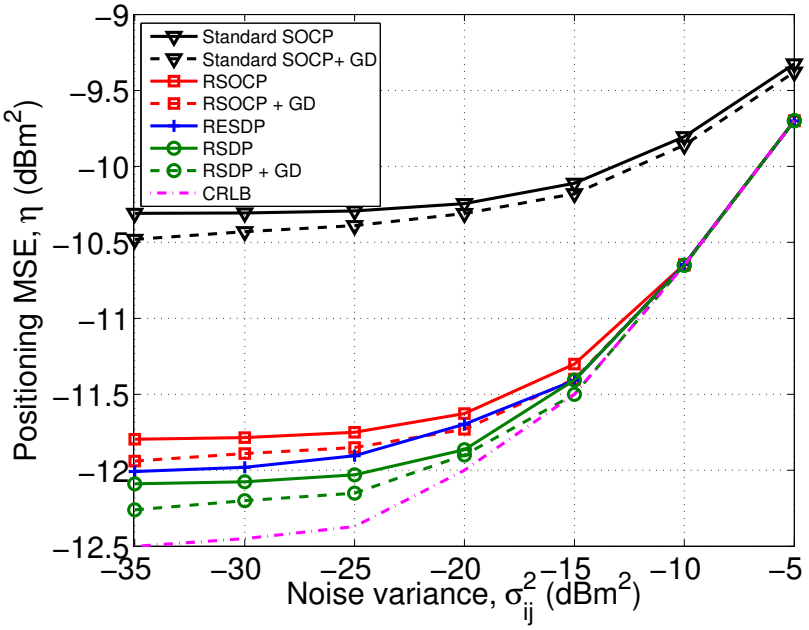

Figure 3.3: The positioning MSE of the standard SOCP, RSOCP, and RSDP with and without gradient descent (GD) refinement as well as the positioning MSE of RESDP in random topologies with $|\mathcal{N}_s| = 35$ sensors, $|\mathcal{N}_a| = 15$ anchors, and $\boldsymbol{\Psi}_i = -10\ \boldsymbol{I}_2$ dBm^2. The CRLB are also shown.

standard SOCP. Furthermore, since RSOCP is able to adjust the location of anchors, the gap between the standard and robust SOCP becomes larger by increasing anchor position uncertainties.

In order to verify the performance of the robust methods in larger scales we perform simulations in a 1 km $\times$ 1 km area with $|\mathcal{N}_s| = 105$ sensors and $|\mathcal{N}_a| = 45$ anchors and show the value of η for RSOCP and RSDP in Figure 3.5. In order to make the simulations closer to a real-life experiment, we also consider 30% chance of link failures in this scenario. In the presence of a link failure, no ranging data is used for the corresponding link in the optimization, i.e. nodes are not neighbours anymore. For this scenario, our

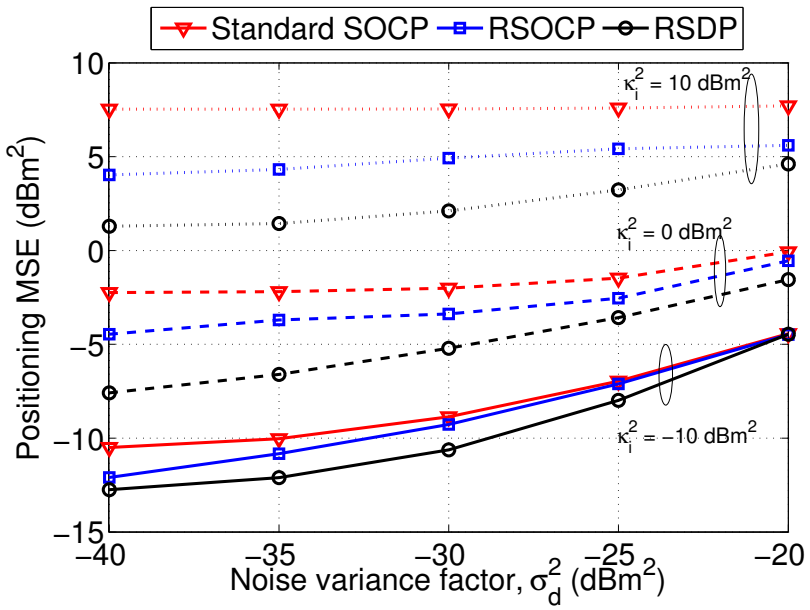

Figure 3.4: The positioning MSE, η, as a function of noise variance factor σ_d^2 in random topologies with $|\mathcal{N}_s| = 18$ sensors, $|\mathcal{N}_a| = 12$ anchors, and $\boldsymbol{\Psi}_i = \kappa_i^2 \boldsymbol{I}_2$, $\kappa_i^2 = \{-10, 0, 10\}$ dBm^2. 8 of the anchors are located at the corners.

RSOCP is able to localize the network in an average of 37 seconds and is more than twice faster than RSDP, which takes 84 seconds on average. The results of RSOCP MSE error provide an acceptable localization accuracy, always within 2.5 dBm^2 of that for RSDP. This translates to an increase of only 1.4 m in the standard deviation of localization error. Note that the localization algorithms would run faster in a network with a lower density compared to the results shown above, for example when the same number of sensors are deployed in a larger area.

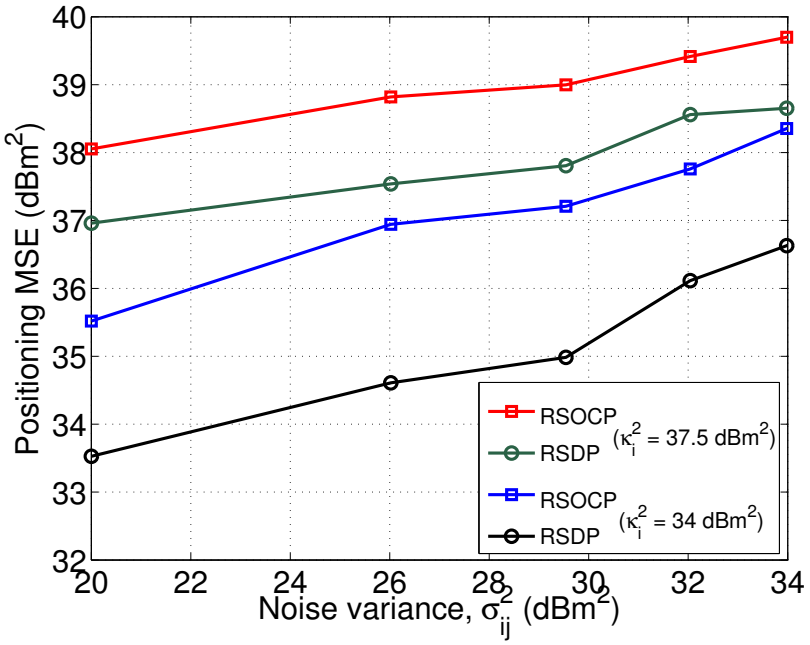

Figure 3.5: The positioning MSE in a 1 km $\times$ 1 km area with $|\mathcal{N}_s| = 105$ sensors and $|\mathcal{N}_a| = 45$ anchors. A link failure probability of 30% is considered. The link noise variance σ_{ij}^2 changes from 20 to 34 dBm^2 (i.e. 10 to 50 m of noise standard deviation) and $\boldsymbol{\Psi}_i = \kappa_i^2 \boldsymbol{I}_2$, $\kappa_i^2 = \{34, 37.5\}$ dBm^2 (i.e. a radius of 50 or 75 m uncertainty around anchors). The anchor positions are randomly chosen based on a uniform distribution.

3.6.2 Combination of RSOCP and RSDP

Next we examine the performance of the combined RSOCP and RSDP algorithm introduced in Section 3.3.2.

Figure 3.6 shows a sample network with $|\mathcal{N}_s| = 11$ sensors and $|\mathcal{N}_a| = 6$ anchors, displayed as blue circles and diamonds, respectively. First, RSOCP is executed over the entire network, resulting in the sensor and anchor estimations shown by the red squares and crosses, respectively. A threshold of 10^{-5} is used for determining the tight links. Note that the RSOCP sensor

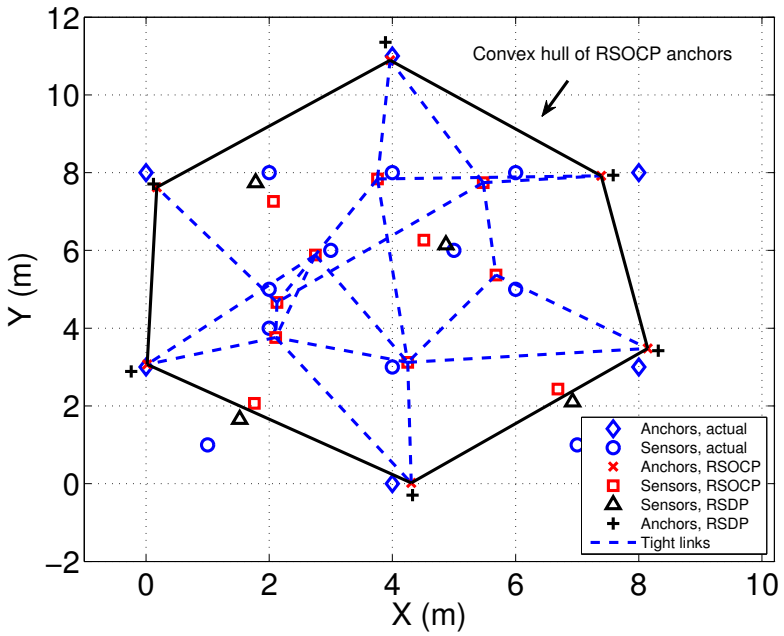

Figure 3.6: Illustration of the RSOCP-RSDP combination algorithm in a sample scenario. Communication range is $R_c = 5$ m ($\overline{|\mathcal{K}_i|} = 7.4$), and the noise variance factor and uncertainty are set to $\sigma_d^2 = -20$ dBm^2, and $\boldsymbol{\Psi}_i = -10\boldsymbol{I}_2$ dBm^2, respectively.

estimations always lie within the convex hull of estimated anchor positions (solid lines), based on Proposition 3.1 c). Seven of the sensors are precisely localized using RSOCP since they are tightly-connected. The total positioning MSE of RSOCP is -4.07 dBm^2. From the remaining four sensors which are not tight, two are located inside the convex hull. This fact shows that a node inside the convex hull is not necessarily unambiguously localizable, while the reverse is always true according to Proposition 3.1. The remaining four sensors, along with anchors, are re-localized using RSDP leading to the black triangle and plus signs for sensors and anchors, respectively, and a

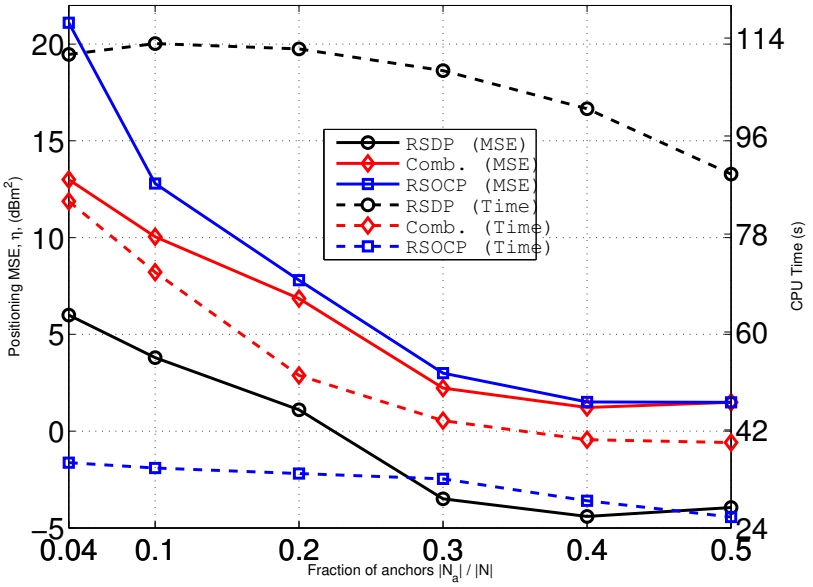

Figure 3.7: Average positioning MSE (solid lines) and time taken (dashed lines) for solving centralized RSDP, RSOCP and their combination for $|\mathcal{N}| = 200$ nodes as a function of the fraction of anchors, $\frac{|\mathcal{N}_a|}{|\mathcal{N}|}$, with $R_c = 6$ m ($\overline{|\mathcal{K}_i|} = 9.3$), $\sigma_{ij}^2 = -35$ dBm^2, and $\kappa_i^2 = 0$ dBm^2. The anchor positions are randomly chosen based on a uniform distribution.

total positioning MSE of -6.22 dBm^2 for the network.

To further demonstrate the complexity advantage of mixed RSOCP-RSDP over pure RSDP, we also investigate a network with $|\mathcal{N}_s| = 105$ sensors and $|\mathcal{N}_a| = 45$ anchors (not shown here). In this scenario, RSOCP takes 33.88 seconds, and unambiguously localizes 83 sensors. The remaining 22 sensors along with anchors are passed through RSDP, resulting in the total MSE of $\eta = 0.38$ dBm^2 in only 6.70 seconds. In the same scenario, pure RSDP over all network takes 75% more time than the combined algorithm (71.39 seconds) and its positioning MSE is $\eta_{\text{rsdp}} = -2.46$ dBm^2.

The average positioning MSE (solid lines) and the total time spent

(dashed lines) for RSOCP, RSDP, and the combined robust SDP-SOCP method in larger networks with $|\mathcal{N}| = 200$ sensors are shown in Figure 3.7. Here, the percentage of anchors $\frac{|\mathcal{N}_a|}{|\mathcal{N}|}$ varies from 4% to 50%. Since, unlike for the results in Figure 3.4, all sensors and anchors are located based on a uniform random distribution (i.e., no anchors are necessarily placed at the corners), RSOCP has a large MSE for small numbers of anchors. In this situation, the combination of RSOCP and RSDP performs significantly better than RSOCP taking twice as much time, while RSDP has the best performance with three times the computation time of RSOCP. Hence, the proposed combined method is an interesting alternative to RSOCP and RSDP, especially in sensor networks with many nodes and a relatively small number of anchors. It can be also observed from Figure 3.7 that as percentage of anchors increases, both positioning MSE and computation time for all three methods decrease. The former is due to availability of more information (i.e. anchor priors) about the network, and the latter is because of the smaller $|\mathcal{E}|$ after removing anchor-anchor links which leads to fewer variables and constraints.

3.6.3 The Distributed RSOCP Method

Now we consider larger network sizes for which it is preferable to use the distributed methods for solving the localization problem. In Figure 3.8, we compare the performance of the distributed RSOCP for $|\mathcal{N}| = 100$ to 500 nodes with the three-phase iterative distributed method in [105]. We consider 10 different topologies for each value of $|\mathcal{N}|$ and show the scatter plots for η and computation time in Figures 3.8(a) and 3.8(b), respectively.

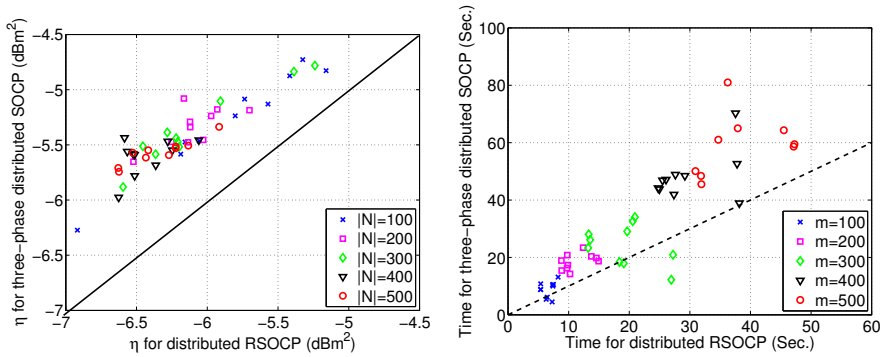

(a) (b)

Figure 3.8: Comparison between the proposed distributed RSOCP and the three-phase heuristic. The scatter plots for (a) η and (b) time are shown for 50 scenarios with $|\mathcal{N}| = 100$ to 500, 40% of which are anchors, $\sigma_d^2 = -20$ dBm^2, and $\mathbf{\Psi}_i = -10\boldsymbol{I}_2$ dBm^2. The diagonal solid and dashed lines are the $x = y$ identity lines.

For obtaining results in this figure, $R_c = 8$ m, 40% of the nodes are randomly selected as anchors, $\sigma_d^2 = -20$ dBm^2 and $\mathbf{\Psi}_i = -10\boldsymbol{I}_2$ dBm^2. For a fair comparison of time complexity, both algorithms are iteratively executed for only six rounds before they converge, i.e. the three-phase algorithm is run twice and our sensor-anchor refinement procedure in (3.17), (3.18) is executed three times. Note that for both distributed methods, only anchors which are reasonably inside the convex hull of their neighbors update their locations [105]. For measuring the computation time, we sum the maximum time taken by the nodes to solve their local problems during each phase. Note that the time for communicating variables to neighbors is not taken into account.

As can be seen from Figure 3.8, in almost all cases, the proposed distributed RSOCP algorithm outperforms the three-phase algorithm both in

terms of η and computation time. The former is due to the fact that our anchor refinement step takes into account the uncertainty and is able to provide a better position estimates for anchors. The latter is because of the simpler structure of our anchor update problem compared to the proposed heuristic in [105]. Note that for obtaining the results in Figure 3.8, we have used $(0, 0)$ as the initial location of nodes. Given a sufficient number of anchors, the distributed algorithm converges to good location estimates in few iterations, as can be seen from Figure 3.8.

3.6.4 EM Performance

Finally, we investigate the performance of the EM algorithm when the anchor uncertainties have unknown covariance matrices. Figure 3.9 compares the value of η for the EM method, after different numbers of iteration with that for the standard and robust SOCP (with known covariance). There are $|\mathcal{N}_s| = 35$ sensors and $|\mathcal{N}_a| = 15$ anchors in the network with $n_{\rm m} = 5$ initial readings for each anchor, $\sigma_{ij}^2 = -20$ dBm^2, and $\boldsymbol{\Psi}_i = \kappa_i^2 \boldsymbol{I}_2$, where κ_i^2 varies from -15 to 15 dBm^2. The initial readings are obtained by generating 5 noisy versions of the actual anchor positions based on the actual $\boldsymbol{\Psi}_i$. As can be seen, the positioning MSE of EM after convergence is very close to that of RSOCP, which indicates that the EM algorithm is able to correctly estimate the covariance matrices. On the other hand, the standard SOCP leads to a larger error, especially for larger values of uncertainty since it is unable to refine the anchor positions. For example, in Figure 3.9, the EM MSE after 3 to 5 iterations is close to its optimal value when $\kappa_i^2 \geq 0$ dBm^2, while additional iterations are needed for smaller uncertainties.

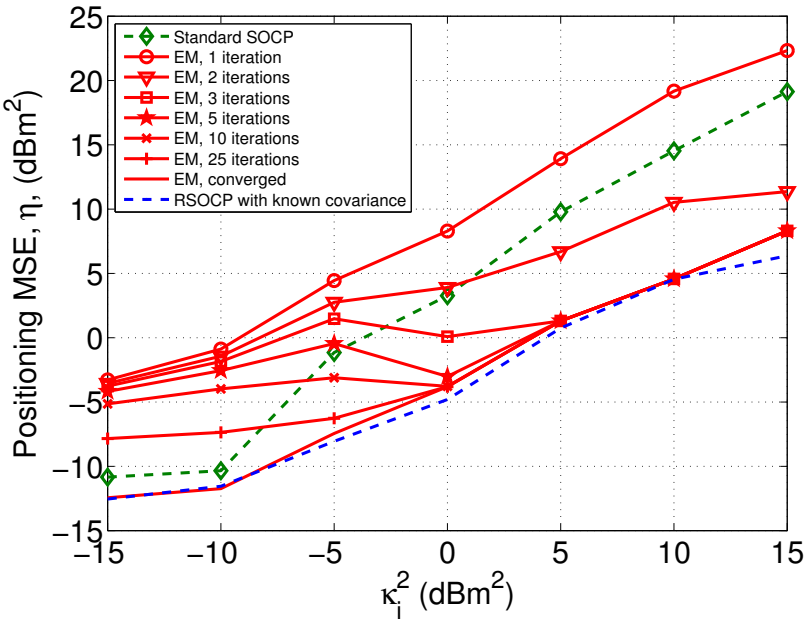

Figure 3.9: Positioning MSE, η, for EM after $1, 2, 3, 5, 10, 25$ iterations and after convergence, compared to the standard and robust SOCP. Number of sensors and anchors are $|\mathcal{N}_s| = 35$ and $|\mathcal{N}_a| = 15$, respectively, and $n_{\mathrm{m}} = 5$ initial readings are used in EM for each anchor. $\sigma_{ij}^2 = -20$ dBm^2, and $\boldsymbol{\Psi}_i = \kappa_i^2 \boldsymbol{I}_2$.

3.6.5 Formation Control

To show the effectiveness of the tightening procedure in making the network unambiguously localized, we consider mobile sensor networks with $|\mathcal{N}| = \{50, 100, 150, 200\}$ and 40% of anchors. Nodes are located in a 40 m $\times$ 40 m area, and the communication range $R_c = 8$m. The noise variance for ranging measurements is $\sigma_{d,ij}^2 = -20$ dBm^2, and the anchor uncertainty covariance matrix is $\boldsymbol{\Psi}_i = -10\ \boldsymbol{I}_2$ dBm^2.

Figure 3.10 shows the average and standard deviation of the number of iterations, over 100 topologies for each $|\mathcal{N}|$, needed for ambiguously-localized

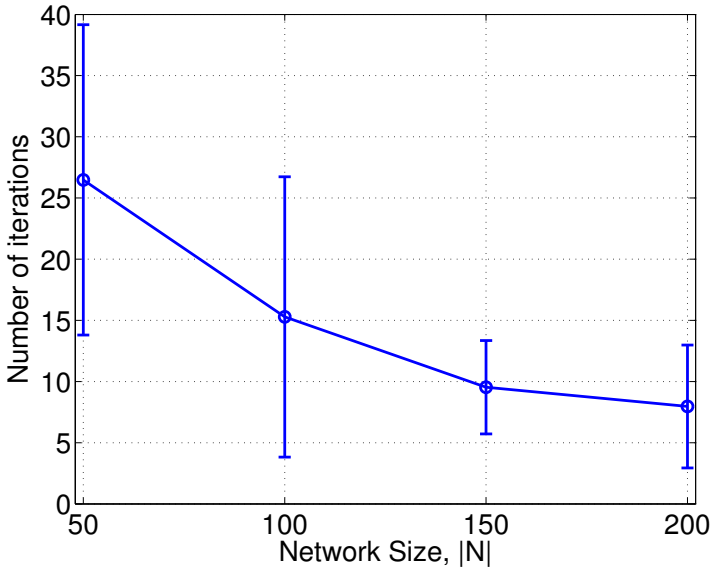

Figure 3.10: Average and standard deviation of number of mobility iterations needed for making the entire network unambiguously localizable. $\sigma^2_{d,ij} = -20$ dBm^2, $\mathbf{\Psi}_i = -10\ \boldsymbol{I}_2$ dBm^2, and $R_c = 8$ m, $|\mathcal{N}| = 50, 100, 150, 200$, and 40% of nodes are static anchors.

nodes to move based on equation (3.24) in order to make *the entire network* unambiguously localizable. As can be seen, only a few iterations, always smaller than 40, is required for making the whole network unambiguously localizable. This result shows that RSOCP can be efficiently used for achieving more reliability in formation control applications. Note that the nodes outside the convex hull will eventually move into the convex hull. Moreover, the number of iterations is a decreasing function of network size, due to the fact that the level of connectivity is higher in a denser network and thus, there are fewer unambiguous spots left in the convex hull. We should point out that according to our simulations for smaller networks in the order of 20 nodes or less, not shown here, the movements based on (3.24) might

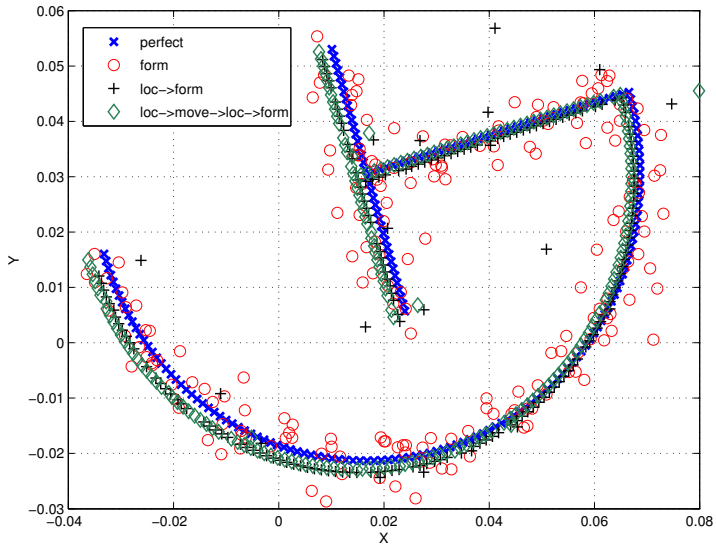

Figure 3.11: Formation of $|\mathcal{N}| = 200$ mobile sensors, into a rotation of the letter **G**. The sensors are initially uniformly-randomly distributed in a unit square around (0,0). The formation with and without prior localization is shown with different colors and markers, and their corresponding performance are provided in Table 3.3.

converge to a configuration where 90% or larger number of nodes in the network, but not necessarily all of them, are unambiguously localized.

We now use the tightening procedure for a robust formation control, as shown in Figure 3.11. We force a rotation constraint [122] ($\theta = \frac{3\pi}{4}$) but allow free scaling and translation in the formation. The sensors are initially uniformly-randomly distributed in a unit square around (0,0). The corresponding traveled time and mean square error (MSE) values for different formation control strategies are provided in Table 3.3.

In Figure 3.11, the blue crosses indicate the perfect formation that would have been established if all nodes knew their actual locations. In the presence of ranging noise with $\sigma^2_{d,ij} = -50$ dBm $^2, \forall (i,j) \in \mathcal{E}$, we compare the

Table 3.3: Performance of formation control with and without prior localization and tightening.

Method	Traveled distance (m) (tightening + formation)	Number of tight nodes	MSE (dB)
Direct Formation (Form.)	74.53 (0.00 + 74.53)	unknown	-12.29
Loc. → Form.	74.14 (0.00 + 74.14)	168	-9.78
Loc. → Tight. → Loc → Form.	75.88 (2.29 + 73.59)	186	-59.91

performance of three strategies. First, directly performing the optimization in [122] leads to the formation of red circles, with an observable deviation from the desired formation.

Second, performing only one localization with 13 anchors (on the convex hull) and 187 sensors without performing the tightening procedure (black + points in Figure 3.11) slightly decreases the total traveled distance but has an adverse effect on the final formation MSE. This can be due to the fact that the number of non-tight nodes with a high error in their location estimate is high (19 out of 168).

Third, performing one round of the tightening procedure followed by the second round of localization, the number of tight nodes is increased from 168 to 186. This leads to an almost perfect formation (-59.91 dB),

and the only node (out of 187) which is not tight can be clearly seen as the only green diamond outlier point at $(0.08, 0.045)$ in Figure 3.11 which further confirms the importance of being a tight node for a good formation. We should also mention that the formed shape in this case (green diamond points) is slightly shifted and scaled compared to the shape resulted from perfect measurements (blue + points), which is possible due to the degrees of freedom in the shape constraint $Ax = 0$, but the rotation angle is fixed because of the applied rotation constraint.

3.6.6 Boundary Trespassing Detection

Figures 3.12(a) and 3.12(b) show the performance of the RSOCP optimization for detecting mobile nodes which enter and exit the convex hull of anchors, respectively. For obtaining the results, $|\mathcal{N}_a| = 40$ static anchors are randomly placed in a 40 m $\times$ 40 m square area, and $|\mathcal{N}_s| = 60$ sensors, with randomly selected initial locations in the same area, move for 2000 seconds according to a random way-point model [163], where a node chooses a uniformly-random velocity vector every 10 seconds. The communication range is $R_c = 8$ m which translates to an average node connectivity of 8.6. The maximum speed of a sensor is set to $v_{\max} = 4$ m/s, and border closeness threshold is set to $\epsilon_d = 5$ m. In these figures, the squares show the actual times where nodes enter and exit the convex hull of anchors, while the crosses show the detections based on RSOCP which is executed after each round of movement. As can be seen, RSOCP is able to detect many of the occurrences of nodes passing the borders with a few false alarms. Quantitatively, the probability of a successful detection (both entering and

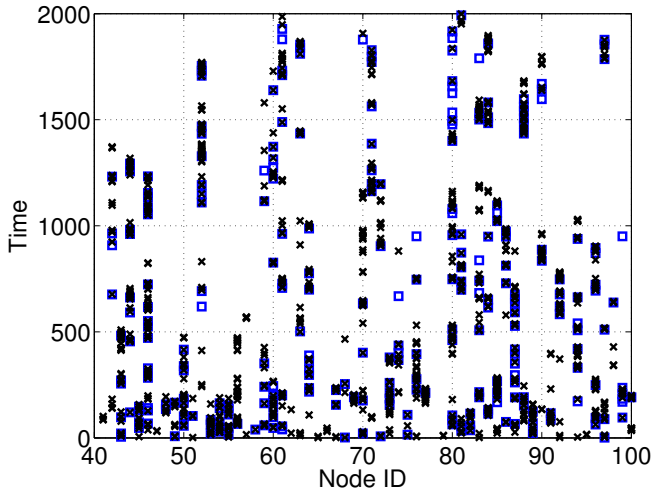

(a)

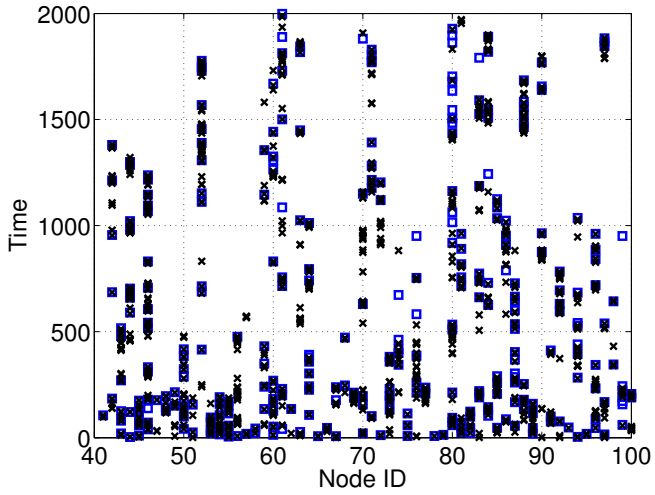

(b)

Figure 3.12: Detecting trespassing of $|\mathcal{N}_s| = 60$ mobile nodes on the convex hull of $|\mathcal{N}_a| = 40$ static anchors, a) entering b) exiting. Squares show actual trespassing and crosses are detections made by RSOCP. $\sigma_d^2 = -20$ dBm^2, $\boldsymbol{\Psi}_i = -10\ \boldsymbol{I}_2$ dBm^2.

exiting) is 83%, while the false alarm probability is 13%. As stated previously, ϵ_d can be adjusted for a tradeoff between probability of detection and

false alarm. To show this fact, we also tried a smaller threshold, $\epsilon_d = 2$ m, leading to a smaller probability of false alarm (7%), and a smaller probability of detection (60%).

3.7 Conclusions

We proposed robust and distributed algorithms for solving the localization problem based on an SOCP relaxation, which is computationally more efficient than the similar SDP methods. We analyzed the relation between the robust SOCP and robust SDP methods and provided a hybrid robust SDP-SOCP approach, which benefits from the lower complexity of robust SOCP and the better accuracy of robust SDP. The necessary and sufficient conditions for unambiguous localizability were also derived. Furthermore, an EM algorithm was proposed for estimating the locations in situations where the covariance matrices of the anchor uncertainties are unknown. Simulation results confirmed that the proposed robust, distributed, and hybrid methods based on the SOCP relaxation can be effectively used for localization in large networks with anchor position uncertainties.

Chapter 4

Coverage Enhancement for LTE MTC

After addressing the challenges of lifetime and localization in *ad hoc* WSNs in the previous two chapters, in this chapter we focus on the related concept of machine-to-machine communications (M2M). We choose the centralized architecture of LTE, and investigate the important problem of LTE coverage for M2M.

As explained in Section 1.1, M2M communication is one of the fastest-growing technologies in the field of telecommunications, and it is expected that the number of devices that need an M2M interface reaches hundreds of millions in the near future [5–8]. Wireless devices for M2M communication generally serve applications whose quality-of-service requirements are different from those handled by conventional (human-operated) LTE user equipment (UE). For example, many M2M applications require transmitting only infrequent and short messages (low average data rate per device) and are often more delay-tolerant compared to the human-to-human (H2H) and human-to-machine (H2M) applications. At the same time, the density of machine-type communication (MTC) UEs can be high. Finally, due to

many similarities between M2M and WSN applications often involving (a large number of) inexpensive battery-operated equipment without maintenance for long periods of time, MTC UEs need to be low cost and operate with low power consumption.

Against this background, the 3GPP standardization process has recognized the need for extending the LTE standard to open the network for M2M applications and to meet the specific requirements of MTC devices. In particular, 3GPP has started to integrate machine-type communication (MTC) into LTE-A starting from the tenth release (Rel-10) of the standard in 2010 [137]. Additional new enhancements have been introduced in the latest release (Rel-12) to improve the performance of MTC in LTE. In particular, the definition of several service requirement classes for different M2M applications, efficient handling of small data transmission requests, and device triggering have been included into LTE Rel-12. Also, several work items are in the final stages of investigation and will potentially appear in Rel-12 [7, 164]. These include the introduction of a new UE category equipped with a single antenna, limited operational bandwidth, half-duplexing frequency-division duplex, and lower transport bock sizes in order to reduce cost.

Table 4.1 shows some of the properties of the new UE category 0 (CAT0) designed for MTC in comparison to legacy UE categories in LTE. We observe that CAT0 UEs lack some of the LTE features and transmission capabilities for the benefit of low-cost design. While estimate cost savings are on the order of 50% compared to CAT1 devices [164], the required signal-to-noise ratio (SNR) for achieving a desired error rate will be higher and thus

Table 4.1: Comparison of some features for different LTE UE categories and LTE MTC UEs (category 0 (CAT0) devices).

Category		1	2	3	4	5	0
Peak rate (Mbps)	DL	10	50	100	150	300	1-2
	UL	5	25	50	50	75	1-2
Capability for physical layer functionalities							
Modulation	DL	QPSK, 16QAM, 64QAM					All
	UL	QPSK, 16QAM				QPSK, 16QAM, 64QAM	QPSK, 16QAM
Multi-antenna							
2 Rx diversity		Assumed in performance requirements					Not required
2×2 MIMO		Not supported	Mandatory				Not required
4×4 MIMO		Not supported				Mandatory	Not required

coverage is reduced for CAT0 UEs. Coverage is particularly critical in the context of MTC though, as some MTC UEs are installed inside buildings or structures with large penetration losses. Since these UEs are not mobile,

methods for coverage enhancement are necessary to provide LTE connectivity. In response to this, a new coverage enhancement work item has been approved in the 3GPP radio access network technical specification group (RAN TSG) in June 2013 [138].

In this chapter we review the coverage enhancement (CE) targets specified in this group and extend one of the CE techniques that are being considered for the inclusion in the standardization. For the former, we first provide a brief description of the LTE resource structure and the coverage in its uplink (UL) and downlink (DL) channels in Section 4.1. Then we focus on the LTE channel with the worst coverage and propose a novel method in Section 4.2 that can provide flexible CE under different network conditions, such as instantaneous link quality and number of active MTC UEs. Implementation of this method does not require modifications of legacy LTE UEs and has little effect on their performance (e.g. by way of limitations to resource scheduling), which is decisive for coexistence of legacy and MTC UEs. Overall cell spectral efficiency is also not compromised, which is important from a cost per bit perspective for mobile network operators. The coverage enhancement and spectral efficiency of the proposed method is evaluated through simulation results in Section 4.3.

While the CE methods discussed in the following are rooted in CE for MTC, we note that their application is by no means limited to LTE CAT0 UEs, and they can also be implemented for other UE categories.

4.1 Overview of Coverage in Uplink and Downlink LTE Channels

We first briefly review LTE physical uplink and downlink channels and present a summary of the current coverage in these channels. This sets the stage for the coverage enhancement methods presented thereafter.

In both of the UL and DL directions, there are different physical channels which are transmitted in specific RBs of the time and frequency radio resources. The physical DL and UL shared channels (PDSCH and PUSCH) are dedicated to data exchange between the eNodeB and the UEs. The size of the data which is transmitted in each data transaction is called the transport block size (TBS), and the time taken for this transmission is referred to as the data transmission time interval (TTI). The TTI is typically equal to the duration of one subframe. The data channels are complemented by a number of control channels, including the physical DL control channel (PDCCH) for allocating physical resource blocks (PRBs) to PDSCH and PUSCH, the physical UL control channel (PUCCH) for transmitting UE resource requests and link quality information, the physical broadcast channel (PBCH) in the DL, which broadcasts the information required at a UE for joining a cell, and the UL physical random access channel (PRACH), which is used for contention-based random access for requesting a resource allocation from the eNodeB.

4.1.1 LTE and MTC Coverage Requirements

Maximum coupling loss (MCL) is a measure for coverage in LTE channels. It is defined as the difference between maximum transmission power in the channel and its corresponding receiver sensitivity [137]. A higher MCL value indicates a smaller required SNR for a target block error rate (BLER), which translates into a better coverage for that channel.

The 3GPP study item [137] focused on identifying the LTE channels with critical MCLs. For this, the study item considered medium data rata and VoIP applications. Table 4.2 summarizes the MCL of the above-mentioned channels in LTE as reported in [137, 164]. It can be seen that the MCL values vary for different LTE channels and that the UL channels have, in general, a worse coverage compared to the DL channels. The issue of coverage imbalance is less pronounced when we consider MTC UEs. In particular, since MTC UEs will be equipped with only one receive antenna as shown in Table 4.1, a 4 dB penalty has been applied to the MCL of downlink channels in Table 4.2. Although the study [137] targeted 20 dB of coverage improvement, to reduce complexity it was agreed in work item [138] that only 15 dB of CE would be targeted. This means that all MTC channels should achieve an MCL of 155.7 dB. The required CEs for CAT0 devices are summarized in the last row in Table 4.2.

We have proposed different MTC CE methods for PUSCH in [165], for PDCCH in [166], and for PBCH in [167]. In the remainder of this chapter, we only focus on the PUSCH and present a transmission strategy based on spreading and bundling the data in order to achieve 15 dB CE in PUSCH.

Table 4.2: MCL for UL and DL LTE channels in FDD mode. eNodeB in 2 transmit and 2 receive antenna configuration. UE with 1 transmit and 2 receive antennas, and UE CAT0 with 1 transmit and 1 receive antenna.

	UL channels			DL channels		
(values in dB)	PUCCH	PRACH	PUSCH	PDCCH	PBCH	PDSCH
MCL for Category 1 Legacy UE	147.2	141.7	140.7	146.1	149.0	145.4
MCL for MTC UE	147.2	141.7	140.7	142.1	145.0	141.4
MCL for 15 dB CE	155.7	155.7	155.7	155.7	155.7	155.7
Required CE for MTC UE	8.5	14.0	15.0	13.6	10.7	14.3

The reason for choosing PUSCH is two-fold. First, PUSCH is the channel which requires the largest CE. Second, the MTC UEs tend to send UL data much more often than receiving the DL data.

4.1.2 LTE Channel Model

Before moving on to the CE methods, we would like to mention that most of the deep coverage holes in a system are due to in-building insertion loss and in this situation almost stationary MTC UEs is assumed. Therefore, in the 3GPP RAN1 working groups, the extended pedestrian type-A channel (EPA) is used as appropriate channel model for numerical evaluations and comparisons of results, usually with a Doppler frequency of 1, 3 or 5 Hz to account for a slight degree of mobility.

4.2 Coverage Enhancement in PUSCH

Data transmitted over PUSCH is encoded with a rate-1/3 turbo encoder. The encoder output is rate-matched and arranged in four redundancy versions (RVs), each of which matches the TBS. Based on this, incremental-redundancy automatic repeat request (ARQ) can be performed after each TTI. That is, the receiver acknowledges the receipt of data, and in case of a negative acknowledgment, the next RV of the current data will be transmitted. The default schedule for PUSCH transmission is to transmit one RV in one TTI, and to only transmit another RV if requested via negative acknowledgment (NACK). Reference [137] tackles the issue of CE for PUSCH through TTI bundling. In TTI bundling, all RVs are transmitted at once, without waiting for a NACK. This leads to CE for delay-limited application, in particular VoIP. The current LTE standard assumes a fixed bundling size of 4.

Since M2M applications are often delay-tolerant, we can think of combin-

ing bundling with repetition for CE. For example, increasing the bundling size from 4 to 8 means that the UE would send each RV twice. Furthermore, bundling size could be adjusted dynamically, considering the UEs need for CE and its delay tolerance [137].

Given the often low data-rate and latency requirements for MTC UEs, data repetition is a generally acceptable solution to improve coverage. But while a trade-off between spectral and power efficiency is mandated by principles of communication theory, repetition is often far from optimal in the sense of spectrum efficiency. An alternative to repetition is the use of spreading. The advantage of spreading is that it enables multiple UEs to transmit concurrently, i.e., to perform code-division multiple-access (CDMA). Therefore, the system spectral efficiency would not be affected by using CDMA if all code indices are used for transmission. CDMA is already used in LTE, namely for PUCCH format 3 to provide multiple user access on the control channel [11].

In the following, we explain a method for simultaneous use of adaptive TTI bundling and spreading for MTC CE, and we present a signalling procedure for the flexible assignment of PUSCH resources to a variable number of UEs.

4.2.1 Flexible TTI Bundling with CDMA Support

Our method extends conventional LTE TTI bundling by adjusting the bundling size and the spreading factor used by UEs, according to the instantaneous cellular network conditions. These are defined through number of "active" MTC UEs, i.e., UEs which have data to transmit, their channel quality and

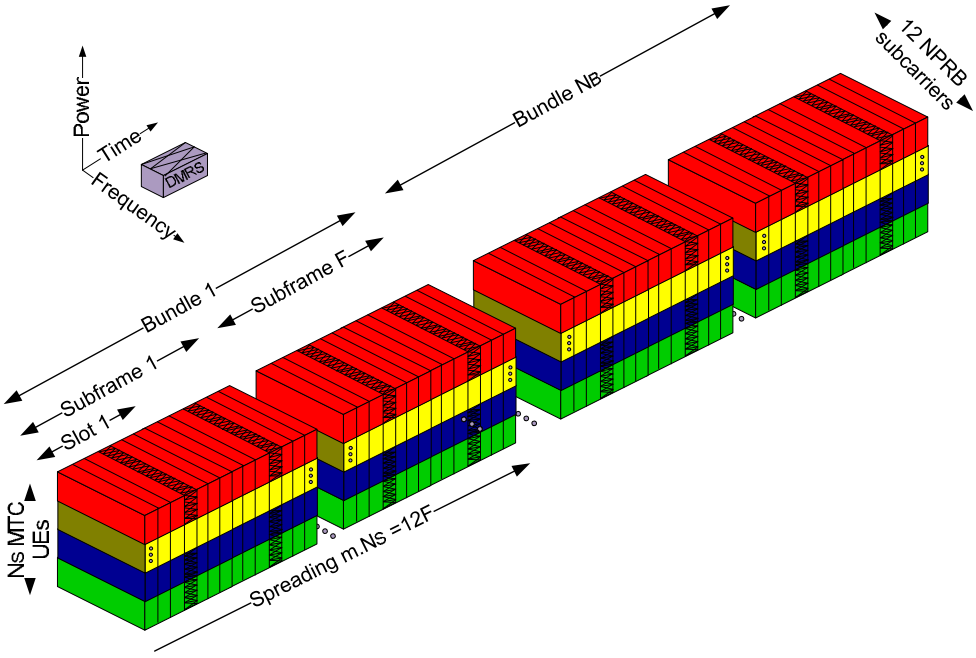

Figure 4.1: A TTI bundle in our invention consists of N_B "spreading blocks". Spreading codes of length N_S are used for spreading A symbols over one or more (F) subframes, enabling concurrent transmission of up to N_S UEs. Different spreading blocks may be scheduled non-consecutively over time and/or frequency. Note that 2 out of 14 OFDM symbols in each subframe are unavailable for spreading since they are dedicated to transmission of demodulation reference symbols (DMRS) for channel estimation.

thus instantaneous coverage, and the available PUSCH resources. The main advantage of using flexible bundling and spreading is that CE is achieved without overly compromising network spectral efficiency. Spreading is performed over REs at the same frequency, which simplifies despreading assuming the channel remains essentially constant over the spreading interval.

Figure 4.1 shows a unit of the code-spread TTI bundling for this new PUSCH sub-frame structure. In this new structure, the coverage gain is

based on:

- The spreading gain, which results from spreading a symbol over N_S single-carrier frequency division multiple access (SC-FDMA) symbols.
- The coding gain, which is achieved by bundling N_B "spreading blocks". The value of N_B can be dynamically chosen for achieving the desired code rate given the TBS, as it will be explained later.

Spreading blocks allow us to enhance coverage based on the spreading gain. A spreading block is defined as $F \geq 1$ subframes over which a variable number of SC-FDMA data symbols (denoted by A) are spread, over time, using spreading codes of length N_S. It can be also observed from Figure 4.1 that 2 symbols per sub-carrier are reserved for demodulation reference symbols (DMRS) in each PUSCH subframe. Consequently, there are $14-2 = 12$ SC-FDMA *data* symbols available per sub-carrier (i.e. we have a total of 144 data REs per RB), and thus we have

$$F = \text{lcm}(N_S, 12),$$

i.e., F is the least common multiplier (LCM) of N_S and 12. Also,

$$A = 144\ M_{\text{RB}}^{\text{PUSCH}}\ F/N_S,$$

where $M_{\text{RB}}^{\text{PUSCH}}$ is the number of allocated PRBs assigned by eNodeB for PUSCH transmission.

Using N_S (possibly orthogonal) spreading codes, up to N_S UEs can be scheduled to transmit over the proposed structure. The value of N_S is

dynamically adjusted by the eNodeB based on the required coverage and the number of active users. Moreover, increasing N_B leads to more coding and repetition gain. Mathematically, the coverage gain offered by the flexible TTI bundling and spreading can be lower bounded as,

$$G = 10 \log_{10} (N_B N_S) . \tag{4.1}$$

The exact gain in coverage is somewhat larger when combining different RVs from the turbo code contained in TTI bundles.

Unlike spreading, coverage enhancement provided by N_B block repetitions comes at the cost of decreasing the spectral efficiency. To see this, note that for a given modulation order (i.e. bits per symbol) of M and TBS, the code rate of bundling can be calculated as $c_r(N_B) = \frac{\text{TBS}}{AMN_B}$. In the special case when $N_B = 1$, i.e. in the normal PUSCH transmission with no bundling, the code rate is $\frac{\text{TBS}}{AM}$. Therefore, bundling size N_B decreases the spectral efficiency by a factor of N_B.

4.2.1.1 Realistic Channel Estimation in CDMA

When CDMA is used for simultaneous transmission of multiple users, channel estimations for each individual MTC UEs is required at the receiver (eNodeB) prior to despreading and decoding the data. Since the legacy RB structure is designed to accommodate the DMRS for only one user, we need to modify the RB structure to allow transmissions of DMRS from multiple users. There are different solutions for achieving this functionality. For instance, we can introduce new REs for DMRS and assign them separately to

different MTC UEs. This reduces the overall spectral efficiency, since the REs that used to carry data are now assigned to reference symbols. Alternatively, the reference symbols can be spread over the available DMRS REs. Applying this method is possible if the bundling size is large enough and accommodates at least N_S reference symbols. Under the assumption that the channel remains constant over the spreading interval, we can first despread the DMRS and use it for despreading the actual MTC UE data. In general, this assumption may not hold for the large values of N_S, and the practical gains of spreading would be less than the predicted $10\log_{10}(N_S)$ due to the effect of noise on the loss in the orthogonality between the CDMA codes.

4.2.2 Protocol for Flexible TTI bundling and CDMA

In order to successfully schedule the active MTC UEs to transmit on the bundling and spreading blocks, the eNodeB should first adjust the values of N_S and N_B based on the number of active UEs and the required coverage gain, respectively. Then, it informs the MTC UE of values of N_B and N_S and its assigned codes. To minimize the impact of this procedure on the current LTE standard, we note that some of the existing control flags in the PDCCH uplink grant are unlikely to be used in the MTC mode and thus can be reused to inform the UE to obtain its TBS, bundling size, spreading length and their code index. This would be done based on a configuration table for flexible TTI bundling and CDMA, which is a modified version of the TBS lookup table used in legacy UEs.

Using a modified TBS table, transmission with flexible TTI bundling and CDMA can be scheduled as follows.

1. When data is available for transmission, the MTC UE sends a scheduling request on PUCCH.

2. The eNodeB waits for a predefined time, collecting requests of MTC UEs as in Step 1, and estimates their required coverage gain from the received channel quality index (CQI).

3. The eNodeB sets N_S to the closest spreading length that is available in the configuration table such that the current number of active MTC UEs can be accommodated.

4. The eNodeB chooses N_B based on the required coverage gain (4.1) with the computed N_S from Step 3.

5. Based on Steps 3 and 4 and available resources, eNodeB assigns resources to UEs. It sends a PDCCH DCI format 0 for PUSCH allocation and sets a flag to indicate that the modified TBS table needs to be used.

Waiting and collecting requests in Step 2 is done to utilize as much of the available CDMA codes as possible, which maximizes system spectral efficiency while providing CE through spreading for individual MTC UEs. Steps 3 and 4 can further be refined to account for MTC UEs in good coverage, which may not need the full spreading gain. For example, those UEs could be assigned shorter spreading sequences, or multiple longer spreading sequences.

4.3 Performance Evaluation

According to LTE coverage enhancement study [137], we evaluate the CE achieved with flexible bundling and CDMA by measuring the SNR required for 2% BLER after jointly decoding all the CDMA blocks in the bundle, which is also known as the residual BLER (rBLER). For CDMA, we use Walsh-Hadamard and discrete Fourier transform (DFT) orthogonal sequences [22, 23] for the even and odd values of N_S, respectively. We choose TBS of 104 bits to be transmitted in one RB (i.e., $M_{\text{RB}}^{\text{PUSCH}} = 1$ in 180 kHz bandwidth) using QPSK modulation (i.e. $M = 2$). Figure 4.2 compares the rBLER obtained in simulations for different bundling and spreading configurations compared to the legacy PUSCH transmission. We show the results both in perfect and imperfect (abbreviated by "im" in the figure) channel state information scenarios. As can be seen from this figure, the proposed transmission based on bundling and spreading can achieve different values of gain by changing the configurations of (N_S, N_B). For example, the $(22, 2)$ configuration, and in general any configuration whose $N_S N_B$ is larger than $32 = \left\lceil 10^{\frac{15.0}{10}} \right\rceil$, reaches the target CE of 15.0 dB.

The first five columns of Table 4.3 compare the results shown in Figure 4.2 with the expected theoretical gain (4.1). As can be seen, the theoretical and simulated gains match well, where the latter include the effect of combing RVs in the turbo decoder, which gives only another about 0.4 dB gain compared to pure repetition due to the already low code rate for only one RV. In addition, it can be observed that the imperfect channel estimation decreases the gain by around 1 to 2 dB. In general, the performance

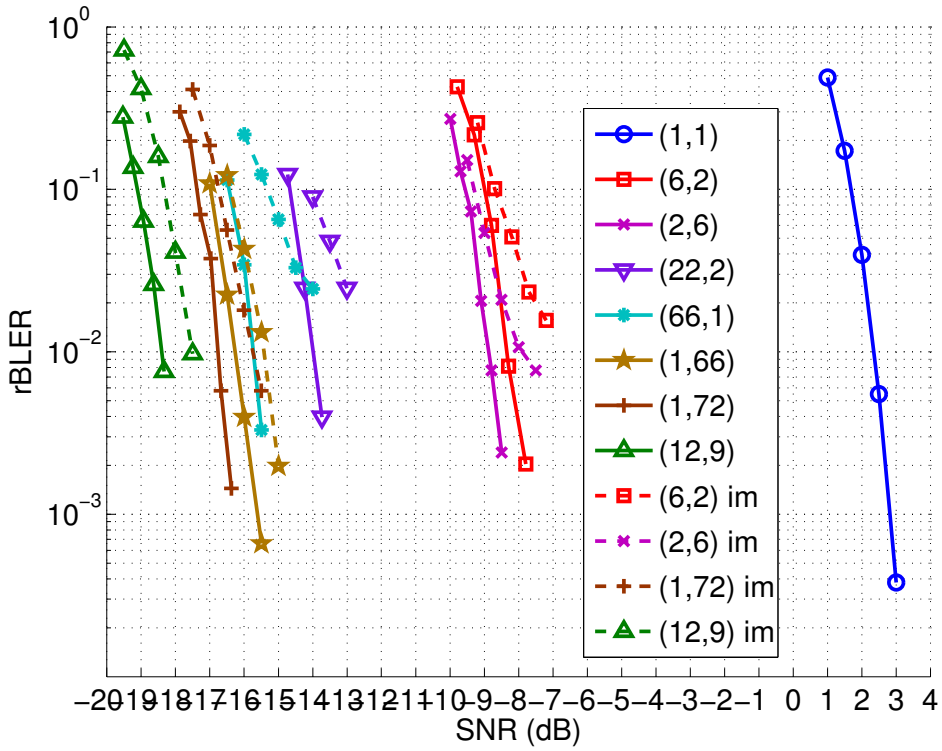

Figure 4.2: Comparison of rBLER as a function of SNR for the legacy $(1, 1)$ PUSCH transmission and different spreading and bundling configurations (N_s, N_B). The rBLER curves are shown for both perfect and imperfect (im) channel estimations.

Table 4.3: Achieved coverage gain, spectral efficiency, and MTC data rates for flexible TTI bundling and spreading. Simulated CE, spectral efficiency and data rate for TBS=104 in one RB using QPSK ($M = 2$).

N_S	N_B	Theoretical CE from (4.1) (dB)	Simulated CE (perfect CSI) (dB)	Simulated CE (Imperfect CSI) (dB)	Spectral Efficiency over all MTC UEs (bps/Hz)	Data Rate per MTC UE (kbps)
1	1	0.0	0.0	0.0	0.578	104.0
2	6	10.8	11.2	10.7	0.097	8.7
6	2	10.8	10.7	9.7	0.290	8.7
22	2	16.4	16.4	15.2	0.289	2.4
12	9	20.3	20.6	19.9	0.067	1.0
1	66	18.2	18.6	17.9	0.009	1.6
66	1	18.2	18.1	16.2	0.578	1.6
1	72	18.6	19.0	18.1	0.008	1.4

difference between the perfect and imperfect channel estimation scenarios is larger for higher coverage gains, because the channel estimation is a more challenging task in the presence of more noise in the low SNR values.

The last two columns of Table 4.3 show the spectral efficiency (over all MTC UEs) and data rate (per MTC UE). As can be seen, system spectral efficiency is affected by bundling but not by spreading, assuming that all spreading codes are used, so that no resources are wasted while benefiting from spreading gain. Note that the amount of spreading that can be applied is also limited by the need for either an essentially time-invariant channel over N_S PRBs, or extra reference symbols for channel estimation. Finally, it can be observed that the achieved data rates are about a few kilo bits per second (kbps) per MTC UE, which is suitable for many M2M applications.

4.4 Conclusions

We addressed the coverage enhancement of low-cost machine-type communication (MTC) user equipments (UEs) in LTE. We focused on the channel with the lowest coverage, namely physical uplink shared channel (PUSCH), and presented a novel transmission method on this channel by combining TTI bundling and CDMA repetition. The coverage enhancement of this method is a function of both the coding gain of turbo codes used in the TTI bundles and the repetition gain of CDMA. Moreover, CDMA transmission gives us the advantage of scheduling multiple MTC UEs at the same time. Therefore, the base station (eNodeB) can flexibly adjust the size of the proposed transmission blocks to provide the desired coverage to the active MTC

UEs. To this end, a simple scheduling protocol was also presented. This protocol reuses the current LTE standard's downlink control information that are unlikely to be used in the MTC mode. Using this protocol, MTC UEs can coexist with the current LTE legacy UES without requiring the LTE specification changes. We performed simulations to confirm that the achieved coverage gains compared to the normal PUSCH transmission reach the desired 15 dB of CE.

Chapter 5

Conclusions

Performing optimization in wireless sensor networks and their successors, machine-type communication networks, is essential for developing energy-efficient, reliable, and cost-effective solutions. In this thesis, we addressed three important aspects of WSN and MTCN operations, and provided optimization frameworks to improve their performance. We provided algorithms with low complexity, for example by using convex optimization, and also achieved scalability by presenting the distributed version of our algorithms.

First, we formulated the lifetime of an ultra-wideband (UWB) event-detection sensor network as a function of sensing and routing parameters in Chapter 2. We derived centralized and distributed convex optimization frameworks for maximizing the lifetime. Detection requirement constraints were added in the optimization to ensure that the sensing task can be accomplished over the span of network lifetime. Our software simulations showed that the network lifetime achieved by solving the proposed convex formula is significantly improved compared to the similar formulations in the literature.

Second, a comprehensive study of different convex formulations for sensor network localization was presented in Chapter 3. We derived a robust

localization framework, where the nodes can be localized in the presence of uncertainty in the location of anchors. Moreover, an algorithm capable of trading off localization accuracy with computational complexity were presented. We also presented a distributed version of our robust localization solution to provide scalability to the network size. We performed extensive computer simulations to quantify the localization errors of our algorithms, and confirmed their high accuracy, low complexity and resilience to uncertainty.

Third, we turned our attention to the newer type of sensor networks, namely machine-type communication over LTE cellular networks, and addressed the coverage enhancement problem. We focused on the LTE uplink data channel which has the worst coverage, and designed a new transmission strategy based on data repetition and code division multiple access (CDMA) for coverage enhancement. We also presented a scheduling algorithm which can be controlled by the LTE base station (eNodeB) to provide the necessary coverage to the MTC UEs. In designing this protocol, we took into account the coexistence criteria by making sure that our algorithm requires minimal changes to the current LTE specifications.

5.1 Directions for Future Research

Lifetime of a network can be further improved by means of data aggregation [59, 67]. This would require analysis of correlation between data generated by the nearby sensors to find out how packets can be merged together to achieve the maximum compression ratio and the minimum transmission

power. Similarly, data aggregation and cooperative routing among MTC UEs in an LTE cell can significantly reduce the workload of the eNodeB, and at the same time improve the coverage [140].

Robust localization problems can benefit from a control on outliers, i.e. the nodes which generate extremely inaccurate ranging information due to for example, their completely asynchronous clocks [100]. Discarding outliers' data from the localization formulation can significantly reduce the final localization error.

Establishing secure connections is another important challenge for both WSNs and MTCNs. In fact, there has been a great interest recently on physical-layer security for UWB [168] and MTC-enabled LTE [169]. Physical-layer security exploits the information present in the channel, e.g. delays and amplitudes of the taps in the channel impulse response, to generate a secure key that is only shared between the transmitter-receiver pair. An advantage of this type of key agreement is that it has a lower complexity compared to the traditional cryptographic key exchange protocols. Providing privacy and security in Internet of Things and MTCNs is another important and related uprising research topic [170].

Bibliography

[1] I. F. Akyildiz, W. Su, Y. Sankarasubramaniam, and E. Cayirci, "Wireless sensor networks: a survey," *Computer Networks*, vol. 38, no. 4, pp. 393 – 422, Mar. 2002.

[2] "First Report and Order: In the matter of Revision of Part 15 of the Commissions Rules Regarding Ultra-Wideband Transmission Systems," Federal Communications Commision (FCC) 02-48, Tech. Rep., Apr. 2002.

[3] Z. Ahmadian, "Multiuser Pre-Filtered Ultra-Wideband Systems," Ph.D. dissertation, The University of British Columbia (Vancouver), Dec. 2013.

[4] International Telecommunication Union (ITU) , *Objectives, Characteristics, and Functional Requirements of Wide-Area Sensor and/or Actuator Network (WASN) Systems*, www.itu.int/rec/R-REC-M.2002-0-201203-I/en, Std. M.2002, Mar. 2012.

[5] D. Boswarthick, O. Elloumi, and O. Hersent, *M2M Communications: a Systems Approach*. John Wiley & Sons, 2012.

[6] "GSMA Predicts 250 Million M2M Connections in 2014," Feb. 2014. [Online]. Available: http://www.gsma.com/newsroom/gsma-predicts-250-million-m2m/

[7] Third Generation Partnership Project (3GPP), "Standardization of Machine-Type Communication, LTE Rel-12," Tech. Rep. [Online]. Available: http://tinyurl.com/mv9ymkp

[8] "Machine to machine (M2M) market global forecast & analysis (2012-2017)," Sep. 2012. [Online]. Available: http://tinyurl.com/pg3xa2a

[9] G. B. Dantzig, *Linear programming and extensions*. Princeton University Press, 1965.

[10] S. Boyd and L. Vandenberghe, *Convex Optimization*, 4th ed. Cambridge University Press, 2004.

[11] S. Sesia, I. Toufik, and M. Baker, *LTE, The UMTS Long Term Evolution: From Theory to Practice*, 2nd ed. John Wiley & Sons, 2011.

[12] M.-G. Di Benedetto, *UWB communication systems: a comprehensive overview*. Hindawi Publishing Corporation, 2006, vol. 5.

[13] J. Wang, *High-Speed Wireless Communications: Ultra-wideband, 3G Long Term Evolution, and 4G Mobile Systems*. Cambridge University Press, 2008.

[14] A. Parihar, L. Lampe, R. Schober, and C. Leung, "Equalization for DS-UWB systemspart I: BPSK modulation," *IEEE Transactions on Communications*, vol. 55, no. 6, pp. 1164–1173, June 2007.

[15] ECMA Standard, "368: High Rate Ultra Wideband PHY and MAC Standard." 2005. [Online]. Available: http://tinyurl.com/256ja4

[16] M. Win and R. Scholtz, "Impulse Radio: How It Works," *IEEE Commun. Lett.*, vol. 2, no. 2, pp. 36–38, 1998.

[17] J.-Y. Lee and R. A. Scholtz, "Ranging in a dense multipath environment using an UWB radio link," *Selected Areas in Communications, IEEE Journal on*, vol. 20, no. 9, pp. 1677–1683, 2002.

[18] "IEEE standard part 15.4a: Wireless medium access control (MAC) and physical layer (PHY) specifications for low-rate wireless personal area networks (WPANs)," *IEEE Std 802.15.4a-2007 (Amendment to IEEE Std 802.15.4-2006)*, pp. 1–203, 2007.

[19] S. Gezici, Z. Tian, G. B. Giannakis, H. Kobayashi, A. F. Molisch, H. V. Poor, and Z. Sahinoglu, "Localization via ultra-wideband radios: a look at positioning aspects for future sensor networks," *Signal Processing Magazine, IEEE*, vol. 22, no. 4, pp. 70–84, 2005.

[20] J. R. Fernandes and D. Wentzloff, "Recent advances in ir-uwb transceivers: An overview," in *Circuits and Systems (ISCAS), Proceedings of 2010 IEEE International Symposium on*. IEEE, 2010, pp. 3284–3287.

[21] B. Radunovic and J.-Y. Le Boudec, "Power control is not required for wireless networks in the linear regime," in *Proceedings of the IEEE International Symposium on a World of Wireless Mobile and Multimedia Networks (WoWMoM)*, June 2005, pp. 417–427.

[22] L. Hanzo, M. Münster, B. Choi, and T. Keller, *OFDM and MC-CDMA*. John Wiley & Sons, 2004.

[23] K. Fazel and S. Kaiser, *Multi-Carrier and Spread Spectrum Systems: From OFDM and MC-CDMA to LTE and WiMAX*, 2nd ed. John Wiley & Sons, 2008.

[24] H. Holma and A. Toskala, *LTE for UMTS: Evolution to LTE-Advanced*. John Wiley & Sons, 2011.

[25] K. S. Low, W. N. N. Win, and M. J. Er, "Wireless sensor networks for industrial environments," in *IEEE International Conference on Computational Intelligence for Modelling, Control and Automation*, vol. 2, 2005, pp. 271–276.

[26] A. Wheeler, "Commercial applications of wireless sensor networks using ZigBee," *Communications Magazine, IEEE*, vol. 45, no. 4, pp. 70–77, 2007.

[27] I. F. Akyildiz, T. Melodia, and K. R. Chowdury, "Wireless multimedia sensor networks: A survey," *IEEE Wireless Communications*, vol. 14, no. 6, pp. 32–39, 2007.

[28] C. Otto, A. Milenkovic, C. Sanders, and E. Jovanov, "System architecture of a wireless body area sensor network for ubiquitous health monitoring," *Journal of Mobile Multimedia*, vol. 1, no. 4, pp. 307–326, 2006.

[29] J. Stankovic, Q. Cao, T. Doan, L. Fang, Z. He, R. Kiran, S. Lin,

S. Son, R. Stoleru, and A. Wood, "Wireless sensor networks for in-home healthcare: Potential and challenges," in *High confidence medical device software and systems (HCMDSS) workshop*, 2005, pp. 2–3.

[30] C. S. Raghavendra, K. M. Sivalingam, and T. Znati, *Wireless sensor networks*. Springer, 2004.

[31] T. Arampatzis, J. Lygeros, and S. Manesis, "A survey of applications of wireless sensors and wireless sensor networks," in *IEEE International Symposium on Intelligent Control*, 2005, pp. 719–724.

[32] S. Kumar and S. Chauhan, "A survey on scheduling algorithms for wireless sensor networks." *International Journal of Computer Applications*, vol. 20, 2011.

[33] A. Manjeshwar and D. P. Agrawal, "Teen: A routing protocol for enhanced efficiency in wireless sensor networks." in *IPDPS*, vol. 1, 2001, p. 189.

[34] K. Akkaya and M. Younis, "A survey on routing protocols for wireless sensor networks," *Ad hoc networks*, vol. 3, no. 3, pp. 325–349, 2005.

[35] S. Biswas and R. Morris, "Exor: opportunistic multi-hop routing for wireless networks," in *ACM SIGCOMM Computer Communication Review*, vol. 35, no. 4. ACM, 2005, pp. 133–144.

[36] M. Win and R. Scholtz, "Ultra-wide bandwidth time-hopping spread-spectrum impulse radio for wireless multiple-access communications," *IEEE Trans. Commun.*, vol. 48, no. 4, pp. 679–689, 2000.

[37] R. Merz, J. Widmer, J. Y. Le Boudec, and B. Radunovic, "A joint PHY/MAC architecture for low-radiated power TH-UWB wireless ad-hoc networks," *Journal of Wireless Communication and Mobile Computing*, vol. 5, no. 5, pp. 567–580, Jul. 2005.

[38] H. Jiang and W. Zhuang, "Effective packet scheduling with fairness adaptation in Ultra-wideband wireless networks," *IEEE Trans. Wireless Commun.*, vol. 6, no. 2, pp. 680–690, Feb. 2007.

[39] B. Radunovic and J. Y. Le Boudec, "Optimal power control, scheduling, and routing in UWB networks," *IEEE J. Sel. Areas Commun.*, vol. 22, no. 7, pp. 1252–1270, Sep. 2004.

[40] I. Oppermann, L. Stoica, A. Rabbachin, Z. Shelby, and J. Haapola, "UWB wireless sensor networks: UWEN - a practical example," *IEEE Commun. Mag.*, vol. 42, no. 12, pp. S27–S32, Dec. 2004.

[41] J. Zhang, P. Orlik, S. Z., A. Molisch, and P. Kinney, "UWB systems for wireless sensor networks," *Proc. IEEE*, vol. 97, no. 2, pp. 313 –331, Feb. 2009.

[42] H. Yang and W. Wu, "UWB-assisted real-time localization in wireless sensor networks," in *Industrial Electronics Society, IECON 2013-39th Annual Conference of the IEEE*. IEEE, 2013, pp. 4500–4505.

[43] T. Melodia and I. F. Akyildiz, "Cross-layer QoS-aware communications for ultra wide band wireless multimedia sensor networks," *IEEE J. Sel. Areas Commun.*, vol. 28, no. 5, pp. 653–663, Jun. 2010.

[44] J. Fu and S. Pan, "Fiber-connected uwb sensor network for high-resolution localization using optical time-division multiplexing," *Optics express*, vol. 21, no. 18, pp. 21 218–21 223, 2013.

[45] F. Cuomo, C. Martello, A. Baiocchi, and F. Capriotti, "Radio resource sharing for ad hoc networking with UWB," *IEEE J. Sel. Areas Commun.*, vol. 20, no. 9, pp. 1722–1732, Dec. 2002.

[46] N. Patwari, J. N. Ash, S. Kyperountas, A. O. Hero III, R. L. Moses, and N. S. Correal, "Locating the nodes: cooperative localization in wireless sensor networks," *Signal Processing Magazine, IEEE*, vol. 22, no. 4, pp. 54–69, 2005.

[47] J. Hill, M. Horton, R. Kling, and L. Krishnamurthy, "The platforms enabling wireless sensor networks," *Communications of the ACM*, vol. 47, no. 6, pp. 41–46, 2004.

[48] W. Ye, J. Heidemann, and D. Estrin, "An energy-efficient MAC protocol for wireless sensor networks," in *INFOCOM, Twenty-First Annual Joint Conference of the IEEE Computer and Communications Societies*, vol. 3, 2002, pp. 1567–1576.

[49] ——, "Medium access control with coordinated adaptive sleeping for wireless sensor networks," *IEEE/ACM Transactions on Networking*, vol. 12, no. 3, pp. 493–506, June 2004.

[50] G. Lu, B. Krishnamachari, and C. S. Raghavendra, "An adaptive energy-efficient and low-latency MAC for data gathering in wireless

sensor networks," in *Parallel and Distributed Processing Symposium, 2004. Proceedings. 18th International*. IEEE, 2004, p. 224.

[51] S. Bandyopadhyay and E. J. Coyle, "An energy efficient hierarchical clustering algorithm for wireless sensor networks," in *INFOCOM, Twenty Second Annual Joint Conference of the IEEE Computer and Communications Societies*, vol. 3. IEEE, 2003, pp. 1713–1723.

[52] D. Tian and N. D. Georganas, "A coverage-preserving node scheduling scheme for large wireless sensor networks," in *Proceedings of the 1st ACM international workshop on Wireless sensor networks and applications*. ACM, 2002, pp. 32–41.

[53] S. Soro and W. B. Heinzelman, "Cluster head election techniques for coverage preservation in wireless sensor networks," *Ad Hoc Networks*, vol. 7, no. 5, pp. 955–972, 2009.

[54] G. Naddafzadeh Shirazi and L. Lampe, "Outage optimal node placement in ultra wideband sensor networks," in *IEEE International Conference on Ultra-Wideband (ICUWB)*, 2009, pp. 343–347.

[55] J.-H. Chang and L. Tassiulas, "Maximum lifetime routing in wireless sensor networks," *IEEE/ACM Transactions on Networking*, vol. 12, no. 4, pp. 609–619, 2004.

[56] H. Wang, N. Agoulmine, M. Ma, and Y. Jin, "Network lifetime optimization in wireless sensor networks," *IEEE Journal on Selected Areas in Communications*, vol. 28, no. 7, pp. 1127–1137, Sep. 2010.

[57] Y. Xi and M. Yeh, "Node-based optimal power control, routing, and congestion control in wireless networks," *IEEE Trans. Inf. Theory*, vol. 54, no. 9, pp. 4081–4106, Sep. 2008.

[58] Q. Dong, "Maximizing system lifetime in wireless sensor networks," in *Proc. Fourth International Symposium on Information Processing in Sensor Networks (IPSN)*, Apr. 15, 2005, pp. 13–19.

[59] D. M. Blough and P. Santi, "Investigating upper bounds on network lifetime extension for cell-based energy conservation techniques in stationary ad hoc networks," in *Proceedings of the 8th annual international conference on Mobile computing and networking*. ACM, 2002, pp. 183–192.

[60] A. Sankar and Z. Liu, "Maximum lifetime routing in wireless ad-hoc networks," in *INFOCOMM, Twenty-third Annual Joint Conference of the IEEE Computer and Communications Societies*, 2004.

[61] C. Pandana and K. R. Liu, "Robust connectivity-aware energy-efficient routing for wireless sensor networks," *Wireless Communications, IEEE Transactions on*, vol. 7, no. 10, pp. 3904–3916, 2008.

[62] S. Olariu and I. Stojmenovic, "Design guidelines for maximizing lifetime and avoiding energy holes in sensor networks with uniform distribution and uniform reporting." in *INFOCOM, Twenty Fifth Annual Joint Conference of the IEEE Computer and Communications Societies*, 2006, pp. 1–12.

[63] H. Kim, Y. Seok, N. Choi, Y. Choi, and T. Kwon, "Optimal multi-sink positioning and energy-efficient routing in wireless sensor networks," in *Information Networking. Convergence in Broadband and Mobile Networking.* Springer, 2005, pp. 264–274.

[64] E. I. Oyman and C. Ersoy, "Multiple sink network design problem in large scale wireless sensor networks," in *Communications, 2004 IEEE International Conference on*, vol. 6. IEEE, 2004, pp. 3663–3667.

[65] R. Madan and S. Lall, "Distributed algorithms for maximum lifetime routing in wireless sensor networks," *IEEE Trans. Wireless Commun.*, vol. 5, no. 8, pp. 2185–2193, Aug. 2006.

[66] V. Shah-Mansouri and V. W. Wong, "Distributed maximum lifetime routing in wireless sensor networks based on regularization," in *IEEE Global Telecommunications Conference (GLOBECOM)*, Washington, DC, USA, Nov. 2007.

[67] C. Hua and T.-S. P. Yum, "Optimal routing and data aggregation for maximizing lifetime of wireless sensor networks," *IEEE/ACM Transactions on Networking*, vol. 16, no. 4, pp. 892–903, Aug. 2008.

[68] T. Q. S. Quek, M. Z. Win, and M. Chiani, "Distributed diversity in ultrawide bandwidth wireless sensor networks," in *Proc. Vehicular Technology Conference (VTC-Spring)*, vol. 2, May 30–Jun. 1, 2005, pp. 1355–1359.

[69] Y. Yang, R. S. Blum, and B. M. Sadler, "Energy-efficient routing

for signal detection in wireless sensor networks," *IEEE Trans. Signal Process.*, vol. 57, no. 6, pp. 2050–2063, Jun. 2009.

[70] J. Li and G. AlRegib, "Network lifetime maximization for estimation in multihop wireless sensor networks," *IEEE Trans. Signal Process.*, vol. 57, no. 7, pp. 2456–2466, Jul. 2009.

[71] K. Lorincz, D. Malan, T. Fulford-Jones, A. Nawoj, A. Clavel, V. Shnayder, G. Mainland, M. Welsh, and S. Moulton, "Sensor networks for emergency response: challenges and opportunities," *Pervasive Computing, IEEE*, vol. 3, no. 4, pp. 16 – 23, Oct. 2004.

[72] N. Kurata, S. Saruwatari, and H. Morikawa, "Ubiquitous structural monitoring using wireless sensor networks," in *Intelligent Signal Processing and Communications, 2006. ISPACS'06. International Symposium on.* IEEE, 2006, pp. 99–102.

[73] Y. Wang, L. Huang, J. Wu, and H. Xu, "Wireless sensor networks for intensive irrigated agriculture," in *Fourth Consumer Communications and Networking Conference (CCNC).* IEEE, 2007, pp. 197–201.

[74] A. Mainwaring, D. Culler, J. Polastre, R. Szewczyk, and J. Anderson, "Wireless sensor networks for habitat monitoring," in *Proceedings of the 1st ACM international workshop on Wireless sensor networks and applications*, ser. WSNA '02, 2002, pp. 88–97.

[75] A. Milenkovic, C. Otto, and E. Jovanov, "Wireless sensor networks for personal health monitoring: Issues and an implementation," *Computer Communications*, vol. 29, no. 13-14, pp. 2521 – 2533, 2006.

[76] H. Alemdar and C. Ersoy, "Wireless sensor networks for healthcare: A survey," *Computer Networks*, vol. 54, no. 15, pp. 2688–2710, 2010.

[77] J. Neyman and E. S. Pearson, "On the problem of the most efficient tests of statistical hypotheses," *Royal Society of London Philosophical Transactions Series A*, vol. 231, pp. 289–337, 1933.

[78] H. V. Poor, *An introduction to signal detection and estimation (2nd ed.)*. New York, NY, USA: Springer-Verlag New York, Inc., 1994.

[79] K. Bai and C. Tepedelenlioglu, "Distributed detection in UWB wireless sensor networks," *IEEE Trans. Signal Process.*, vol. 58, no. 2, pp. 804–813, Feb. 2010.

[80] J. Xu, Y. Hong, and L. Chen, "Bound on the operational lifetime of ultra wideband sensor network," in *Proc. of the First International Conference on Innovative Computing, Information and Control (ICICIC)*, 2006, pp. 80–84.

[81] Y. Shi, Y. T. Hou, H. D. Sherali, and S. F. Midkiff, "Optimal routing for UWB-based sensor networks," *IEEE Journal on Selected Areas in Communications*, vol. 24, no. 4, pp. 857–863, Apr. 2006.

[82] R. Szewczyk, E. Osterweil, J. Polastre, M. Hamilton, A. Mainwaring, and D. Estrin, "Habitat monitoring with sensor networks," *Communications of the ACM*, vol. 47, pp. 34–40, Jun. 2004.

[83] L. Blazevic, J. Y. Le-Boudec, and S. Giordano, "A location-based

routing method for mobile ad hoc networks," *IEEE Trans. Mobile Comput.*, vol. 4, pp. 97–110, Mar. 2004.

[84] J. Wang, R. Ghosh, and S. K. Das, "A survey on sensor localization," *Journal of Control Theory and Applications*, vol. 8, no. 1, pp. 2–11, 2010.

[85] J. Ibriq and I. Mahgoub, "Cluster-based routing in wireless sensor networks: issues and challenges," in *SPECTS*, vol. 4, 2004, pp. 759–766.

[86] T. Eren, O. Goldenberg, W. Whiteley, Y. Yang, A. Morse, B. D. O. Anderson, and P. Belhumeur, "Rigidity, computation, and randomization in network localization," in *INFOCOM, Twenty Third Annual Joint Conference of the IEEE Computer and Communications Societies*, Mar. 2004, pp. 2673 – 2684.

[87] J. Aspnes, T. Eren, D. K. Goldenberg, A. S. Morse, W. Whiteley, Y. R. Yang, B. D. O. Anderson, and P. N. Belhumeur, "A theory of network localization," *IEEE Trans. Mobile Comput.*, vol. 5, no. 12, pp. 1663–1678, Dec. 2006.

[88] Z. Zhu, A. M. So, and Y. Ye, "Universal rigidity: Towards accurate and efficient localization of wireless networks," in *INFOCOM, Twenty Ninth Annual Joint Conference of the IEEE Computer and Communications Societies*, Mar. 2010, pp. 1–9.

[89] Z. Yang, Y. Liu, and X.-Y. Li, "Beyond trilateration: On the localiz-

ability of wireless ad hoc networks," *IEEE/ACM Trans. Netw.*, vol. 99, no. 99, pp. 1–9, May 2010.

[90] N. Patwari, J. N. Ash, S. Kyperountas, A. O. Hero, R. L. Moses, and N. S. Correal, "Locating the nodes: cooperative localization in wireless sensor networks," *IEEE Signal Process. Mag.*, vol. 22, no. 4, pp. 54–69, Jul. 2005.

[91] P. Bahl and V. N. Padmanabhan, "RADAR: An in-building RF-based user location and tracking system," in *INFOCOM, Nineteenth Annual Joint Conference of the IEEE Computer and Communications Societies*, Mar. 2000, pp. 775–784.

[92] P. Rong and M. Sichitiu, "Angle of arrival localization for wireless sensor networks," in *IEEE Sensor and Ad Hoc Communications and Networks (SECON)*, Sept. 2006, pp. 374 – 382.

[93] G. Mao, B. Fidan, and B. D. O. Anderson, "Wireless sensor network localization techniques," *Computer Networks*, vol. 51, no. 10, pp. 2529 – 2553, Jul. 2007.

[94] X. Cheng, A. Thaeler, G. Xue, and D. Chen, "TPS: A time-based positioning scheme for outdoor wireless sensor networks," in *IEEE Infocom*, Mar. 2004, pp. 2685 – 2696.

[95] J. Aspnes, D. Goldenberg, and Y. R. Yang, "On the computational complexity of sensor network localization," in *Proc. ALGOSENSORS*, ser. Lecture Notes in Computer Science. Springer-Verlag, 2004, pp. 32–44.

[96] M. Jadliwala, S. Upadhyaya, and M. Taneja, "ASFALT: A Simple Fault-Tolerant Signature-based Localization Technique for Emergency Sensor Networks," in *IEEE International Symposium on Reliable Distributed Systems (SRDS)*, Oct 2007, pp. 3–12.

[97] M. Meurer, S. Heilmann, D. Reddy, T. Weber, and P. Baier, "A signature based localization technique relying on covariance matrices of channel impulse responses," in *Proc. 2nd Workshop Positioning Navigation and Communication (WPNC)*, 2005, pp. 31–40.

[98] Y. Shang, W. Ruml, Y. Zhang, and M. Fromherz, "Localization from connectivity in sensor networks," *IEEE Trans. Parallel Distrib. Syst.*, vol. 15, no. 11, pp. 961–974, Nov. 2004.

[99] J. Zheng and Y.-C. Wu, "Robust joint localization and time synchronization in wireless sensor networks with bounded anchor uncertainties," in *IEEE International Conference on Acoustics, Speech, and Signal Processing (ICASSP)*, Apr. 2009, pp. 2793–2796.

[100] J. S. Picard and A. J. Weiss, "Bounds on the number of identifiable outliers in source localization by linear programming," *IEEE Trans. Signal Process.*, no. 5, pp. 2884–2895, May 2010.

[101] L. Doherty, K. S. J. Pister, and L. El Ghaoui, "Convex position estimation in wireless sensor networks," in *INFOCOM, Twentieth Annual Joint Conference of the IEEE Computer and Communications Societies*, vol. 3, Apr. 2001, pp. 1655–1663.

[102] S. Zhu and Z. Ding, "A simple approach of range-based positioning with low computational complexity," *IEEE Trans. Wireless Commun.*, vol. 8, no. 12, pp. 5832–5836, Dec. 2009.

[103] C. Feng, W. S. A. Au, S. Valaee, and Z. Tan, "Compressive sensing based positioning using RSS of WLAN access points," in *INFOCOM, Twenty Ninth Annual Joint Conference of the IEEE Computer and Communications Societies*, Mar. 2010, pp. 1–9.

[104] L. Yang and K. C. Ho, "An approximately efficient TDOA localization algorithm in closed-form for locating multiple disjoint sources with erroneous sensor positions," *IEEE Trans. Signal Process.*, vol. 57, no. 12, pp. 4598–4615, Dec. 2009.

[105] S. Srirangarajan, A. Tewfik, and Z.-Q. Luo, "Distributed sensor network localization using SOCP relaxation," *IEEE Trans. Wireless Commun.*, vol. 7, no. 12, pp. 4886–4895, Dec. 2008.

[106] P. Tseng, "Second-order cone programming relaxation of sensor network localization," *SIAM Journal on Optimization*, vol. 18, no. 1, pp. 156–185, Feb. 2007.

[107] A. M.-C. So and Y. Ye, "Theory of semidefinite programming for sensor network localization," *Math. Program.*, vol. 109, no. 2, pp. 367–384, Jan. 2007.

[108] P. Biswas, T.-C. Liang, K.-C. Toh, Y. Ye, and T.-C. Wang, "Semidefinite programming approaches for sensor network localization with

noisy distance measurements," *IEEE Trans. Autom. Sci. Eng.*, vol. 3, no. 4, pp. 360–371, Oct. 2006.

[109] P. Biswas and Y. Ye, "A distributed method for solving semidefinite programs arising from ad hoc wireless sensor network localization," *Multiscale optimization methods and applications*, vol. 82, pp. 69–84, Jan. 2006.

[110] K. Lui, W.-K. Ma, H. So, and F. Chan, "Semi-definite programming algorithms for sensor network node localization with uncertainties in anchor positions and/or propagation speed," *IEEE Trans. Signal Process.*, vol. 57, no. 2, pp. 752–763, Feb. 2009.

[111] J. A. Costa, N. Patwari, and A. O. Hero, "Distributed weighted-multidimensional scaling for node localization in sensor networks," *ACM Trans. Sensor Networks*, vol. 2, no. 1, pp. 39–64, Feb. 2006.

[112] Z. Wang, S. Zheng, Y. Ye, and S. Boyd, "Further relaxations of the semidefinite programming approach to sensor network localization," *SIAM J. on Optimization*, vol. 19, no. 2, pp. 655–673, Jul. 2008.

[113] T. K. Pong and P. Tseng, "(robust) edge-based semidefinite programming relaxation of sensor network localization," *Mathematical Programming, ser. A*, 2010.

[114] Q. Shi, C. He, H. Chen, and L. Jiang, "Distributed wireless sensor network localization via sequential greedy optimization algorithm," *IEEE Trans. Signal Process.*, vol. 58, no. 6, pp. 3328–3340, Jun. 2010.

[115] P. gren, E. Fiorelli, and N. E. Leonard, "Cooperative control of mobile sensor networks: Adaptive gradient climbing in a distributed environment," *IEEE Trans. Autom. Control*, vol. 49, no. 8, Aug. 2004.

[116] L. Hu and D. Evans, "Localization for mobile sensor networks," in *Proc. ACM MobiCom*, 2004, pp. 45–57.

[117] S. Zhang, J. Cao, L. Chen, and D. Chen, "Accurate and energy-efficient range-free localization for mobile sensor networks," *IEEE Trans. Mobile Comput.*, vol. 9, no. 6, Jun. 2010.

[118] J. Teng, H. Snoussi, C. Richard, and R. Zhou, "Distributed variational filtering for simultaneous sensor localization and target tracking in wireless sensor networks," *IEEE Trans. Veh. Technol.*, vol. 61, no. 5, pp. 2305–2318, 2012.

[119] S. Thrun, D. Fox, W. Burgard, and F. Dellaert, "Robust monte carlo localization for mobile robots," *Artificial Intelligence*, vol. 128, no. 1-2, pp. 99–141, 2000.

[120] Z. Zhong, T. Zhu, D. Wang, and T. He, "Tracking with unreliable node sequences," in *INFOCOMM, Twenty Eighth Annual Joint Conference of the IEEE Computer and Communications Societies*, 2009, pp. 1215–1223.

[121] X. Chen, A. Edelstein, Y. Li, M. Coates, M. Rabbat, and A. Men, "Sequential monte carlo for simultaneous passive device-free tracking and sensor localization using received signal strength measurements,"

in *Proc. 10th Int Information Processing in Sensor Networks (IPSN) Conf.*, 2011, pp. 342–353.

[122] J. C. Derenick and J. R. Spletzer, "Convex optimization strategies for coordinating large-scale robot formations," *IEEE Trans. Mobile Comput.*, vol. 23, no. 6, Dec. 2007.

[123] A. Jadbabaie, J. Lin, and A. S. Morse, "Coordination of groups of mobile autonomous agents using nearest neighbor rules," *IEEE Trans. Autom. Control*, vol. 48, no. 6, pp. 988–1001, 2003.

[124] S.-Y. Lien, K.-C. Chen, and Y. Lin, "Toward ubiquitous massive accesses in 3GPP machine-to-machine communications," *IEEE Commun. Mag.*, vol. 49, no. 4, pp. 66–74, 2011.

[125] S. Lucero. Maximizing Mobile Operator Opportunities in M2M The Benefits of an M2M-Optimized Network. White Paper. ABI Research - Cisco. [Online]. Available: http://tinyurl.com/kt345s9

[126] R. Lu, X. Li, X. Liang, X. Shen, and X. Lin, "Grs: The green, reliability, and security of emerging machine to machine communications," *IEEE Commun. Mag.*, vol. 49, no. 4, pp. 28–35, 2011.

[127] Y. Liang, H. V. Poor, and L. Ying, "Secure communications over wireless broadcast networks: Stability and utility maximization," *IEEE Trans. Inf. Forensics Security*, vol. 6, no. 3, pp. 682–692, 2011.

[128] Third Generation Partnership Project (3GPP), "Service requirements for machine-type communications (MTC); stage 1," Technical Spec-

ification Group Services and System Aspects;, Tech. Rep. 22.368 V12.3.0, Dec. 2013.

[129] K.-R. Jung, A. Park, and S. Lee, "Machine-Type-Communication (MTC) Device Grouping Algorithm for Congestion Avoidance of MTC Oriented LTE Network," in *Security-Enriched Urban Computing and Smart Grid*, 2010, vol. 78, pp. 167–178.

[130] S.-Y. Lien and K.-C. Chen, "Massive access management for QoS guarantees in 3GPP machine-to-machine communications," *IEEE Commun. Lett.*, vol. 15, no. 3, pp. 311–313, 2011.

[131] S.-Y. Lien, T.-H. Liau, C.-Y. Kao, and K.-C. Chen, "Cooperative access class barring for machine-to-machine communications," *IEEE Trans. Wireless Commun.*, vol. 11, no. 1, pp. 27–32, 2012.

[132] R. Yu, Y. Zhang, Y. Chen, C. Huang, Y. Xiao, and M. Guizani, "Distributed rate and admission control in home M2M networks: A non-cooperative game approach," in *Proc. IEEE Conf. Computer Communications Workshops (INFOCOM WKSHPS)*, 2011, pp. 196–200.

[133] R. Liu, W. Wu, H. Zhu, and D. Yang, "M2M-Oriented QoS Categorization in Cellular Network," in *Proc. 7th Int Wireless Communications, Networking and Mobile Computing (WiCOM) Conf*, 2011, pp. 1–5.

[134] J. Zhou, M. Li, L. Liu, X. She, and L. Chen, "Energy source aware target cell selection and coverage optimization for power saving in

cellular networks," in *Proc. Physical and Social Computing (CPSCom) Green Computing and Communications (GreenCom) IEEE/ACM Int'l Conf. & Int'l Conf. Cyber*, 2010, pp. 1–8.

[135] G. Wang, X. Zhong, S. Mei, and J. Wang, "An adaptive medium access control mechanism for cellular based machine to machine (M2M) communication," in *Proc. IEEE International Wireless Information Technology and Systems (ICWITS) Conference*, 2010, pp. 1–4.

[136] M. Hasan, E. Hossain, and D. Niyato, "Random access for machine-to-machine communication in LTE-advanced networks: issues and approaches," *Communications Magazine, IEEE*, vol. 51, no. 6, 2013.

[137] Third Generation Partnership Project (3GPP), "LTE coverage enhancements," Technical Specification Group Radio Access Network (RAN), Tech. Rep. 36.824 V11.0.0, 2012.

[138] Third Generation Partnership Project (3GPP) Work Item Description, "Low Cost and Enhanced Coverage MTC UE for LTE," Tech. Rep. RP-130848, Jun. 2013.

[139] J. Berglund, "Extended LTE coverage for indoor machine type communication," Master's thesis, Ericsson Research, Jun. 2013.

[140] S. Andreev, O. Galinina, and Y. Koucheryavy, "Energy-efficient client relay scheme for machine-to-machine communication," in *Proc. IEEE Global Telecommunications Conf. (GLOBECOM 2011)*, 2011, pp. 1–5.

[141] R. Schoenen, W. Zirwas, and B. H. Walke, "Capacity and coverage

analysis of a 3gpp-lte multihop deployment scenario," in *Communications Workshops, 2008. ICC Workshops' 08. IEEE International Conference on.* IEEE, 2008, pp. 31–36.

[142] T. Beniero, S. Redana, J. Hamalainen, and B. Raaf, "Effect of relaying on coverage in 3GPP LTE-Advanced," in *Vehicular Technology Conference (VTC-Spring).* IEEE, 2009, pp. 1–5.

[143] T. Banerjee, B. Xie, and D. P. Agrawal, "Fault tolerant multiple event detection in a wireless sensor network," *J. Parallel Distrib. Comput.*, vol. 68, pp. 1222–1234, Sep. 2008.

[144] J. Li and G. AlRegib, "Rate-constrained distributed estimation in wireless sensor networks," *IEEE Trans. Signal Process.*, vol. 55, no. 5, pp. 1634–1643, May 2007.

[145] J.-J. Xiao, S. Cui, Z.-Q. Luo, and A. J. Goldsmith, "Power scheduling of universal decentralized estimation in sensor networks," *IEEE Trans. Signal Process.*, vol. 54, no. 2, pp. 413–422, Feb. 2006.

[146] H. L. V. Trees, *Detection, Estimation, and Modulation Theory: Radar-Sonar Signal Processing and Gaussian Signals in Noise.* Melbourne, FL, USA: Krieger Publishing Co., Inc., 1992.

[147] A. Rajeswaran, G. Kim, and R. Negi, "Joint power adaptation, scheduling, and routing for ultra wide band networks," *IEEE Trans. Wireless Commun.*, vol. 6, no. 5, pp. 1964–1972, May 2007.

[148] A. F. Molisch, K. Balakrishnan, D. Cassioli, C. Chong, S. Emami,

A. Fort, J. Karedal, J. Kunisch, H. Schantz, U. Schuster, and K. Siwiak, "IEEE 802.15.4a channel model-final report," IEEE 802.15.4a, Tech. Rep., 2005.

[149] A. Krasnopeev, J.-J. Xiao, and Z.-Q. Luo, "Minimum energy decentralized estimation in a wireless sensor network with correlated sensor noises," *EURASIP J. Wirel. Commun. Netw.*, vol. 2005, no. 4, pp. 473–482, 2005.

[150] L. Xiao, M. Johansson, and S. Boyd, "Simultaneous routing and resource allocation via dual decomposition," *IEEE Trans. Commun.*, vol. 52, no. 7, pp. 1136–1144, Jul. 2004.

[151] J. Ryckaert et al., "A CMOS Ultra-Wideband Receiver for Low Data-Rate Communication," *IEEE J. Solid-State Circuits*, vol. 42, no. 11, pp. 2515–2527, Nov. 2007.

[152] W.-G. Seah, Z. A. Eu, and H. Tan, "Wireless sensor networks powered by ambient energy harvesting (WSN-HEAP) - survey and challenges," in *First International Conference on Wireless Communication, Vehicular Technology, Information Theory and Aerospace Electronic Systems Technology (VITAE)*, May 2009, pp. 1–5.

[153] K. Yu, J. P. Montillet, A. Rabbachin, P. Cheong, and I. Oppermann, "UWB location and tracking for wireless embedded networks," *Elsevier Signal Processing, Special Section: UWB Communications*, vol. 86, no. 9, pp. 2153 – 2171, Sept. 2006.

[154] C. Hide, T. Moore, and M. Smith, "Adaptive Kalman filtering for low cost INS/GPS," *The Journal of Navigation*, vol. 56, pp. 143–152, Jan. 2003.

[155] Global Positioning System (GPS), *Standard Positioning Service Performance Standard*, www.gps.gov/technical/ps/2008-SPS-performance-standard.pdf, Std. Ed. 4, Sep. 2008.

[156] F. Alizadeh and D. Goldfarb, "Second-order cone programming," *Mathematical Programming*, vol. 95, pp. 3–51, 2001.

[157] T. K. Pong, "Edge-based semidenite programming relaxation of sensor network localization with lower bound constraints," *Journal of Computational Optimization and Applications*, vol. 53, pp. 23–44, 2010.

[158] J. Nocedal and S. Wright, *Numerical Optimization*. Springer, 1999.

[159] P. Tseng, "Convergence of a block coordinate descent method for nondifferentiable minimization," *Journal of Optimization Theory and Applications*, vol. 109, pp. 475–494, 2001.

[160] M. S. Lobo, L. Vandenberghe, S. Boyd, and H. Lebret, "Applications of second-order cone programming," *Linear algebra and its applications*, vol. 284, no. 1, pp. 193–228, 1998.

[161] A. Logothetis and V. Krishnamurthy, "Expectation maximization algorithms for map estimation of jump markov linear systems," *IEEE Trans. Signal Process.*, vol. 48, no. 7, pp. 2139–2156, Aug. 1999.

[162] M. Grant and S. Boyd., *MATLAB software for disciplined convex programming (web page and software)*. [Online]. Available: http://stanford.edu/~boyd/cvx

[163] T. Camp, J. Boleng, and V. Davies, "A survey of mobility models for ad hoc network research," *Wireless Communications & Mobile Computing (WCMC)*, vol. 2, pp. 483–502, 2002.

[164] Third Generation Partnership Project (3GPP), "Study on provision of low-cost MTC UEs based on LTE," Technical Specification Group Radio Access Network (RAN), Tech. Rep. 36.888 V12.0.0, Jun. 2013.

[165] G. Naddafzadeh-Shirazi, L. Lampe, G. Vos, and S. Bennett, "Enhancement for LTE communication systems," Patent United States App. No. 14/046 733, International App. No. PCT/CA2013/050 749, (Filed October 4, 2013).

[166] G. Vos, G. Naddafzadeh-Shirazi, S. Bennett, L. Lampe, and R. Khalona, "Method and system for hybrid automatic request combining on an LTE downlink control channel," Patent United States App. No. 13/730 244, International App. No. PCT/CA2013/730 244, (Filed December 28, 2012).

[167] G. Vos, S. Bennett, L. Lampe, and G. Naddafzadeh-Shirazi, "Method and apparatus for broadcast channel decoding," Patent United States App. No. 61/807 641, (Filed April 2, 2013).

[168] R. Wilson, D. Tse, and R. A. Scholtz, "Channel identification: Secret

sharing using reciprocity in ultrawideband channels," *IEEE Trans. Inf. Forensics Security*, vol. 2, no. 3, pp. 364–375, Sep. 2007.

[169] C. Lai, H. Li, R. Lu, X. Shen, and J. Cao, "A unified end-to-end security scheme for machine-type communication in LTE networks," in *IEEE/CIC International Conference on Communications in China (ICCC)*, Aug. 2013, pp. 698–703.

[170] R. H. Weber, "Internet of things–new security and privacy challenges," *Computer Law & Security Review*, vol. 26, no. 1, pp. 23–30, Jan. 2010.

Appendix A

Proof of Proposition 3.1

We can write (3.7) with the relaxation (3.8) in the form:

$$v^*_{\text{socp}} \doteq \min_{\{\boldsymbol{x}_i\},\{q_{ij}\}} \| \Big[[g_{ij}\,|q_{ij}-d_{ij}|]_{(i,j)\in\mathcal{E}} \;;\; [\|\boldsymbol{\Psi}_i^{-1/2}(\boldsymbol{a}_i-\boldsymbol{x}_i)\|]_{i\in\mathcal{N}_a} \Big] \| \tag{A.1a}$$

$$\text{subject to} \quad \|\boldsymbol{x}_i-\boldsymbol{x}_j\| \le q_{ij}, \quad (i,j)\in\mathcal{E}, \tag{A.1b}$$

where intermediate variables $t_{ij}, s_i, \boldsymbol{u}, v$ are removed.

a) Since the Euclidean norm is strictly convex, the problem (A.1) must have a unique optimal with regard to all variables that appear in the norm [10]. Hence, $\boldsymbol{x}_i,\ i\in\mathcal{N}_a$, is unique at the optimal. Note that $\boldsymbol{x}_i,\ i\in\mathcal{N}_s$ does not appear in the norm in the objective.

b) The proof of this part is identical to [106, Proposition 5.1c], and we briefly show it here for completeness. Note that according to part a) $q_{ij},\ (i,j)\in\mathcal{E}$, is unique over all solutions. For a tight link $(i,j)\in\mathcal{B},\ i\in\mathcal{N}_s$,

$$\frac{1}{2}\|\boldsymbol{x}_i-\boldsymbol{x}_j\|^2+\frac{1}{2}\|\boldsymbol{x}'_i-\boldsymbol{x}'_j\|^2 = \|\frac{\boldsymbol{x}_i+\boldsymbol{x}'_i}{2}-\frac{\boldsymbol{x}_j+\boldsymbol{x}'_j}{2}\|^2+\|\frac{\boldsymbol{x}_i-\boldsymbol{x}'_i}{2}-\frac{\boldsymbol{x}_j-\boldsymbol{x}'_j}{2}\|^2, \tag{A.2}$$

with $(\boldsymbol{x}_i', \boldsymbol{x}_j')$ being another optimal solution. Since the solution set of a convex problem is convex [20], $(\frac{\boldsymbol{x}_i+\boldsymbol{x}_i'}{2},\ \frac{\boldsymbol{x}_j+\boldsymbol{x}_j'}{2})$ must be another optimal solution, and thus (A.2) implies that $q_{ij}^2/2 + q_{ij}^2/2 = q_{ij}^2 + \|\frac{\boldsymbol{x}_i-\boldsymbol{x}_i'}{2} - \frac{\boldsymbol{x}_j-\boldsymbol{x}_j'}{2}\|^2$, and thus

$$\boldsymbol{x}_i - \boldsymbol{x}_i' = \boldsymbol{x}_j - \boldsymbol{x}_j',\ \forall j \in \mathcal{J}_i, \tag{A.3}$$

where $\mathcal{J}_i$ is the set of nodes which are *directly* connected to node i through tight links. Now, denote the set of all nodes which are connected to node i through tight links, possibly through multiple hops, by $\mathcal{T}_i$. According to [106, Proposition 5.1b], there is at least one anchor $\boldsymbol{x}_k,\ k \in \mathcal{N}_a$ in $\mathcal{T}_i$. We can then apply (A.3) to this anchor and its immediate tight neighbor $\boldsymbol{x}_l \in \mathcal{N}_s$ in $\mathcal{T}_i$, and conclude that $\boldsymbol{x}_l = \boldsymbol{x}_l'$ since $\boldsymbol{x}_k = \boldsymbol{x}_k'$ holds according to part a). We can repeat the same procedure between the nodes that are proven to be invariant and their immediate neighbours to conclude that all nodes in $\mathcal{T}_i$ are invariant over all solutions. Now, since $j \in \mathcal{T}_i$, (A.3) implies that $\boldsymbol{x}_i$ is also invariant over all solutions of the robust SOCP.

For the proof of the reverse part, note that for a node $\boldsymbol{x}_i\ i \in \mathcal{N}_s$ with $\|\boldsymbol{x}_i - \boldsymbol{x}_j\| < q_{ij},\ \forall j \in \mathcal{K}_i$, another distinct relative interior solution can be obtained as $\boldsymbol{x}_i' = \boldsymbol{x}_i + \Delta\boldsymbol{x}$ with $\Delta\boldsymbol{x}$ small enough such that $\|(\boldsymbol{x}_i' - \boldsymbol{x}_j)\| < q_{ij},\ \forall j \in \mathcal{K}_i$, and all other variables remain unchanged.

c) We first show that for the analytic center solution, each sensor node is estimated within the convex hull of its neighbours, i.e. $\boldsymbol{x}_i \in \mathcal{C}\{\boldsymbol{x}_j\}_{j\in\mathcal{K}_i},\ \forall i \in \mathcal{N}_s$. Similar to [106, Proposition 6.2], we argue by contradiction. Suppose that at the analytic center solution, for a sensor node $i \in \mathcal{N}_s$, $\boldsymbol{x}_i$ is outside the convex hull of its neighbours. Then, let $\boldsymbol{p}_i$ be its projection on this

convex hull and thus for each neighbor $j \in \mathcal{K}_i$ we can write,

$$\begin{aligned} \|\boldsymbol{p}_i - \boldsymbol{x}_j\| \quad &< \quad \|\boldsymbol{x}_i - \boldsymbol{x}_j\| \Rightarrow \log(q_{ij} - \|\boldsymbol{p}_i - \boldsymbol{x}_j\|) > \log(q_{ij} - \|\boldsymbol{x}_i - \boldsymbol{x}_j\|) \\ &\Rightarrow \quad \sum_{(i,j)\in\mathcal{E}-\mathcal{B}} \log(q_{ij} - \|\boldsymbol{p}_i - \boldsymbol{x}_j\|) > \sum_{(i,j)\in\mathcal{E}-\mathcal{B}} \log(q_{ij} - \|\boldsymbol{x}_i - \boldsymbol{x}_j\|), \end{aligned}$$

where the second clause follows from the uniqueness of q_{ij} over all solutions, and in the third clause, summation is taken overall non-tight links. Therefore $\boldsymbol{x}_i$ can not be the analytical center solution of node i. Thus, $\boldsymbol{x}_i$ must be inside the convex hull of its neighbours. Now, since, only anchor nodes are allowed to be localized outside the convex hull of their neighbours, it follows that anchors form the convex hull of the analytic center solution.

Appendix B

Proof of Proposition 3.2

In order to prove Proposition 2, we first construct a variation of the robust SDP optimization problem (3.9):

$$v'_{\text{sdp}} \doteq \min_{\boldsymbol{X},\boldsymbol{Y},\{\boldsymbol{M}_i\},\{\gamma_{ij}\},\{r_{ij}\}} \left(\sum_{(i,j)\in\mathcal{E}} g_{ij}^2 \left(\gamma_{ij} - 2d_{ij}r_{ij} + d_{ij}^2\right) + \sum_{i\in\mathcal{N}_a} \mathbf{tr}\left(\boldsymbol{\Psi}_i^{-1}\boldsymbol{M}_i\right) \right)^{\frac{1}{2}} \tag{B.1a}$$

$$\text{subject to} \quad \gamma_{ij} = y_{ii} + y_{jj} - y_{ij} - y_{ji}, \quad (i,j) \in \mathcal{E}, \tag{B.1b}$$

$$r_{ij}^2 \leq \gamma_{ij}, \quad (i,j) \in \mathcal{E}, \tag{B.1c}$$

$$\mathbf{tr}(\boldsymbol{M}_i) = y_{ii} - 2\boldsymbol{a}_i^T\boldsymbol{x}_i + \boldsymbol{a}_i^T\boldsymbol{a}_i, \qquad i \in \mathcal{N}_a, \tag{B.1d}$$

$$\boldsymbol{x}_i = \left[y_{im+1}\ y_{im+2}\right]^T, \quad i \in \mathcal{N}, \tag{B.1e}$$

$$\begin{bmatrix} y_{m+1m+1} & y_{m+1m+2} \\ y_{m+2m+1} & y_{m+2m+2} \end{bmatrix} = \boldsymbol{I}_2, \tag{B.1f}$$

$$\begin{bmatrix} \boldsymbol{M}_i & \boldsymbol{a}_i - \boldsymbol{x}_i \\ (\boldsymbol{a}_i - \boldsymbol{x}_i)^T & 1 \end{bmatrix} \succeq \mathbf{0}_3, \qquad i \in \mathcal{N}_a, \tag{B.1g}$$

$$\boldsymbol{Y} \succeq \mathbf{0}_{m+2}, \tag{B.1h}$$

where $\boldsymbol{M}_i$ is defined in (3.11). The SDP relaxation (B.1) is equivalent to (3.9) because there is a one-to-one mapping between the feasible solution set of (3.9) to the feasible solution set of (B.1). Let $S_{\text{sdp}} = \{\boldsymbol{X}, \boldsymbol{Y}, \{\boldsymbol{M}_i\}, \{\gamma_{ij}\}, \{r_{ij}\}\}$ be a feasible solution for robust SDP satisfying constraints (B.1b)-(B.1h). We show that the variables defined in (3.11) satisfy the SOCP constraints (3.7c)-(3.7e) and (3.8), and hence any feasible solution for robust SDP (B.1) (equivalently (3.9)) is a feasible solution for (3.7).

In fact, constraints (3.7c) and (3.7d)) are clearly satisfied with equality by definition of v and t_{ij} in (3.11). To see that constraint (3.7e) is satisfied, first note that since SDP constraint (B.1g) is satisfied, $\boldsymbol{M}_i - (\boldsymbol{a}_i - \boldsymbol{x}_i)(\boldsymbol{a}_i - \boldsymbol{x}_i)^T$, $i \in \mathcal{N}_a$, is a positive semidefinite matrix. It is then clear that

$$\mathbf{tr}\left(\boldsymbol{\Psi}_i^{-1}\left(\boldsymbol{M}_i - (\boldsymbol{a}_i - \boldsymbol{x}_i)(\boldsymbol{a}_i - \boldsymbol{x}_i)^T\right)\right) \geq 0, \quad i \in \mathcal{N}_a, \tag{B.2}$$

due to the fact that the trace of the product of two positive semidefinite matrix is always non-negative. Using this inequality we obtain

$$\begin{aligned} s_i^2 &= \mathbf{tr}\left(\boldsymbol{\Psi}_i^{-1}\boldsymbol{M}_i\right) \geq \mathbf{tr}\left(\boldsymbol{\Psi}_i^{-1}(\boldsymbol{a}_i - \boldsymbol{x}_i)(\boldsymbol{a}_i - \boldsymbol{x}_i)^T\right) \\ &= \|\boldsymbol{\Psi}_i^{-1/2}(\boldsymbol{a}_i - \boldsymbol{x}_i)\|^2, \quad i \in \mathcal{N}_a, \end{aligned}$$

which leads to constraint (3.7e) by taking the square root of both sides.

For constraint (3.8), we follow the same line of reasoning as [21]. Specifically, since constraint (B.1h) is satisfied, $\boldsymbol{Y} \doteq \begin{bmatrix} \boldsymbol{Y}_m & \boldsymbol{X}^T \\ \boldsymbol{X} & \boldsymbol{I}_2 \end{bmatrix}$ is positive semidefinite, and $\boldsymbol{Z} \doteq \boldsymbol{Y}_m - \boldsymbol{X}^T\boldsymbol{X} \succeq \boldsymbol{0}_m$. Moreover, since any 2×2 principal submatrix of the positive semidefinite matrix $\boldsymbol{Z}$ is also positive semidefinite, we get

$$\begin{bmatrix} y_{ii} - \|\boldsymbol{x}_i\|^2 & y_{ij} - \boldsymbol{x}_i^T\boldsymbol{x}_j \\ y_{ji} - \boldsymbol{x}_j^T\boldsymbol{x}_i & y_{jj} - \|\boldsymbol{x}_j\|^2 \end{bmatrix} \succeq \boldsymbol{0}_2, \quad (i,j) \in \mathcal{E}. \tag{B.3}$$

Hence,

$$[1,-1] \begin{bmatrix} y_{ii} - \|\boldsymbol{x}_i\|^2 & y_{ij} - \boldsymbol{x}_i^T\boldsymbol{x}_j \\ y_{ji} - \boldsymbol{x}_j^T\boldsymbol{x}_i & y_{jj} - \|\boldsymbol{x}_j\|^2 \end{bmatrix} \begin{bmatrix} 1 \\ -1 \end{bmatrix} \geq 0, \Rightarrow$$

$$y_{ii} - \|\boldsymbol{x}_i\|^2 + y_{jj} - \|\boldsymbol{x}_j\|^2 - 2(y_{ij} - \boldsymbol{x}_i^T\boldsymbol{x}_j) \geq 0.$$

Consequently,

$$q_{ij}^2 = y_{ii} + y_{jj} - 2y_{ij} \geq \|\boldsymbol{x}_i\|^2 - 2\boldsymbol{x}_i^T\boldsymbol{x}_j + \|\boldsymbol{x}_j\|^2 = \|\boldsymbol{x}_i - \boldsymbol{x}_j\|^2.$$

Therefore, constraint (3.8) is also satisfied.

We have shown that all constraints of the robust SOCP are satisfied and thus any feasible solution of the robust SDP is also a feasible solution of the robust SOCP. Also, the optimum value of the robust SOCP in (3.7) is

smaller than or equal to that for the robust SDP in (B.1) because at the optimal point of SDP, which is a feasible point for SOCP, we have

$$\begin{aligned}
v'_{\text{sdp}} &= \sqrt{v_{\text{sdp}} + v_0} \\
&= \left(\sum_{(i,j)\in\mathcal{E}} g_{ij}^2 \left(\gamma_{ij} - 2d_{ij}r_{ij} + d_{ij}^2\right) + \sum_{i\in\mathcal{N}_a} \mathbf{tr}\left(\boldsymbol{\Psi}_i^{-1}\boldsymbol{M}_i\right) \right)^{\frac{1}{2}} \\
&= \left(\sum_{(i,j)\in\mathcal{E}} g_{ij}^2 \left(\gamma_{ij} - 2d_{ij}\sqrt{\gamma_{ij}} + d_{ij}^2\right) + \sum_{i\in\mathcal{N}_a} s_i^2 \right)^{\frac{1}{2}} \\
&= \left(\sum_{(i,j)\in\mathcal{E}} g_{ij}^2 \left(q_{ij} - d_{ij}\right)^2 + \sum_{i\in\mathcal{N}_a} s_i^2 \right)^{\frac{1}{2}} \\
&= \left(\sum_{(i,j)\in\mathcal{E}} t_{ij}^2 + \sum_{i\in\mathcal{N}_a} s_i^2 \right)^{\frac{1}{2}} = v_{\text{socp}},
\end{aligned}$$

where the third equality holds because at the optimum solution of the robust SDP, $r_{ij}^2 = \gamma_{ij}$, i.e. constraint (B.1e) is satisfied with equality [25]. The proof is complete by noting that, by definition, any non-optimal solution of SDP has a value of objective which is larger than v'_{sdp}.